



**EVALUATING
POTENTIAL
GROUNDWATER
RESOURCES ON
STATE LANDS
IN EL PASO
COUNTY, TEXAS
USING
AIRBORNE
GEOPHYSICS**

**BY
JEFFREY G. PAINE AND
EDWARD W. COLLINS**

BUREAU OF ECONOMIC GEOLOGY

SCOTT W. TINKER, DIRECTOR

JOHN A. AND KATHERINE G. JACKSON SCHOOL OF GEOSCIENCES

THE UNIVERSITY OF TEXAS AT AUSTIN

AUSTIN, TEXAS 78713-8924



AUGUST 2002

EVALUATING POTENTIAL GROUNDWATER RESOURCES ON STATE LANDS
IN EL PASO COUNTY, TEXAS USING AIRBORNE GEOPHYSICS

by

Jeffrey G. Paine and Edward W. Collins
Bureau of Economic Geology
The University of Texas at Austin

Mail address:
University Station, Box X
Austin, Texas 78713-8924

Street address:
J. J. Pickle Research Campus, Building 130
10100 Burnet Road
Austin, Texas 78758-4445
jeff.paine@beg.utexas.edu
eddie.collins@beg.utexas.edu

Report prepared for the General Land Office
under Interagency Cooperation Contract No. 02-306R

August 2002

Page intentionally blank

SUMMARY	vii
INTRODUCTION	1
Geologic Setting	4
Groundwater Depth	7
Groundwater Quality	12
METHODS	17
Ground Geophysics	20
Airborne Geophysics	27
GROUND GEOPHYSICAL SURVEY	32
AIRBORNE GEOPHYSICAL SURVEY	40
Magnetic Field Data	40
EM Data	41
Average Conductivity Profile and Achieved Exploration Depth	47
Conductivity–Depth Slices	50
RELATIONSHIP BETWEEN WATER QUALITY AND CONDUCTIVITY	53
FAVORABLE GROUNDWATER EXPLORATION AREAS	59
CONCLUSIONS	63
ACKNOWLEDGMENTS	64
REFERENCES AND RELATED PUBLICATIONS	64
APPENDIX A: CONDUCTIVITY-DEPTH SLICES BETWEEN 10- AND 200-M DEPTH	71
APPENDIX B: CD-ROM CONTENTS	83

FIGURES

1. Location of the airborne survey area in eastern El Paso County, Texas	2
2. Aerial photographic map of the airborne survey area	3

3.	Geologic map of the survey area	6
4.	Relationship between land-surface elevation and depth to water	8
5.	Depth to water superimposed on map of land-surface elevation	9
6.	Water-level elevation superimposed on map of land-surface elevation	10
7.	Water levels and depths to the top and bottom of slotted casing	11
8.	Relationship between TDS concentration and measured electrical conductivity in groundwater samples	14
9.	Total dissolved solids (TDS) concentration in samples from water wells	15
10.	Distribution of fresh, slightly saline, and moderately saline water	16
11.	Specific capacity measured for selected water wells	19
12.	Time-domain EM transmitter input and receiver response	21
13.	Survey area flight lines, State Lands tracts, and ground-based TDEM sites	23
14.	Central loop instrument configuration for ground-based TDEM soundings	25
15.	Ground-based transmitter operating at site TDEM-2	26
16.	Ground-based receiver at site TDEM-2	26
17.	Fugro Airborne Surveys' Megatem II airborne TDEM system	29
18.	Megatem II system acquiring data over the northern part of the survey area	29
19.	Estimated exploration depth of the Megatem II system	31
20.	Decay of the ground TDEM signal following termination of the transmitter current at site TDEM-1	35
21.	Vertical (z) and horizontal (x and y) components of the ground TDEM signal at site 1	36
22.	Apparent conductivity and the best-fit conductivity model for ground TDEM site 1	38
23.	Comparison of the best-fit, 4-layer conductivity model for data collected at ground TDEM site 1 with the best 1-, 2-, and 3-layer models	39
24.	Residual magnetic field strength measured with an airborne magnetometer	42
25.	Shallow-depth transform of magnetic field data	43
26.	Powerline noise intensity measured during the airborne survey	45
27.	Apparent conductance calculated from TDEM data	46
28.	Average conductivity over the geophysical survey area	48

29.	Apparent conductivity at a depth of 70 m and mapped faults	52
30.	Apparent conductivity at a depth of 120 m and TDS values for water samples	54
31.	Comparison of TDS values from one low-TDS water well and one high-TDS water well with conductivity profiles	55
32.	Relationship between TDS concentration in groundwater samples and apparent conductivi- ties calculated from airborne data	57
33.	Favorable exploration areas for relatively low-TDS groundwater at a depth of 120 m	60
34.	Favorable exploration areas for relatively low-TDS groundwater superimposed on an aerial photograph	61
A1.	Apparent conductivity at a depth of 10 m	73
A2.	Apparent conductivity at a depth of 20 m	73
A3.	Apparent conductivity at a depth of 30 m	74
A4.	Apparent conductivity at a depth of 40 m and TDS values	74
A5.	Apparent conductivity at a depth of 50 m and TDS values	75
A6.	Apparent conductivity at a depth of 60 m and TDS values	75
A7.	Apparent conductivity at a depth of 70 m and TDS values	76
A8.	Apparent conductivity at a depth of 80 m	76
A9.	Apparent conductivity at a depth of 90 m	77
A10.	Apparent conductivity at a depth of 100 m and TDS values	77
A11.	Apparent conductivity at a depth of 110 m and TDS values	78
A12.	Apparent conductivity at a depth of 120 m and TDS values	78
A13.	Apparent conductivity at a depth of 130 m and TDS values	79
A14.	Apparent conductivity at a depth of 140 m and TDS values	79
A15.	Apparent conductivity at a depth of 150 m and TDS values	80
A16.	Apparent conductivity at a depth of 160 m and TDS values	80
A17.	Apparent conductivity at a depth of 170 m and TDS values	81
A18.	Apparent conductivity at a depth of 180 m and TDS values	81
A19.	Apparent conductivity at a depth of 190 m and TDS values	82
A20.	Apparent conductivity at a depth of 200 m and TDS values	82

TABLES

1.	Salinity classifications based on TDS concentration	13
2.	Water-quality statistics for samples from survey-area water wells	18
3.	Best-fit conductivity models for ground-based TDEM soundings	24
4.	Survey and flight parameters for the El Paso County airborne survey	28
5.	Acquisition parameters for the El Paso County airborne TDEM survey	30
6.	Acquisition parameters for the El Paso County airborne magnetometer survey	33
B1.	File name, measurement units, low and high data values, and file description	84

SUMMARY

We employed ground-based and high-resolution airborne geophysical methods in combination with an analysis of available water-well data and geologic information to identify potentially favorable groundwater resources in a 372 km² area within the Hueco Bolson in eastern El Paso County, Texas. Analysis of water-well data from the survey area demonstrates that (a) good quality groundwater (less than 1,000 mg/L total dissolved solids) is present in places, (b) water-level depths on the floor of the basin range from 90 to 130 m and are strongly correlated with surface elevation, (c) most groundwater sampled in this area is classified as fresh or slightly saline, (d) water salinity increases with depth, and (e) reported specific capacities of wells range from 0.5 to 36 gal/min/ft. Most existing wells draw from depths of 110 to 180 m, which is within the exploration range of the airborne time-domain electromagnetic (TDEM) instrument.

Ground-based geophysical studies conducted before the airborne survey demonstrated that (a) conditions were favorable for the acquisition of good quality electromagnetic (EM) data, (b) changes in electrical conductivity with depth are likely to be related to changes in water saturation, host sediment type, and water quality, and (c) increases in conductivity detected at depths below the water table are likely to be caused by increasing groundwater salinity with depth.

An airborne geophysical survey flown by Fugro Airborne Surveys in August 2001 acquired TDEM and passive magnetic field data at 64,773 locations along north–south flight lines spaced at 400-m intervals. Magnetic field data correlated well with mapped fault locations. The Megatem II airborne TDEM system used in this survey achieved exploration depths that exceeded the depth to water over more than 90 percent of the survey area. Exploration depths exceeded 280 m over more than half the survey area. Airborne TDEM data were processed to produce horizontal slices that depict apparent conductivity changes at 10-m depth intervals across the area. Above the zone of water saturation, geologic features such as faults are prominent in the data. At deeper depths below the water table at about 100 m, apparent conductivity

values correlate reasonably well with existing groundwater quality data for water wells with accurate locations that are near flight lines.

Largely on the basis of airborne survey results, we identified two areas of low conductivity below the water table that are favorable locations for groundwater exploration on State-owned land. The largest, with an area of 23 km², includes a State tract (T&P Railroad, block 78T2, section 18) located southwest of Montana Vista at depths of 110 to 140 m. The other covers about 8 km² in the northwest corner of the survey area at depths of 100 to 150 m. Three State tracts (T&P Railroad, block 79T2, sections 15, 16, and 21) are included within this area. Although these areas are favorable sites for groundwater exploration, geophysical and available water-well data suggest that these resources are limited and that local, high-volume production will likely be accompanied by significant water-level decline and salinity increase.

INTRODUCTION

The Bureau of Economic Geology (Bureau) conducted airborne and supporting ground-based geophysical studies in eastern El Paso County, Texas (fig. 1) to delineate potentially favorable groundwater resources in the shallow subsurface (upper few hundred meters) of the Hueco Bolson, where the State of Texas owns extensive tracts of land (fig. 2). The project area is a rectangular block covering 372 km² (144 mi²) that is about 17 km (10.6 mi) across in an east-west direction and about 22 km (13.7 mi) across in a north-south direction. This area includes all of the tracts delineated for more in-depth study in a 1997 GLO-sponsored evaluation of groundwater resources on State lands in El Paso County (Mullican and others, 1997). These tracts were interpreted to contain potential water resources of relatively low total dissolved solids concentrations (about 1,500 milligrams per liter [mg/L] or less) at relatively shallow depths (about 120m).

The principal geophysical method employed in this study is time-domain electromagnetic induction (TDEM), in which changes in electrical currents flowing in a transmitter wire induce changes in the local magnetic field, which in turn induce currents to flow in the ground beneath the transmitter wire. The recorded decay of the magnetic field produced by the ground currents contains information about the electrical conductivity of the ground. Electrical conductivity of the ground is influenced both by sediment type (clayey sediments are more conductive than sandy sediments) and by water quality (saline water is more conductive than fresh water). Areas within the survey area that have the best potential for good water resource quality will have low electrical conductivity (fresh water in sandy or gravelly sediments), whereas areas with poor water-resource potential will have high conductivity (saline water or clayey sediments).

Dense spatial data obtained by mounting the geophysical instruments in an aircraft and flying at low altitude on a tight grid over the survey area should allow subsurface changes in water quality and sediment type to be interpreted. The airborne geophysical data were verified by (1) acquiring ground-based TDEM data at representative locations and comparing ground and airborne results, (2) comparing available water well data to conductivity patterns evident in the

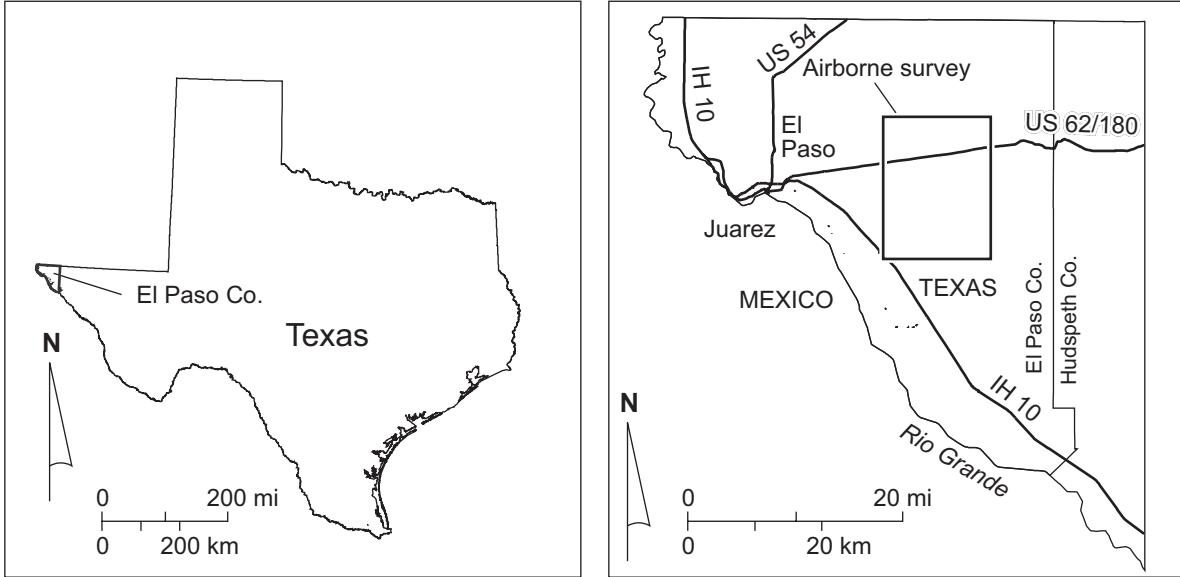


Figure 1. Location of the airborne survey area in eastern El Paso County, Texas.

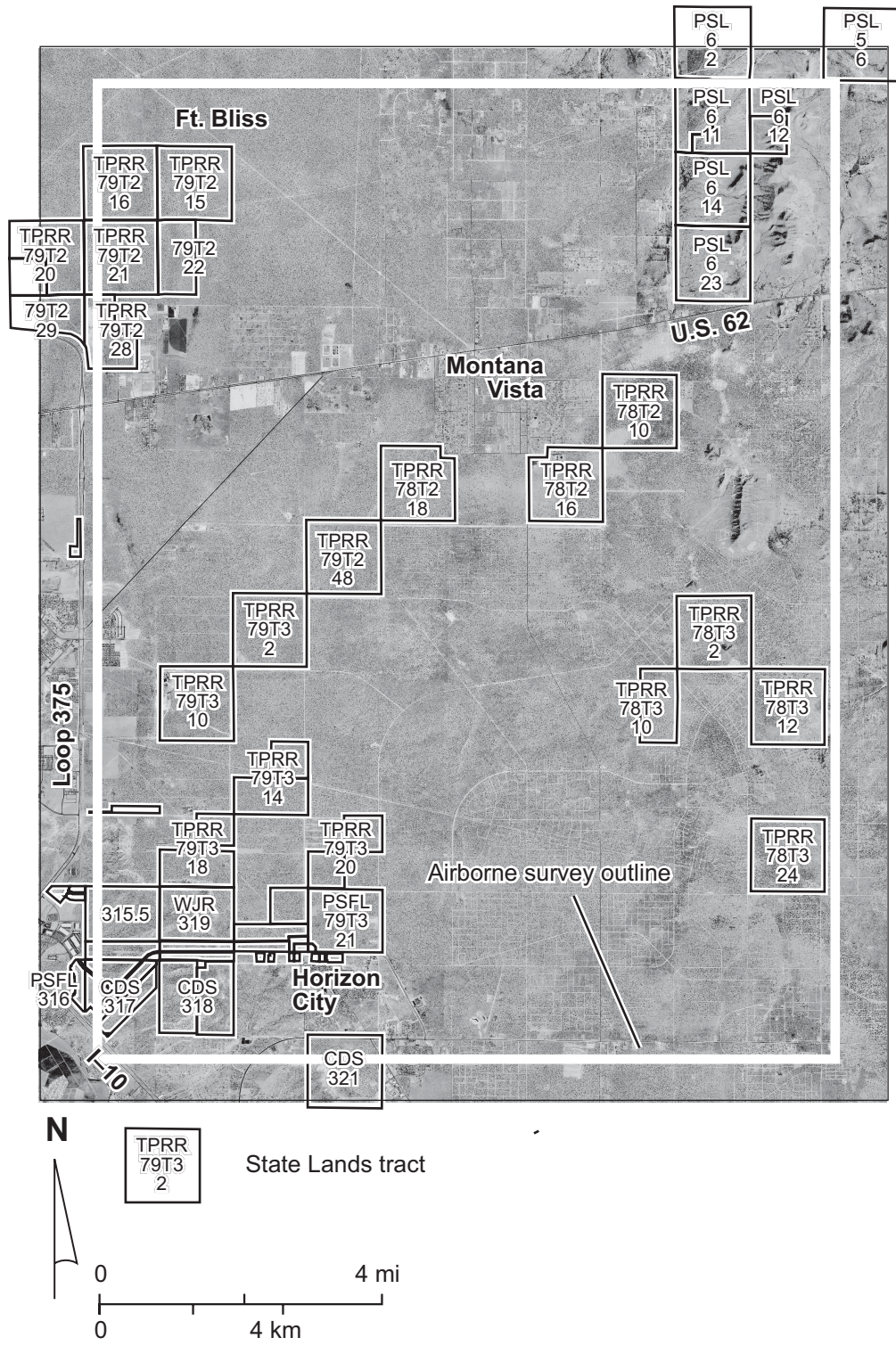


Figure 2. Aerial photographic map of the airborne survey area in eastern El Paso County. Also shown are State-owned tracts including survey, block, and section number for major parcels. Aerial photograph modified from originals provided by the Texas Natural Resources Information System.

airborne data set, and (3) incorporating existing geological and hydrological information into the interpretation of the airborne geophysical data.

Geologic Setting

The Hueco Bolson, El Paso region of west Texas is a desert basin surrounded by fault-bound mountains and the Diablo Plateau. This area is located where the well-defined southern Rio Grande rift merges with the southern Basin and Range province. Rocks, unconsolidated to slightly friable sediments, and the landscape of the Hueco Bolson record a long history of Precambrian (more than 570 million years ago [mya]) to recent geologic events (Henry and Price, 1985; Muehlberger and Dickerson, 1989). The geologic framework for the water resources of the Hueco Bolson have been mostly influenced by tectonic and depositional events that began during the middle Cenozoic, about 24 to 30 mya, when the regional stress regime became extensional and normal faulting uplifted the fault-bound mountain ranges relative to the down-dropped Hueco Bolson. Fault-bounded sub-basins have formed within the Hueco Bolson, and faulting and coincident subsidence and infilling have occurred episodically (Collins and Raney, 1991). Cenozoic basin-fill sediments in outcrops within the Hueco Bolson date back to the Pliocene (Albritton and Smith, 1965; Strain, 1966, 1971; Vanderhill, 1986), but in some parts of the basin they extend to depths of more than 2.5 km, where their age is unknown. The basin-fill sediments reflect the development of the Rio Grande, which forms the border between Texas and Mexico, and the ancestral drainage systems that preceded the modern Rio Grande (Albritton and Smith, 1965; Strain, 1966, 1971; Hawley and others, 1969; Stuart and Willingham, 1980; Mack and Seager, 1990; Gustavson, 1991). The ancestral Rio Grande system drained into Lake Cabeza de Vaca, which encompassed much of the Hueco Bolson. Breaching of the Hueco Bolson by about 2.2 mya resulted in a through-flowing ancestral river system across the basin. Basin-fill deposition associated with the ancestral river system continued into the early Pleistocene to about 0.78 mya (Mack and others, 1998). Since the early Pleistocene, periods of downcutting, backfilling deposition, and stability have been recorded in the series of modern Rio Grande and large arroyo

terraces, alluvial-fan and piedmont deposits, and soils that are well exposed locally in the basin. Even though the Hueco Bolson does not currently exhibit internal drainage, the term bolson is commonly used in the formal name of the area because this intermontane basin contains deposits that were deposited in a bolson setting (Strain, 1966, 1971).

The study area lies within the eastern side of the Hueco Bolson, west of the Hueco Mountains and its foothills and east of the Franklin Mountains. Between the Franklin and Hueco Mountains the fault-bound basin has an asymmetric geometry with the western side containing thicker basin-fill deposits than the eastern side (Mattick, 1967; Ramberg and others, 1978; Seager, 1980; Collins and Raney, 1991, 2000). Cliett (1969) reported the best water-bearing sediments to be thick gravel and sand deposits of the Camp Rice Formation's fluvial channel facies that occurs west of the study area along the east side of the Franklin Mountains. Although basin-fill deposits are as thick as 1.5 to 2.5 km across the basin, relatively fresh water within the study area is mostly encountered within the most recent deposits at shallower depths of 100 to 150 m.

At the study area the basin-floor contains mostly wind-blown sand deposits that overlie Pliocene-middle Pleistocene Camp Rice sand and gravel and lesser amounts of silt and clay (fig. 3). Regionally, Camp Rice deposits represent a system of dominantly fluvial and alluvial-fan deposition, along with some floodplain and minor lacustrine deposition (Albritton and Smith, 1965; Strain, 1966; 1971; Stuart and Willingham, 1980; Gustavson, 1991). It's likely that the main fluvial axis during Camp Rice deposition was west to south of the study area and that basin-fill sediments in the study area were laid down in dominantly alluvial-fan and floodplain settings. Beneath Camp Rice deposits are Fort Hancock lacustrine clay and silt and lesser amounts of alluvial-fan and fluvial gravel, sand, silt, and clay. North-striking normal faults cut the basin-fill deposits and are expressed at the surface as subtle sand-covered scarps. These faults may have partly controlled the basin's surface drainage and sedimentation, although precise geometries of coarser basin-fill intervals are difficult to determine with the currently available lithologic data from drillers' logs.

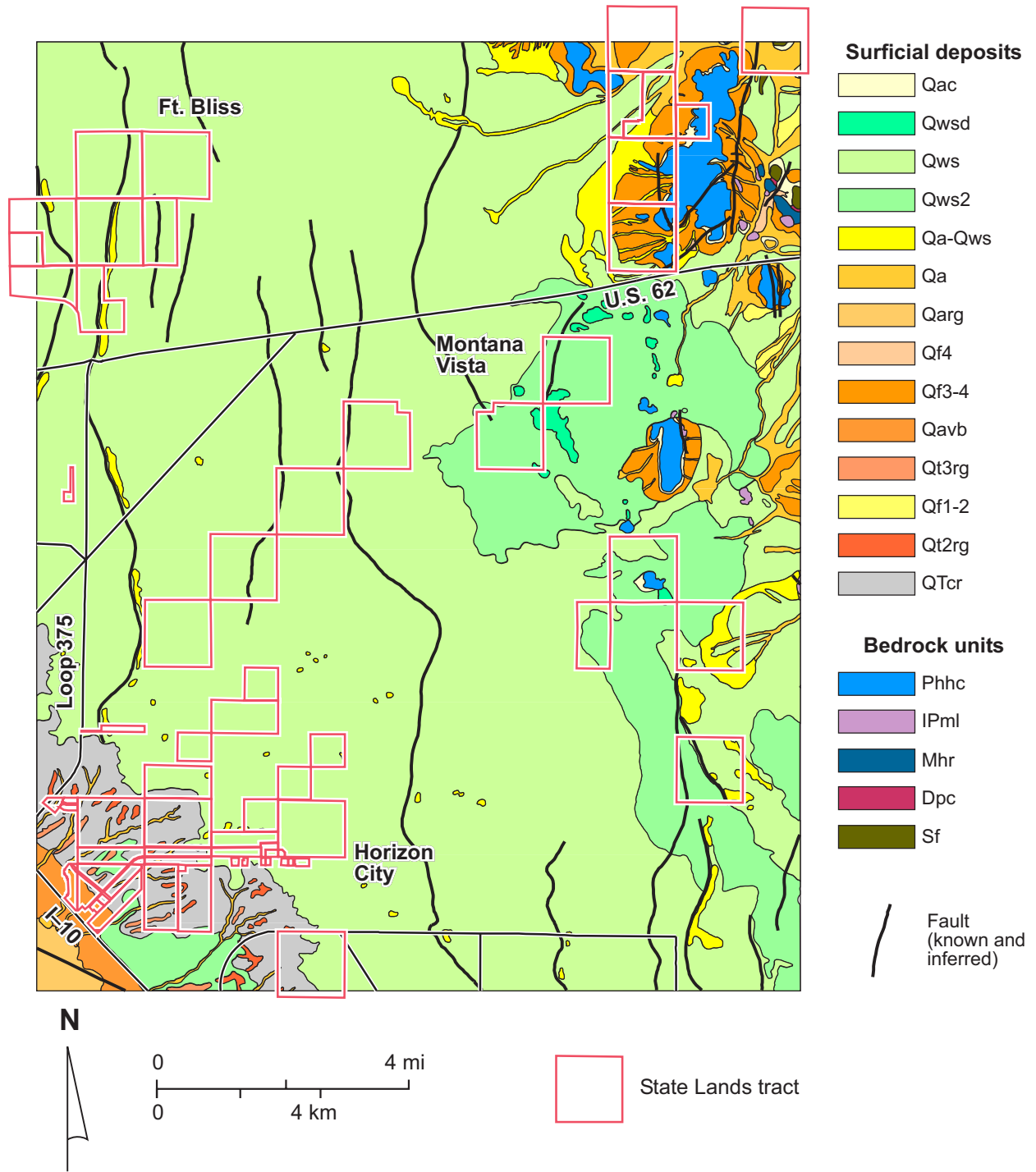


Figure 3. Geologic map of the survey area. Adapted from Collins and Raney (2000).

Groundwater Depth

To ensure that the exploration depth of the airborne and ground-based geophysical instruments is sufficient to reveal information about groundwater resources, we examined water depths reported from available wells in the survey area. Data from 59 eastern El Paso County water wells indicate that water levels correlate strongly with surface elevation (fig. 4): as elevation increases, depth to water also increases. To provide information on groundwater resources in an unconfined aquifer, the instruments must explore deeper than the depth to water. Gates and others (1980) consider the Hueco Bolson aquifer to be under water-table conditions in this area.

Because water depths vary with surface elevation, we superimposed water-level depths on a detailed topographic map constructed from altimeter and GPS data acquired by the survey aircraft (fig. 5). Over most of the study area, depths are generally between 90 and 130 m. Shallower depths below 30 m are found in the southwest corner of the study area where surface elevation falls toward the Rio Grande. An isolated water depth of 32 m in the southeast corner of the study area among nearby deeper depths may be attributed to a shallow and local water saturated zone above the main Hueco Bolson aquifer. The most recent water-level data from 94 survey-area wells show that water depths range from less than 4 m nearest the Rio Grande to as much as 130 m. The average water depth is about 102 m.

Surface elevation within the survey area, measured using instruments on the survey aircraft, ranges from 1133 to 1453 m. Most wells are located on the low-relief floor of the bolson, where elevations average about 1220 m. Water-level elevations, obtained by subtracting water depths from surface elevation, average 1120 m. Water levels generally fall within a narrow elevation range between 1112 and 1126 m for wells across the basin floor (fig. 6). Higher surface elevations are associated with higher water-level elevations.

There are 50 wells within the survey area for which well casing information has been reported (fig. 7). Slotted casings are generally installed by drillers within depth zones that may contribute water to be pumped from the well. Slotted casing depths can serve as a guide for

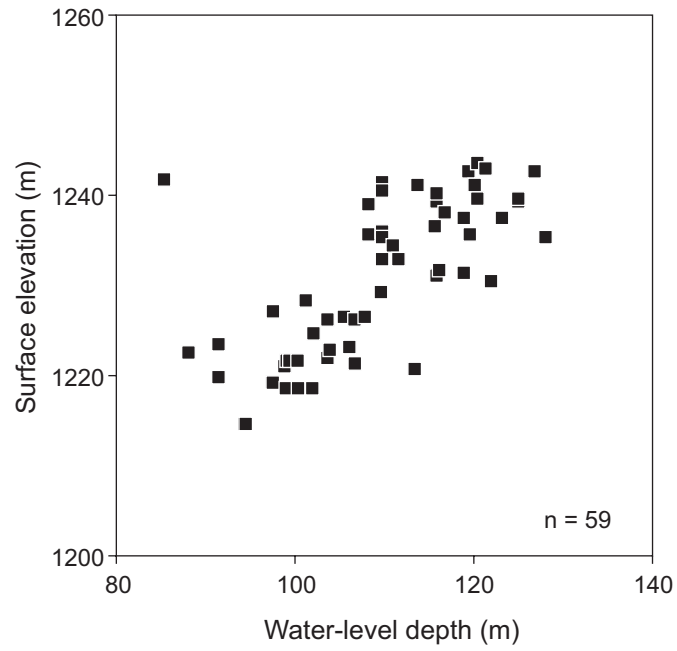


Figure 4. Relationship between land-surface elevation and depth to water in water wells in eastern El Paso County. Water-level data from the Texas Water Development Board (TWDB).

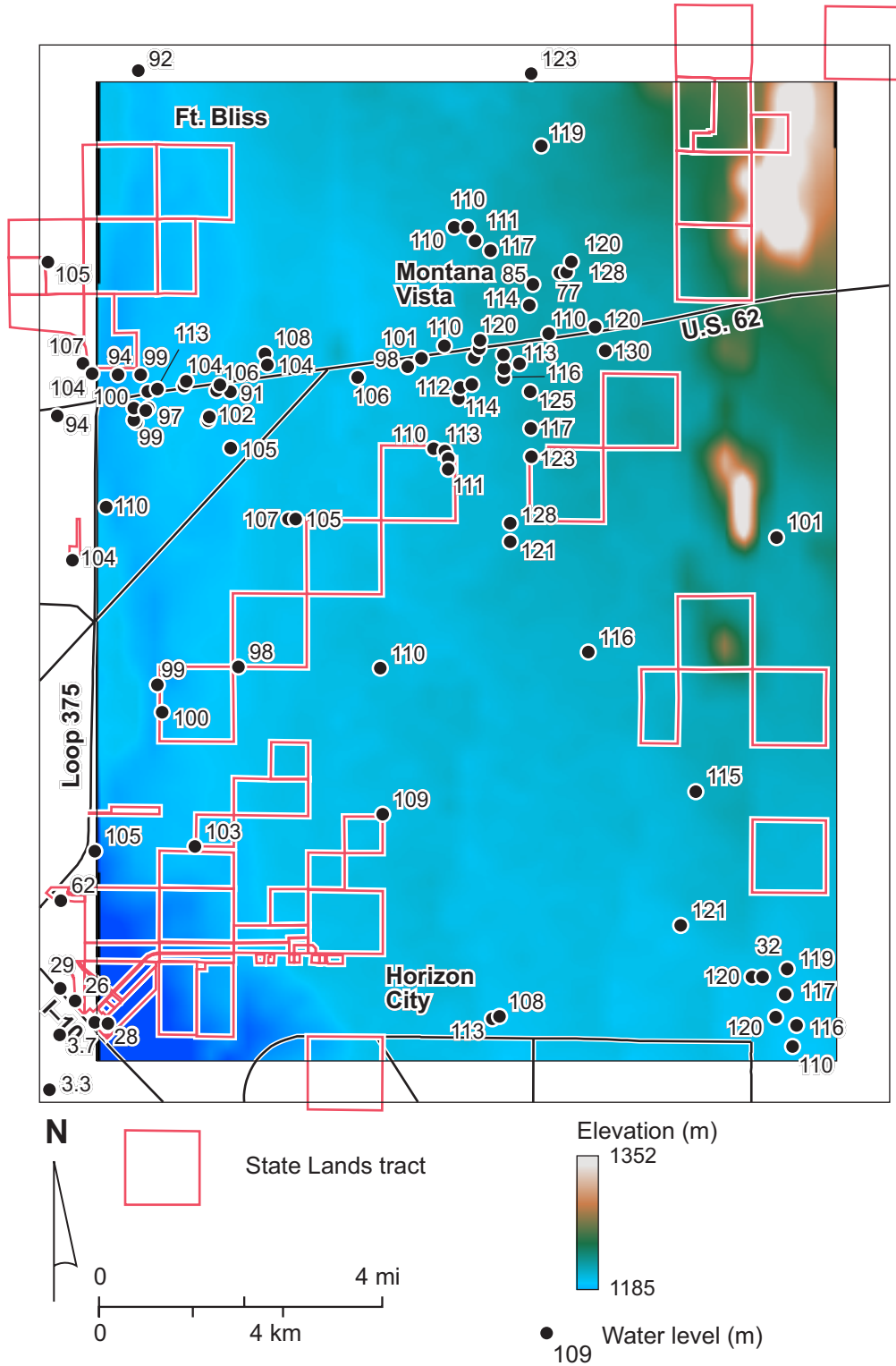


Figure 5. Depth to water superimposed on map of land-surface elevation. Elevation data from airborne geophysical survey. Water-level data from the TWDB.

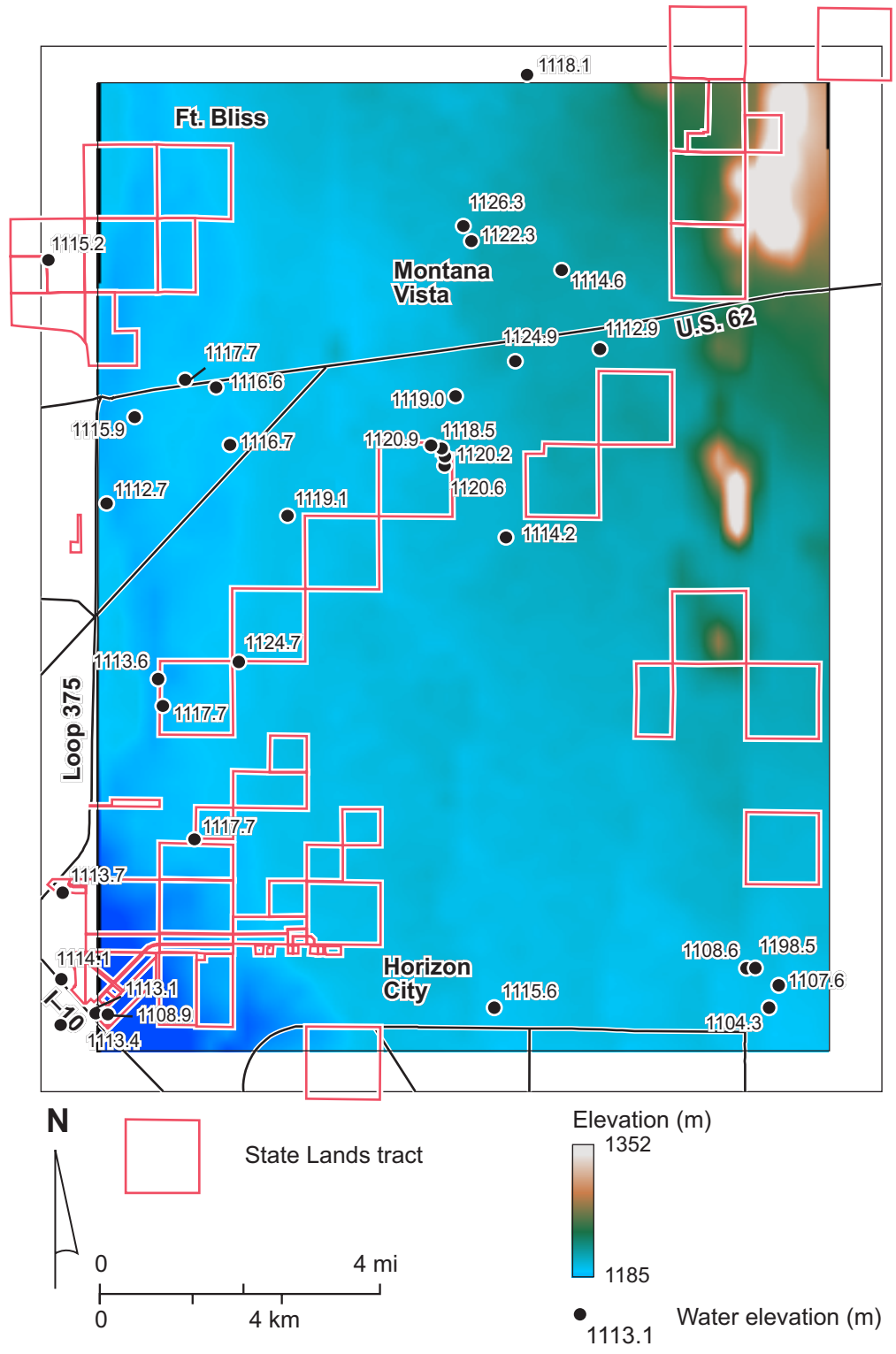


Figure 6. Water-level elevation superimposed on map of land-surface elevation. Elevations calculated from surface elevations and water depths measured since 1993. Water-level data from the TWDB.

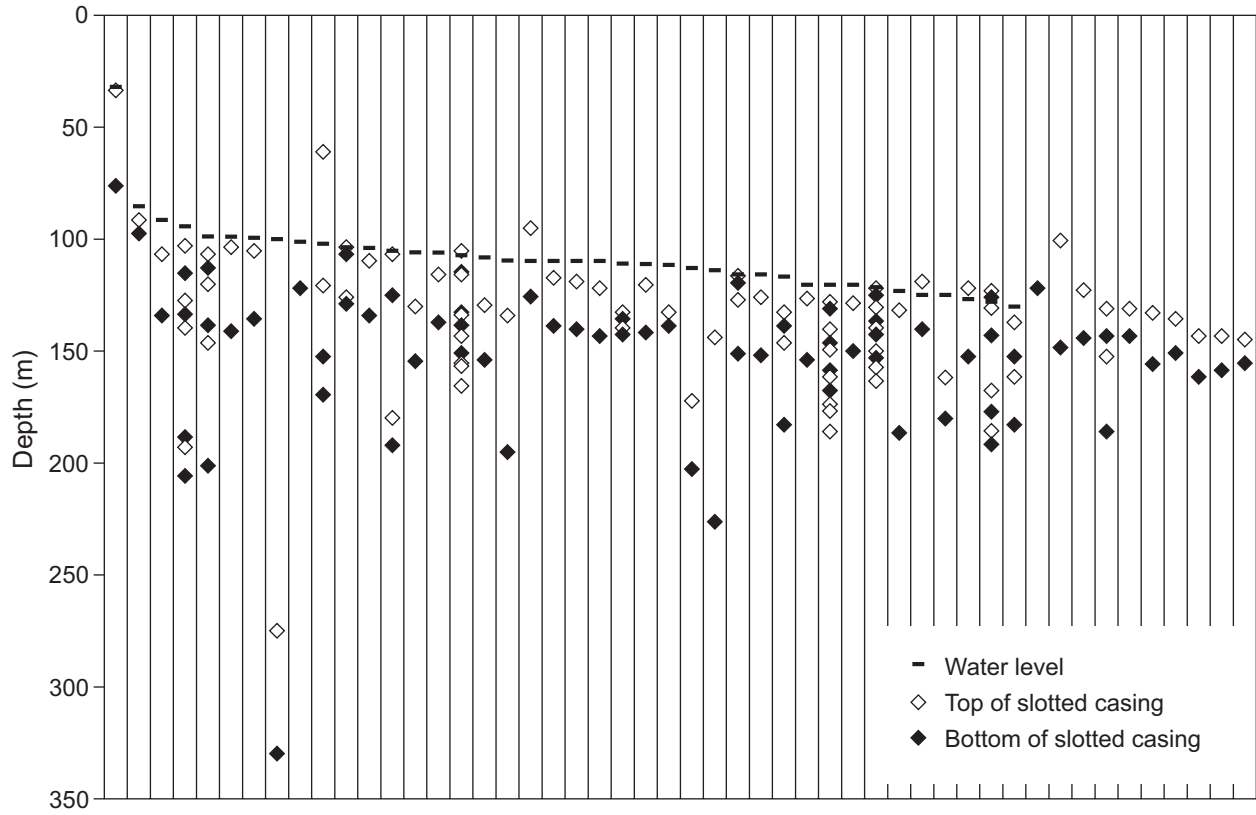


Figure 7. Water levels and depths to the top and bottom of slotted casing in 50 water wells within the survey area. Well data from the TWDB.

determining the proper depths to examine within the airborne geophysical data. Depths to the top of the uppermost slotted casing in these wells range widely from 34 to 275 m. The average depth is 124 m, somewhat deeper than the average water level of 109 m reported for these wells. The deepest reported bottom of slotted well casing is 330 m.

Groundwater Quality

Water quality can be classified according to the concentration of dissolved minerals in the water (TDS, or total dissolved solids, table 1). Water-quality data, including TDS values and electrical conductivity, are available for 135 samples from wells in and near the study area (fig. 8). These data show that most groundwater samples from wells in eastern El Paso County are classified as fresh to slightly saline. As the TDS concentration in a water sample increases, so does its ability to conduct electricity. Because most of the sediments filling the Hueco Bolson have naturally low conductivities (generally less than 100 millisiemens per meter [mS/m]), and because the conductivity of most water samples is higher than 100 mS/m, geophysical measurements of the conductivity of the ground will be strongly influenced by water quality. Areas of relatively low conductivity will represent the best potential groundwater resources.

The most recent measurements of TDS concentration in samples from 91 wells vary considerably across the survey area (fig. 9). These data can be used to establish how well conductivity measurements made using airborne instruments correlate with water quality. TDS values reported for the area range from 213 to 8,079 mg/L, averaging 1,159 mg/L. In the north-central part of the study area, TDS concentrations vary from values as low as 255 mg/L in one well to 1,593 mg/L in another well less than 1 km away. Samples from multiple depths in some wells show increasing TDS concentrations with depth.

Of the 91 wells with reported TDS values, about half (46) are classified as fresh (fig. 10). These low-TDS samples come from wells in the north-central part of the study area near Montana Vista, in the southeast corner of the study area and near Horizon City, and in two wells just

Table 1. Salinity classifications based on TDS concentration. The Robinove and others (1958) classification is used in this report because it has more subdivisions within the 0 to 4,000 mg/L TDS range that encompasses most El Paso County groundwater samples.

From Robinove and others (1958):

Classification	TDS range (mg/L)
Fresh	0 - 1,000
Slightly saline	1,000 - 3,000
Moderately saline	3,000 - 10,000
Very saline	10,000 - 35,000
Briny	35,000

From Freeze and Cherry (1979):

Classification	TDS range (mg/L)
Fresh	0 - 1,000
Brackish	1,000 - 10,000
Saline	10,000 - 100,000
Brine	100,000

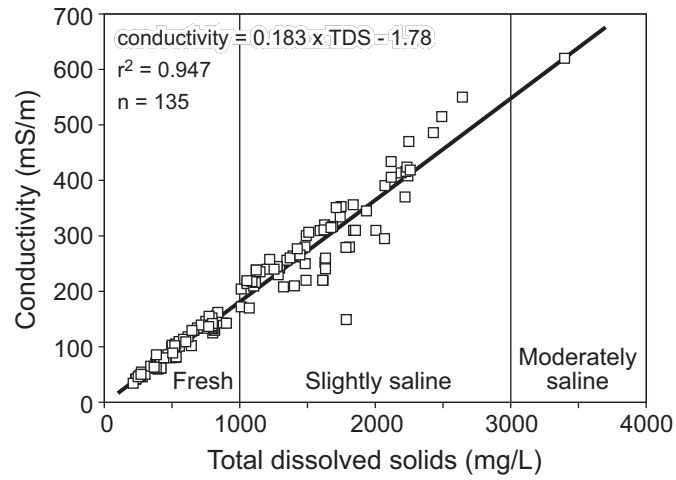


Figure 8. Relationship between TDS concentration and measured electrical conductivity in groundwater samples from eastern El Paso County. Water quality data from the TWDB. Salinity classification from Robinove and others (1958).

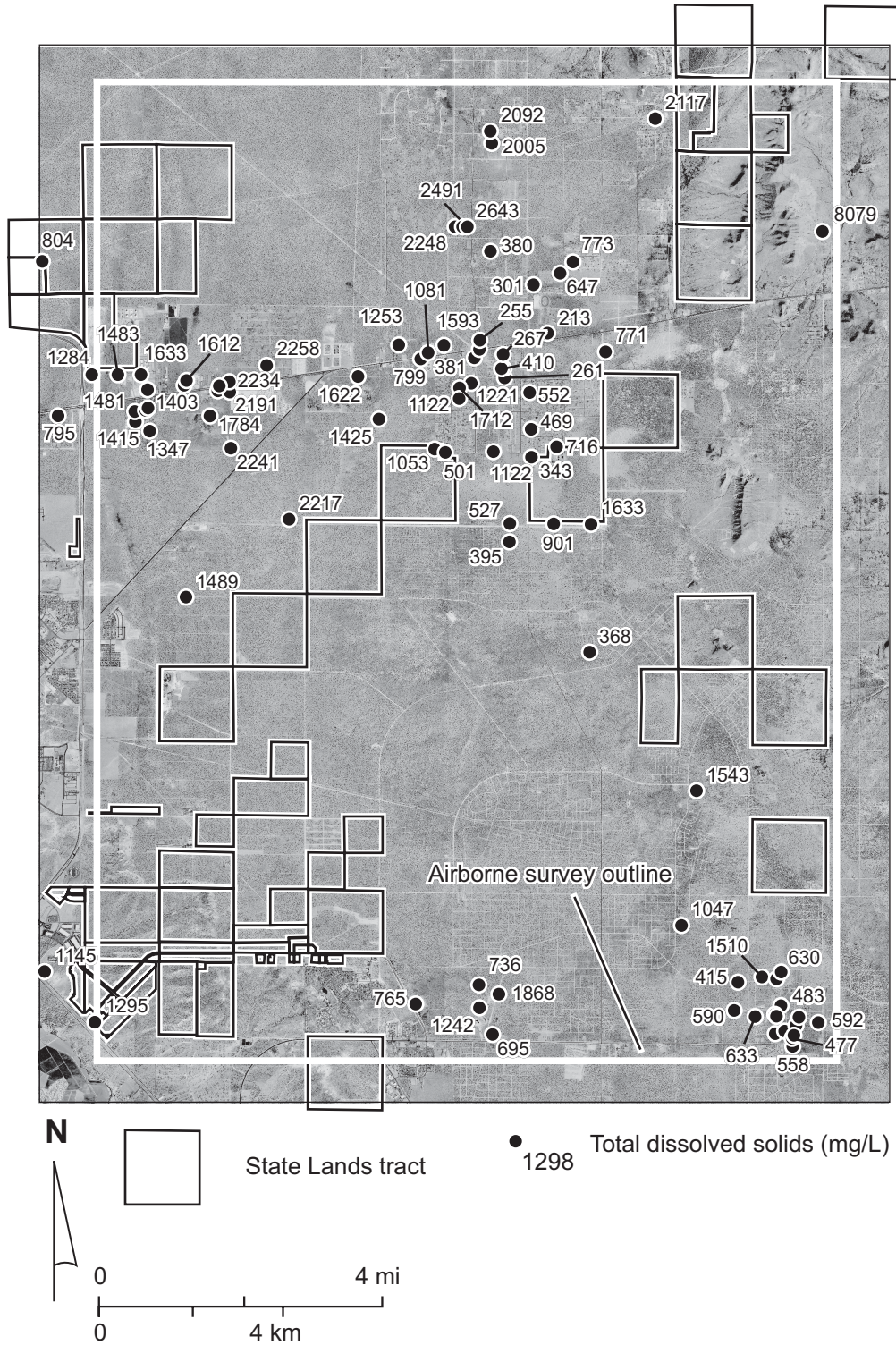


Figure 9. Total dissolved solids (TDS) concentration in samples from water wells in the survey area. Water quality data from the TWDB.

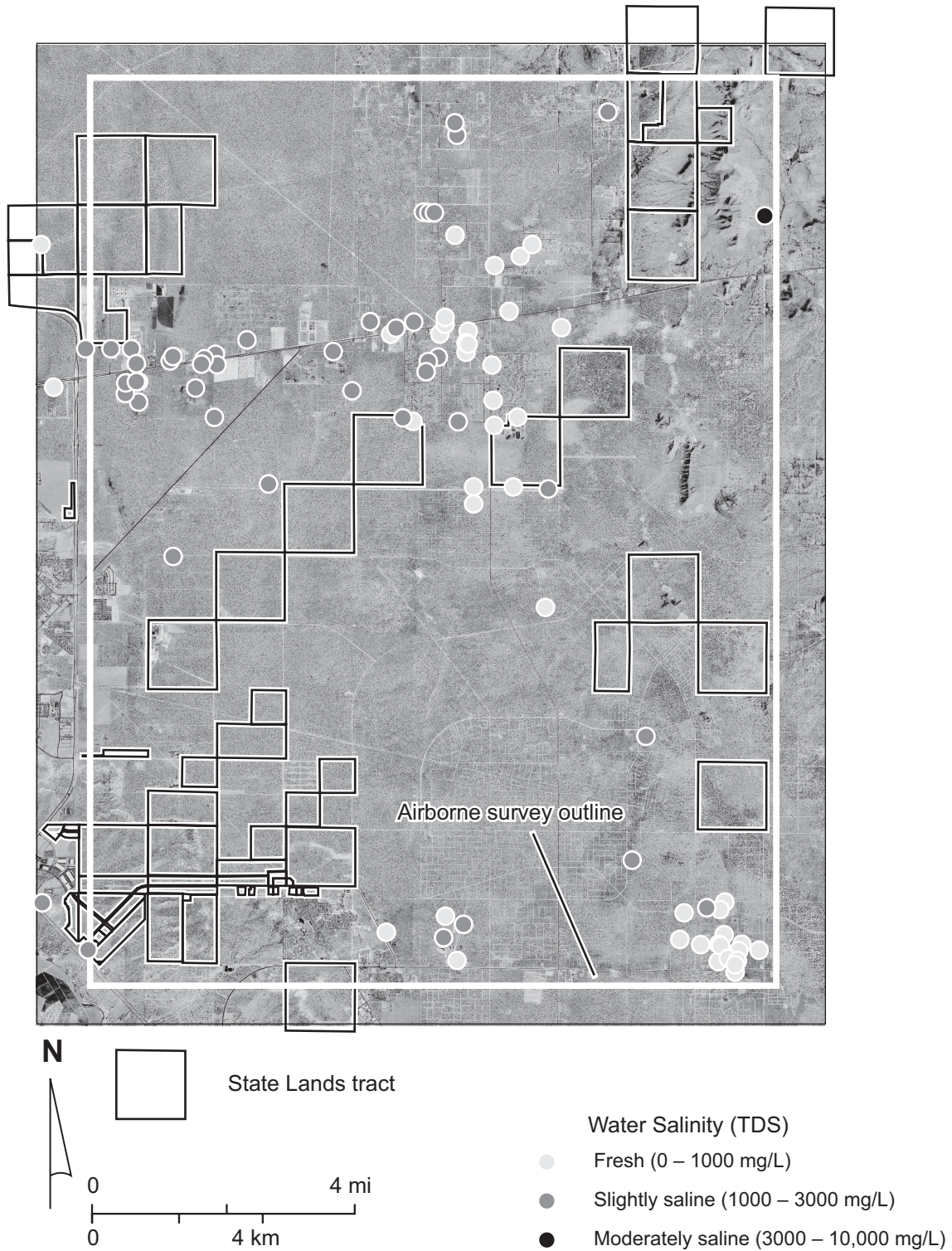


Figure 10. Distribution of fresh, slightly saline, and moderately saline water from survey-area wells. Data from the TWDB.

west of the area surveyed. Nearly half the samples (44) are classified as slightly saline. These values are common north and west of Montana Vista, in the southwest corner of the survey area, and scattered among fresher wells in and east of Horizon City in the southern part of the survey area. Moderately saline water is reported at only one well in the bedrock outcrop area in the northeastern corner of the survey area.

Common dissolved constituents (table 2) in the fresh to moderately saline groundwater that help carry electrical current include the cations (positively charged ions) sodium (average concentration 340 mg/L) and calcium (61 mg/L average) and the anions (negatively charged ions) chloride (concentration 352 mg/L average), sulfate (313 mg/L average), and bicarbonate (127 mg/L average).

Specific capacities are available for 23 wells within the survey area (fig. 11). Reported values are low, ranging from 0.8 to 3.6 gal/min/ft in the southern and central areas. Higher values of 2.6 to 36 gal/min/ft are found along U.S. 62 near the western survey boundary and 10.1 gal/min/ft in the southwest corner of the survey. Higher rates suggest the ability of wells in these areas to produce water at greater rates and smaller amounts of water-level decline.

METHODS

We employed airborne and ground-based geophysical methods to rapidly and noninvasively explore for groundwater in the El Paso area by measuring changes in electrical conductivity with depth. The principal geophysical method in the airborne and ground surveys is electromagnetic induction, or EM (Parasnis, 1973; Frischknecht and others, 1991; West and Macnae, 1991). This family of geophysical methods employs a changing primary magnetic field that is created around a current-carrying transmitter wire to induce a current to flow within the ground, which in turn creates a secondary magnetic field that is sensed by a receiver coil. In general, the strength of the secondary field is proportional to the conductivity of the ground.

Table 2. Water-quality statistics for samples from survey-area water wells in eastern El Paso County. Data from the TWDB.

Parameter	Units	Analyses	Average	Maximum	Minimum
Silica	mg/L	42	23.4	41	0
Calcium	mg/L	90	60.7	364	3
Magnesium	mg/L	92	15.2	114	0.71
Sodium	mg/L	86	339.7	2645	22.6
Potassium	mg/L	18	8.71	18	1.62
Strontium	mg/L	2	0.42	0.66	0.17
Carbonate	mg/L	91	1.05	10.8	0
Bicarbonate	mg/L	89	129	378	25.6
Sulfate	mg/L	93	313	1054	25
Chloride	mg/L	94	352	4050	20
Fluoride	mg/L	82	0.97	6.1	0
Nitrate	mg/L	74	9.27	48.7	0
pH		93	7.96	9.2	6.6
TDS	mg/L	91	1159	8079	213
Alkalinity	mg/L	90	107	310	34
Hardness	mg/L	90	207	1089	7
Specific conductivity	mS/m	72	218	550	34.5

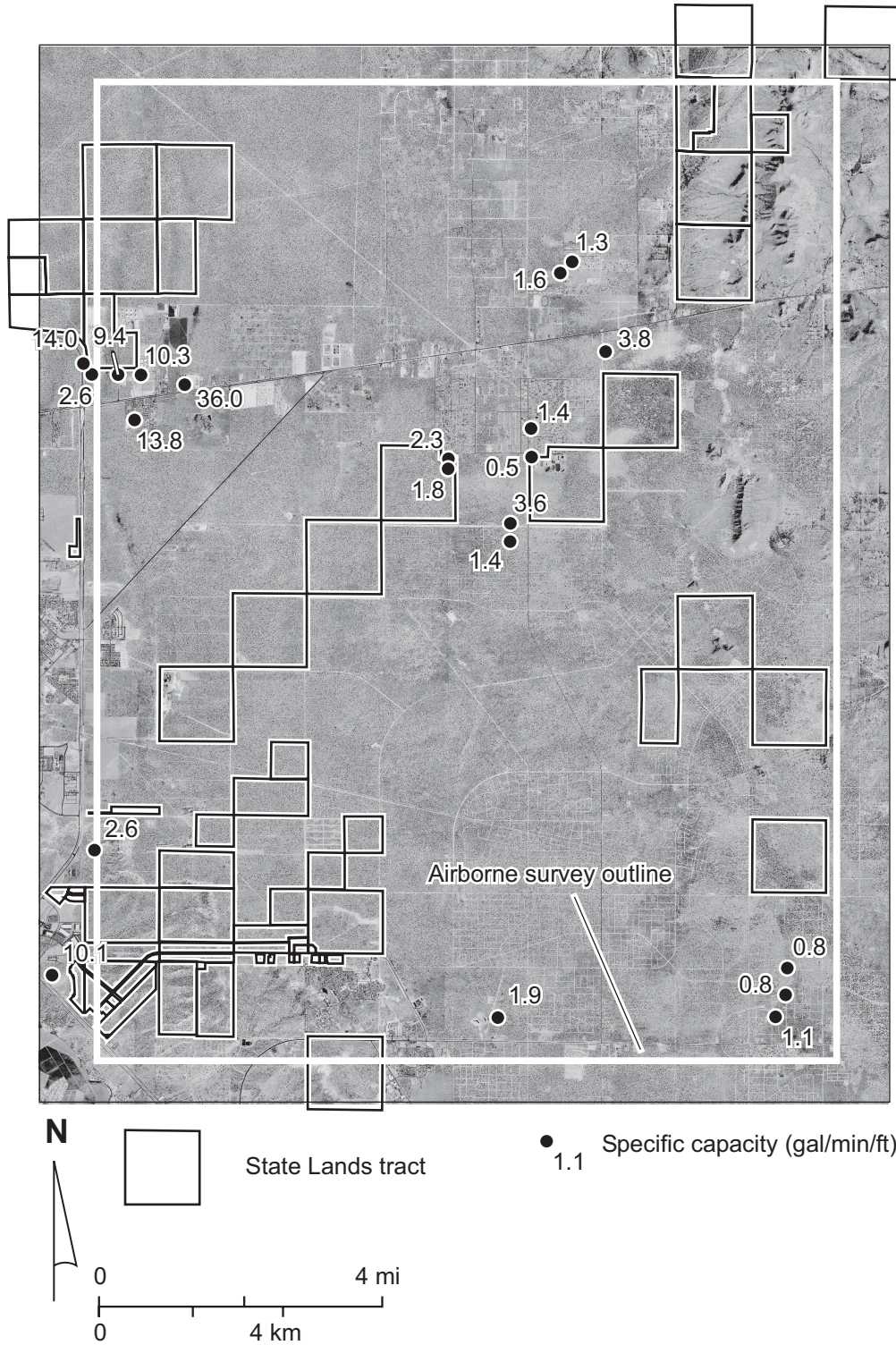


Figure 11. Specific capacity measured for selected water wells within the survey area. Data from the TWDB.

Time-domain EM methods (Kaufman and Keller, 1983; Spies and Frischknecht, 1991), used in both the airborne and ground-based surveys, measure the decay of a transient, secondary magnetic field produced by the termination of an alternating primary electric current in the transmitter loop (fig. 12). The secondary field, generated by current induced to flow in the ground, is measured by the receiving coil following transmitter current shutoff. Secondary field, or transient, strength at an early time gives information on conductivity in the shallow subsurface; transient strength at later times is influenced by conductivity at depth.

Ground Geophysics

Before the airborne geophysical data can be analyzed and interpreted, it is important to verify that the data are reasonably accurate. In other words, do the conductivity models derived from the airborne geophysical data accurately portray generalized conductivity variations in the subsurface? At the most rigorous level, borehole geophysical logs can be compared with vertical conductivity profiles constructed from the airborne data. This comparison is commonly futile because TDEM systems have far less vertical resolution than can be obtained using borehole logs, few wells are logged at the depths investigated in this study, and borehole logs may not be calibrated. The most that can be done to verify the airborne data is to compare those data with similar data acquired using ground-based instruments. At several representative sites in the El Paso area, we examined the transients measured using ground instruments and used those to verify the feasibility of the method and compared the conductivity models derived from both data sets to validate the airborne data.

Ground-based TDEM systems, such as the Geonics Protem 57 used in this study, operate on the same principle as the airborne systems (fig. 12). Compared with airborne systems, ground systems have fewer problems with EM noise and it is easier to keep the transmitter and receiver geometry constant, but data are more difficult to acquire. For example, an airborne system can acquire tens of thousands of measurements (soundings) per day, whereas a ground system might

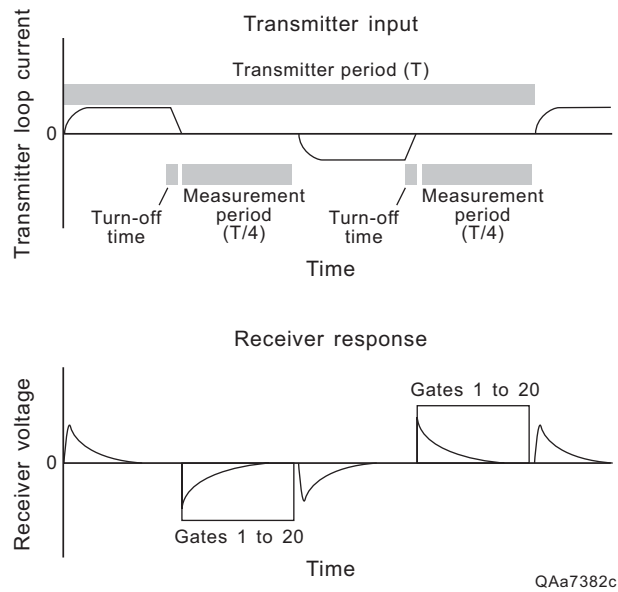


Figure 12. Time-domain EM transmitter input (upper graphic) and receiver response (lower graphic). Adapted from Geonics Limited (1992).

optimally acquire tens of soundings per day. Airborne systems make it possible to produce high-resolution images of subsurface conductivity over large areas that cannot be practically surveyed on the ground.

We acquired 9 TDEM soundings in eastern El Paso County in March 2001 (fig. 13, table 3). We selected the sites to represent the variety of environments present in the area. The location of each TDEM sounding was determined using a GPS receiver and was imported into the GIS to allow us to identify nearby soundings collected with the airborne systems. In the ground-based soundings, we used a large transmitter loop (100×100 m) and placed the receiver in the center of the transmitter loop (figs. 14, 15, and 16). The area of the transmitter loop was $10,000 \text{ m}^2$, and the effective area of the receiver coil was 100 m^2 . At typical transmitter current of about 8 amperes, the transmitter dipole moment is $80,000 \text{ A}\cdot\text{m}^2$. We operated the ground transmitters at 30, 7.5, and 3 Hz at each location. Current shutoff times were about 40 microseconds (μs). The resulting transients were measured at 20 time gates ranging from 0.0881 to 6.97 milliseconds (ms) after current shutoff at 30 Hz, 0.352 to 27.9 ms after shutoff at 7.5 Hz, and 0.881 to 70 ms after shutoff at 3 Hz (fig. 12). Lower transmitter frequencies (and later measuring times) allow the ground-based systems to explore deeper than airborne systems if the transient is strong enough.

Ground-based data were processed using TEMIX, a software package published by Interpex. Beginning with one-layer conductivity models, we increased the number of layers at each site until there was no significant decrease in the fitting error (the difference between the observed transient and the transient predicted from the model and the acquisition parameters) when an additional layer was added. Three- or four-layer models were sufficient to produce fitting errors ranging from 1.1 to 4.9 percent (table 3). Because more than one model can produce a similar transient, we used TEMIX to analyze models that produced equivalent fits to the observed data.

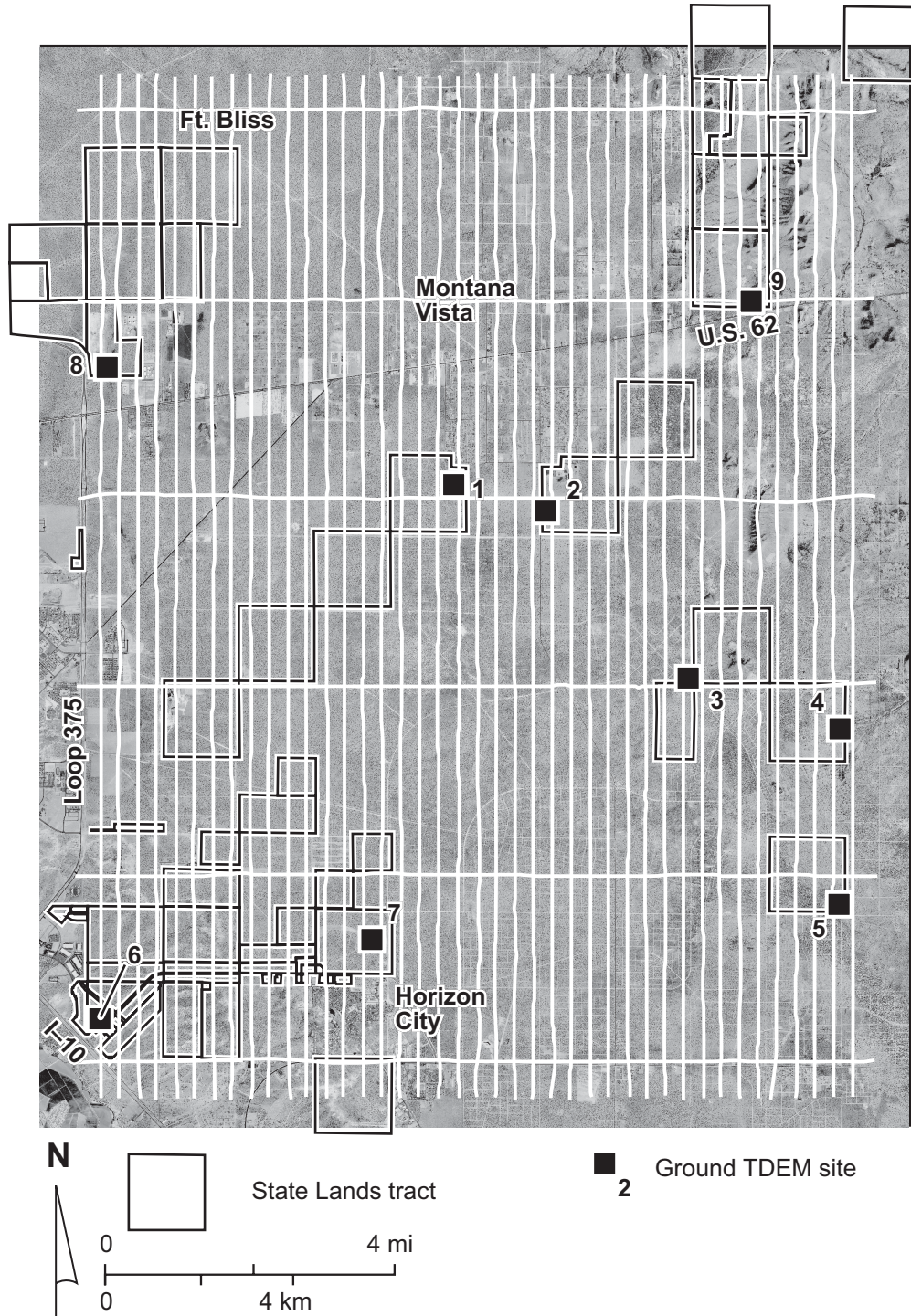


Figure 13. Survey area flight lines, State Lands tracts, and ground-based TDEM sites.

Table 3. Best-fit conductivity models for ground-based TDEM soundings in eastern El Paso County (fig. 13). Locations given in UTM metric coordinates, zone 13, using the 1983 North American Datum.

Sounding	Location (UTM-m)	Fitting error (%)	Layer	Conductivity (mS/m)	Thickness (m)	Depth to top (m)
1	387802.1 E 3518180.2 N	1.11	1	5.7	9.3	0
			2	25.6	105.3	9.3
			3	248.8	106.9	114.6
			4	389.1	—	221.5
2	389744.9 E 3517596.6 N	2.54	1	23.3	99.4	0
			2	295.9	110.8	99.4
			3	724.6	—	210.2
3	392782.8 E 3514041.4 N	3.62	1	7.1	32.3	0
			2	81.3	53.7	32.3
			3	227.3	132.1	86.0
			4	5.0	—	218.1
4	395998.7 E 3512950.6 N	2.88	1	21.6	65.7	0
			2	155.0	86.8	65.7
			3	662.3	20.3	152.5
			4	218.8	—	172.8
5	395992.5 E 3509226.1 N	4.15	1	21.7	57.5	0
			2	82.4	54.0	57.5
			3	183.5	—	111.5
6	380245.2 E 3506780.1 N	1.85	1	18.0	42.9	0
			2	117.1	110.9	42.9
			3	440.5	90.7	153.8
			4	885.0	—	244.5
7	386048.6 E 3508485.1 N	1.76	1	5.1	19.0	0
			2	36.7	79.4	19.0
			3	233.6	65.3	98.4
			4	411.5	—	163.7
8	380412.3 E 3520653.8 N	2.75	1	26.4	21.7	0
			2	124.4	9.1	21.7
			3	43.3	135.3	30.8
			4	186.9	—	166.1
9	394126.1 E 3522063.5 N	4.94	1	16.5	18.0	0
			2	43.1	118.2	18.0
			3	18.5	—	136.2

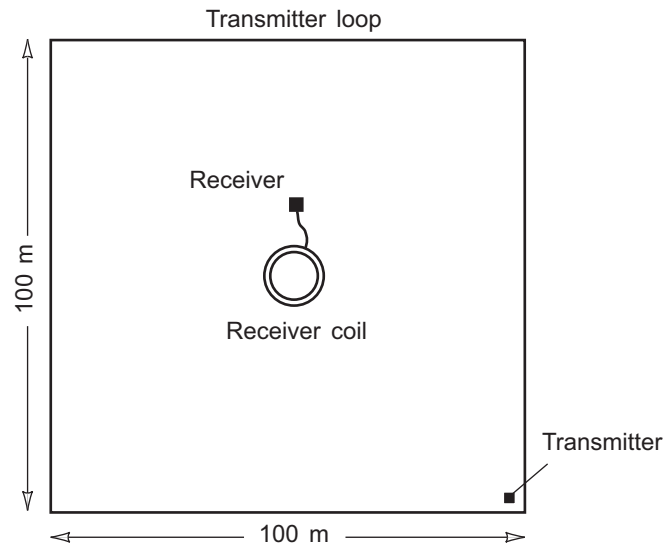


Figure 14. Central loop instrument configuration for ground-based TDEM soundings in eastern El Paso County.



Figure 15. Ground-based transmitter operating at site TDEM-2 (fig. 13).

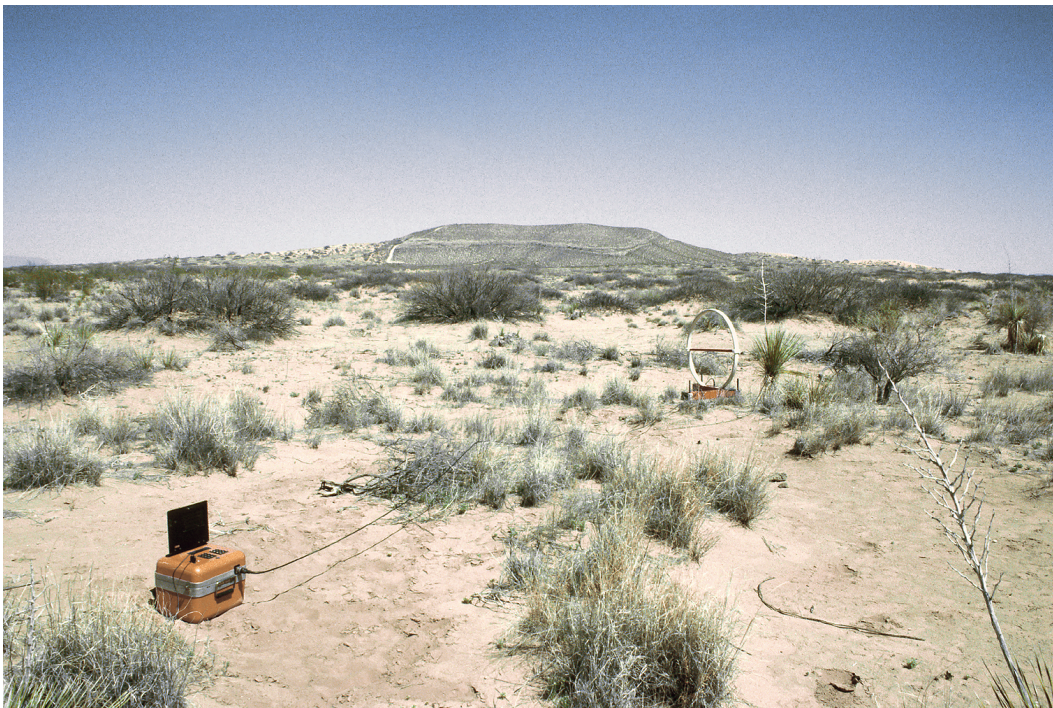


Figure 16. Ground-based receiver at site TDEM-2 (fig. 13). Loop is set to measure the horizontal component of the TDEM signal.

Airborne Geophysics

Airborne geophysical data, including time-domain EM (TDEM) and magnetic-field data, were acquired over eastern El Paso County in August 2001 by Fugro Airborne Surveys (table 4). The 372-km² (144-mi²) area was covered by flying north-south lines spaced at 400 m and east-west tie lines spaced at 4 km. Fugro collected EM and magnetic-field data using its Megatem II TDEM system and a cesium magnetometer towed behind a DeHavilland Dash 7 four-engine aircraft (figs. 17 and 18). Flight height was 120 m; the three-axis EM receiver was towed 131 m behind the transmitter at a height of 75 m above the ground (table 5). The primary EM field was generated by a four-turn wire loop fixed to the aircraft carrying a 30-Hz, discontinuous sinusoidal current of 1,330 amperes (A). The dipole moment, a measure of transmitter strength, was 2.1×10^6 A-m², more than an order of magnitude larger than the moment calculated for the ground-based system. Transients were recorded during the 11.6-ms window following termination of the 4-ms transmitter pulse. EM diffusion depth, the depth below which currents will not have diffused during the measurement period, is commonly used as a proxy for exploration depth. It is calculated using the equation

$$d = k (t \rho)^{0.5}$$

where d = diffusion depth (in m), $k = 503.3$ (m/ohm-s)^{0.5}, t = latest time measured, and ρ = resistivity (in ohm-m) (Parasnis, 1986).

Assuming a ground conductivity range of 20 to 80 mS/m (50 to 13 ohm-m resistivity) estimated from ground-based TDEM data and a latest measurement time of 11.6 ms, expected exploration depth for the El Paso area is about 190 m for the most conductive ground and about 380 m for the least conductive ground (fig. 19). Measurement locations were determined from global-positioning-system (GPS) data by using a base station south of the El Paso airport and a roving receiver on the aircraft. Locational accuracy is 10 m or better. At the 30-Hz transmitter frequency (60-Hz sample frequency) and a nominal airspeed of 250 km/hr, transients were acquired every 1.2 m along the flight line. Recording stacked transients at 4 Hz resulted in a

Table 4. Survey and flight parameters for the El Paso County airborne survey acquired by Fugro Airborne Surveys.

Acquisition date	August 21 to 24, 2001
Aircraft	DeHavilland DHCC-7EM (Dash 7)
Principal line spacing	400 m
Tie line spacing	4,000 m
Principal line, length and direction	21.9 km, 0 and 180 degrees
Tie line, length and direction	17.0 km, 90 and 270 degrees
Aircraft and transmitter height	120 m
Location	Differential GPS
Flight speed	70 m/s (252 km/hr)
Distance flown	953.5 km
Samples	64,773
Area surveyed	372 km ²



Figure 17. Fugro Airborne Surveys' Megatem II airborne TDEM system in El Paso, Texas, August 22, 2001. The transmitter loop is attached to the wing tips and booms at the front and rear of the aircraft. Cables trailing the aircraft tow the EM receiver and magnetometer (not shown). Photograph by David M. Stephens.



Figure 18. Megatem II system acquiring data over the northern part of the survey area, August 23, 2001.

Table 5. Acquisition parameters for the El Paso County airborne TDEM survey.

System	Megatem II
Transmitter loop area	406 m ²
Transmitter loop turns	4
Transmitter loop current	1331 A
Transmitter dipole moment.....	2,111,000 A-m ²
Transmitter frequency	30 Hz
Transmitter on time	3.85 ms
Receiver type	Towed 3 axis
Receiver height	64 m
Receiver trailing distance	131 m
Number of recording windows	20
Recording time (from end of pulse).....	-3.6 to 11.6 ms
Sample rate	4 Hz
Sample interval	~18 m

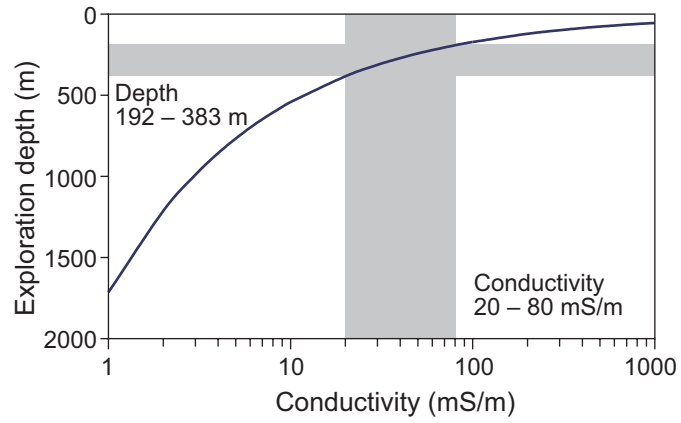


Figure 19. Estimated exploration depth of the Megatem II system assuming ground conductivities between 20 and 80 mS/m.

sample spacing of about 17 m. Fugro processed and delivered the data in December 2001 (Hefford, 2001).

Along with the transients measured in the x (parallel to the flight path), y (horizontal and perpendicular to the flight path), and z (vertical) axes by the towed receiver coils, Fugro performed conductivity-depth transforms to produce relatively smooth conductivity models depicting a conductivity value at 10-m-depth intervals. These transforms were performed for all 64,773 stacked transients.

We produced horizontal images of subsurface conductivity for each survey area by (1) extracting modeled conductivity values at 10-m-depth intervals; (2) gridding the values within the image processing software ERMapper using a cell size of 50 m; (3) rescaling the color bar to cover 99 percent of the data range (cutting off 0.5 percent of the values at the low and high “tails” of the data spectra), and (4) exporting the georeferenced images using the Universal Transverse Mercator (UTM) zone 13 north projection and the 1983 North American Datum.

Digital images were imported into a GIS database. Coverages used to analyze the relationship between the geophysical data and geological and hydrological characteristics of the region included water-well locations and depths, water-quality analyses, well casing types and depths, well production data, and roads (and associated power lines).

The aircraft also towed a cesium magnetometer at a height of 73 m above the ground (table 6) to measure changes in the magnetic field strength caused by natural effects and local features such as pipelines that contain significant amounts of iron. Magnetometer data were acquired at 10 Hz, yielding a 7-m sample spacing for magnetic field data.

GROUND GEOPHYSICAL SURVEY

We acquired nine TDEM soundings in a representative set of environments in eastern El Paso County (fig. 13 and table 3). The purpose of these soundings was to establish the electrical properties of the subsurface, estimate the achievable exploration depth of the airborne TDEM

Table 6. Acquisition parameters for the El Paso County airborne magnetometer survey.

Magnetometer	Towed cesium vapor
Magnetometer height	73 m
Sample rate	10 Hz
Sample interval	~7 m
Sensitivity	0.01 nT

system, examine whether the data were influenced by groundwater quality and depth, and serve as a basis for assessing the quality of the airborne geophysical data.

Raw TDEM data are recorded as voltages induced in the receiver divided by the area of the receiver (in nanovolts per square meter, or nV/m^2 , fig. 20). These voltages depend on the strength of the field generated by currents flowing in the ground and the field's rate of decay. Because the primary field generated by the transmitter propagates downward with time, receiver voltages recorded at early times after transmitter shutoff reflect the response to shallow conditions and the receiver voltages recorded at late times are more influenced by deeper conditions. The shape of the decay and the magnitude of the signal are used to construct a conductivity model that would produce a similar decay curve and thus represents an estimate of changes in conductivity with depth for the sounding. At site TDEM-1 (fig. 13), the receiver recorded signals from the ground from early times at about 0.1 ms to late times of about 30 ms (fig. 20). The signals decay very rapidly; the signal at 0.1 ms is about 5 orders of magnitude stronger than the signal at 20 ms. Below a signal strength of about $1 \text{ nV}/\text{m}^2$, ambient noise is stronger than the induced signal and represents the effective limit of exploration. Masked data points represent times when data were recorded but were too noisy to include in the analysis of the conductivity profile at the site.

In processing TDEM data, an assumption is made that the ground beneath the instrument is composed of layers in which conductivity changes downward but not laterally. We test this assumption by measuring signals in the vertical direction and two horizontal directions. If there are no lateral heterogeneities, the vertical signal will be much stronger than the horizontal signal and the horizontal signals will be approximately equal. At site TDEM-1, the lateral homogeneity assumption is valid; the vertical signal component (z) is about two orders of magnitude stronger than the horizontal components (x and y) at all times and the signal strengths for the horizontal components are approximately equal (fig. 21). If this assumption were not valid, the vertical component of the signal would be reduced or increased by the signal produced by the lateral heterogeneity and would lead to an erroneous vertical conductivity model for the site.

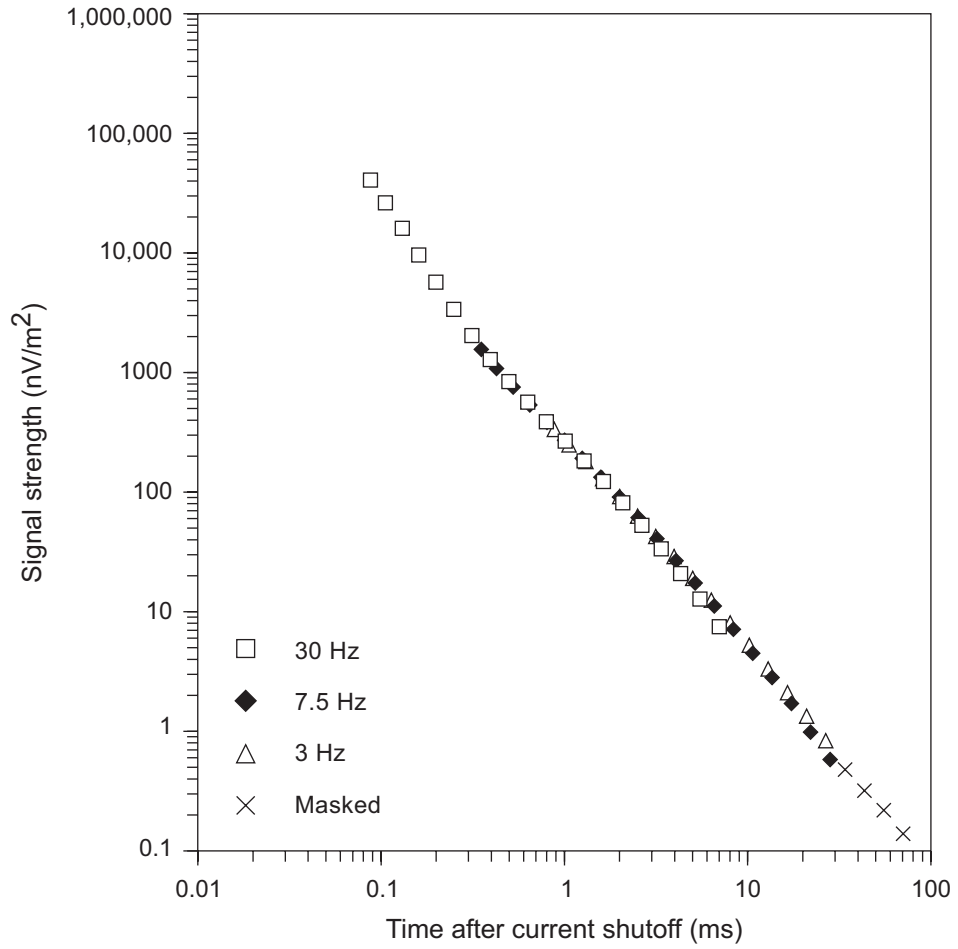


Figure 20. Decay of the ground TDEM signal following termination of the transmitter current at site TDEM-1. Data recorded at transmitter frequencies of 30, 7.5, and 3 Hz.

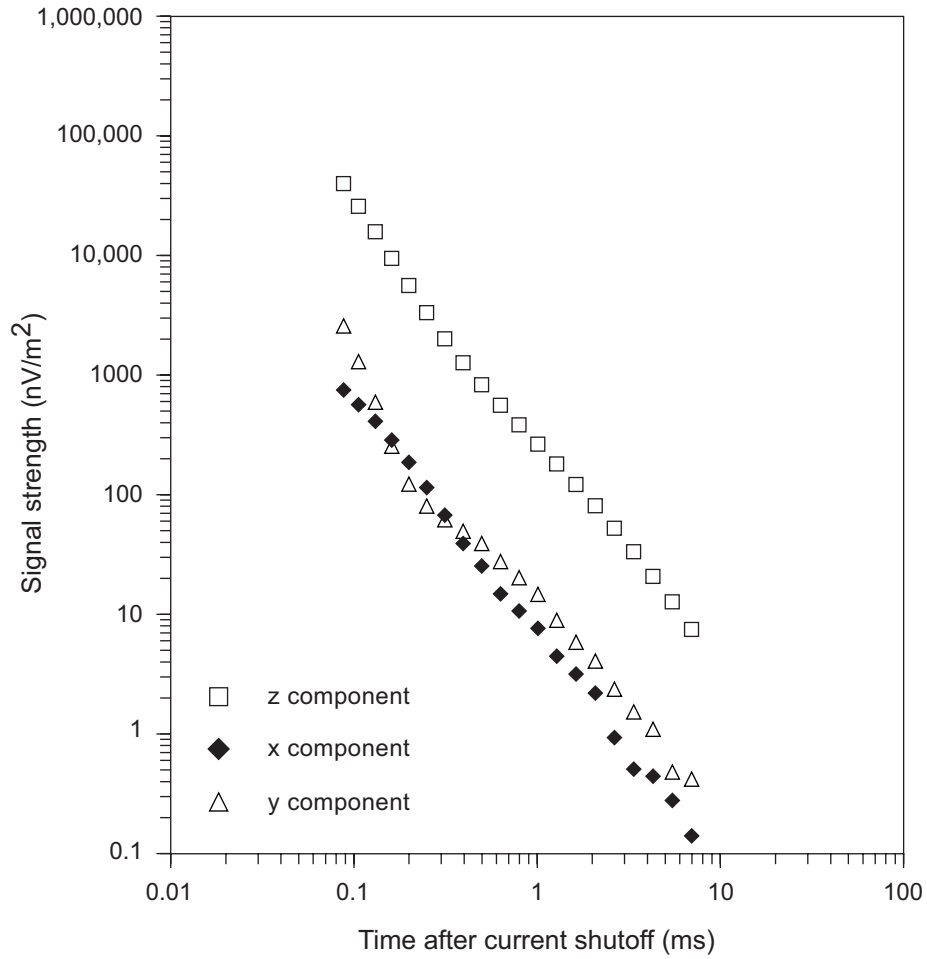


Figure 21. Vertical (z) and horizontal (x and y) components of the ground TDEM signal at site 1.

Once the noise levels have been established and the lateral homogeneity assumption validated, conductivity models are constructed by trial and error and computer assistance to produce a model that fits the observed signal decay reasonably well. Modeling begins with the simplest case of a single layer of fixed conductivity. The conductivity of that layer is adjusted to provide the best fit possible to the data, but the fit provided by a single layer is commonly poor. As additional layers of differing conductivity are added, the fit to the observed data improves. If the addition of one or more layers does not appreciably improve the fit, those layers are removed and the simplest model that reasonably fits the data is used. At site TDEM-1, a four-layer model produced a transient decay that fit the observed decay with a 1.1 percent residual error (fig. 22 and table 3). This model consists of a thin, poorly conductive surface layer that is underlain by layers of increasing conductivity. Conductivity is modeled to increase from 26 to 249 mS/m at a depth of 115 m, and again increases to 389 mS/m at a depth of 222 m, the deepest layer detected. A comparison with the best-fit models obtained for 1-, 2-, and 3-layer solutions (fig. 23) shows that only the poorly fitting 1-layer model fails to show the large conductivity increase at about 115 m depth.

Water depth and salinity have been reported for the water well (State well number 49-15-523) adjacent to site TDEM-1. Depth to water in this well is 121 m, which closely matches the depth at which the conductivity models show a large increase in conductivity (fig. 23). The TDS concentration of the water in this well is 1,053 mg/L, which is classified as slightly saline (fig. 8 and table 1). The increase in conductivity modeled at a depth of 220 m may be caused by the presence of water that becomes increasingly saline with depth.

Three- to four-layer conductivity models produced acceptable fits to the observed decays at the other 8 ground TDEM sites (table 3). Most of these sites had best-fit conductivity profiles that showed conductivity increasing downward, similar to the pattern observed at site TDEM-1. Tops of the deepest layers detected ranged from 112 m for TDEM-5 to 245 m for TDEM-6. Modeled layer conductivities were as low as 5 mS/m to as high as 885 mS/m, reflecting the opposing influences of sediment type, degree of water saturation, and water salinity. Conductivity

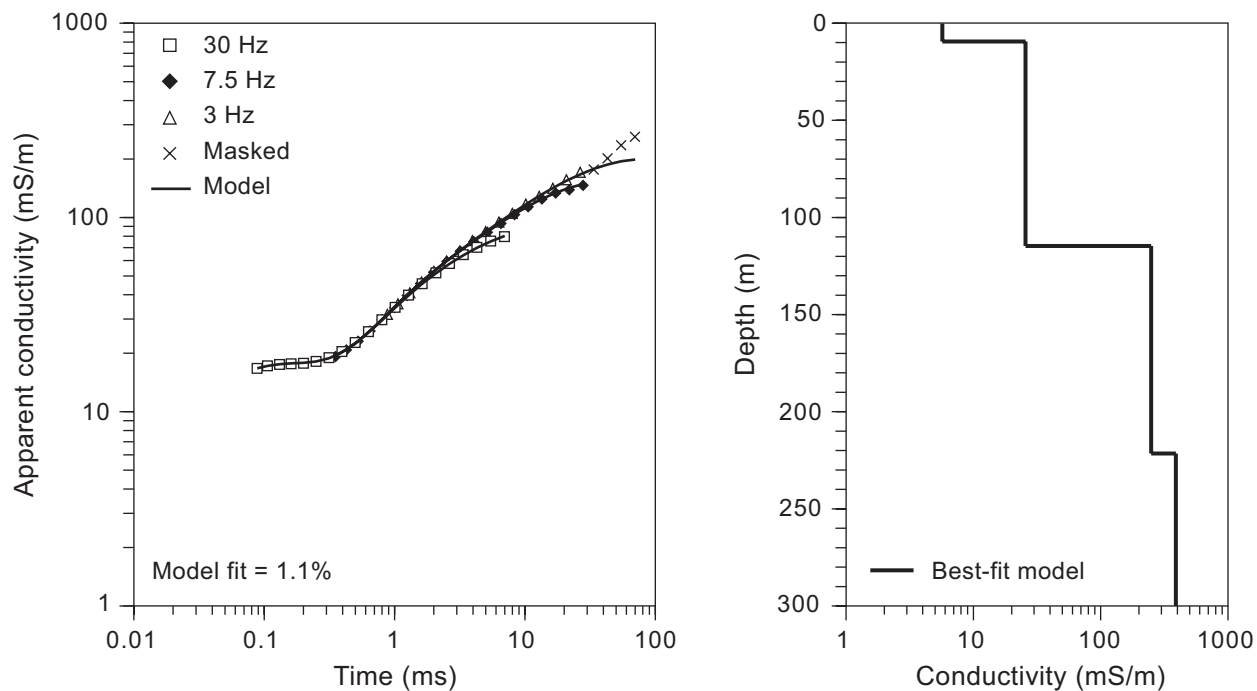


Figure 22. Apparent conductivity and the best-fit conductivity model for ground TDEM site 1. (left) Symbols represent the actual TDEM data; solid lines represent the data produced using the model shown at right. The error shown at bottom is the difference between the actual measurements and those produced using the best-fit model. (right) The four-layer conductivity model that produced the best fit to the observed TDEM data.

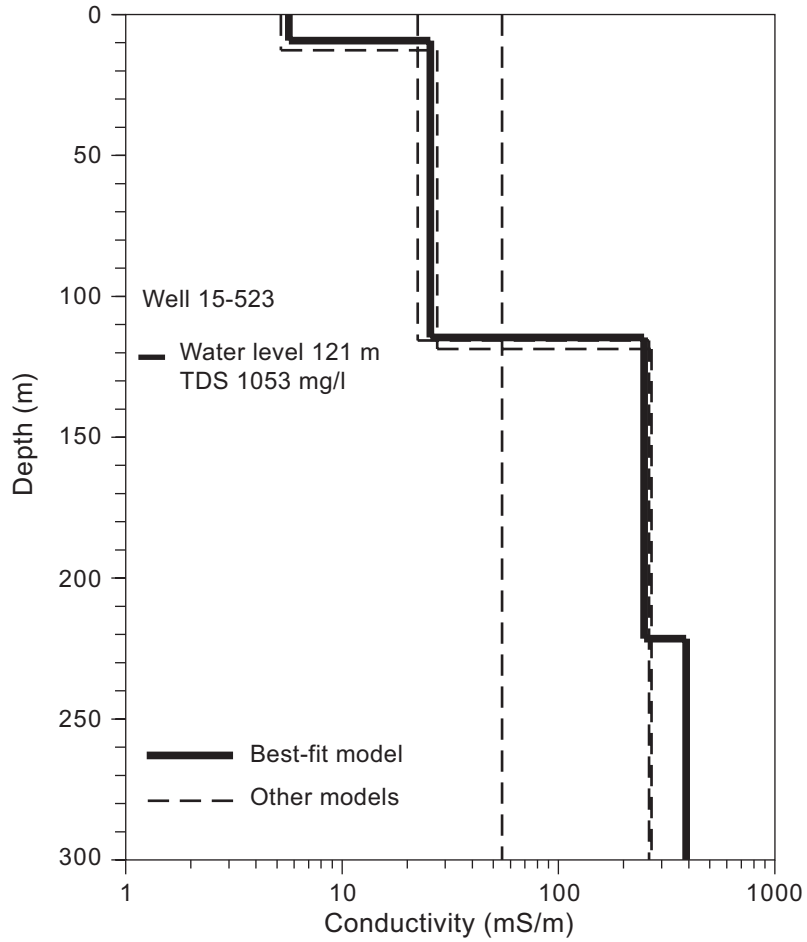


Figure 23. Comparison of the best-fit, 4-layer conductivity model for data collected at ground TDEM site 1 with the best 1-, 2-, and 3-layer models for the same data. The 2-, 3-, and 4-layer models all show a significant increase in conductivity at a depth near that of the water depth reported in adjacent well 49-15-523.

models from these sites were compared to models derived from airborne geophysical data to verify the accuracy of the recorded signals.

AIRBORNE GEOPHYSICAL SURVEY

Three types of data acquired during the airborne geophysical survey have been used in this analysis of potential water resources of eastern El Paso County. Surface elevation data, produced by subtracting radar altimeter heights from GPS-determined aircraft elevation, are used as a high-resolution backdrop for depicting depths to water (fig. 5), water elevations (fig. 6), and the relationship of these two critical exploration parameters to surface elevation. Although surface elevations accompanying the water-level data in the TWDB database are used to calculate water depths and elevations for specific wells, the topographic context provided by the airborne data is a helpful interpretational tool. The airborne magnetometer towed by the aircraft passively measured the ambient magnetic field strength across the survey area. Magnetic field data are often used in minerals exploration, but the primary use in this study is to help delineate faults that may play an important role in the subsurface distribution of sediments. Most important are the EM data, which were acquired using an active transmitter and a towed receiver. If properly acquired, processed, and interpreted, these data detect subsurface changes in electrical conductivity that reveal information about groundwater quality and depth and the type of sediment hosting the water.

Magnetic Field Data

Recent models of the Earth's magnetic field, such as the International Geomagnetic Reference Field (IGRF 2001.67) calculated by the International Association of Geomagnetism and Aeronomy, depict a gentle, smooth regional magnetic field gradient across the survey area. This model shows magnetic field strength increasing to the north-northeast from 49,161 nanoteslas (nT) in the southwest corner to 49,303 nT in the northeast corner, a net increase of 142 nT. The

actual magnetic field strength measured during the survey using airborne and ground-based magnetometers was lower, varied over a wider range of values, and shows perturbations caused by local geologic features and human activity. Measured magnetic field strengths ranged from 48,507 to 49,065 nT, several hundred nT below the IGRF values.

Local magnetic field features are enhanced by subtracting the IGRF from the values measured using the airborne instrument and correcting for secular drift and other minor effects. The residual magnetic field intensity map of the survey area (fig. 24) displays difference values ranging from 660 nT below IGRF along the western margin where the Hueco Bolson is the deepest, to values as high as 165 nT below IGRF in the southeast and northeast areas where basin-fill sediments are shallow and bedrock is exposed. Several linear anomalies cross the area that are coincident with major pipelines. In contrast to the north–northeast to south–southwest magnetic field gradient predicted by the IGRF, the dominant local gradient reflects magnetic field strength that decreases from east–southeast to north–northwest. This difference is attributed to local- to regional-scale geologic structure that is not considered in the IGRF model.

Fugro produced shallow-depth transforms of the magnetic field data that remove the larger, longer spatial wavelength features and emphasize shallow anomalies (fig. 25). This enhances narrow, linear pipeline anomalies over the narrower display range (only –10 to 9 nT). This display also emphasizes several curvilinear features that correspond well to the locations of faults mapped and inferred from aerial photographs and field mapping (Collins and Raney, 2000). These features may be hydrologically significant because they are related to the development and evolution of the Hueco Bolson and may have influenced drainage patterns during the filling of the basin.

EM Data

Water-resource interpretations made from remotely sensed geophysical data rely on the quality of the original data, the validity of the assumptions made during processing, and the

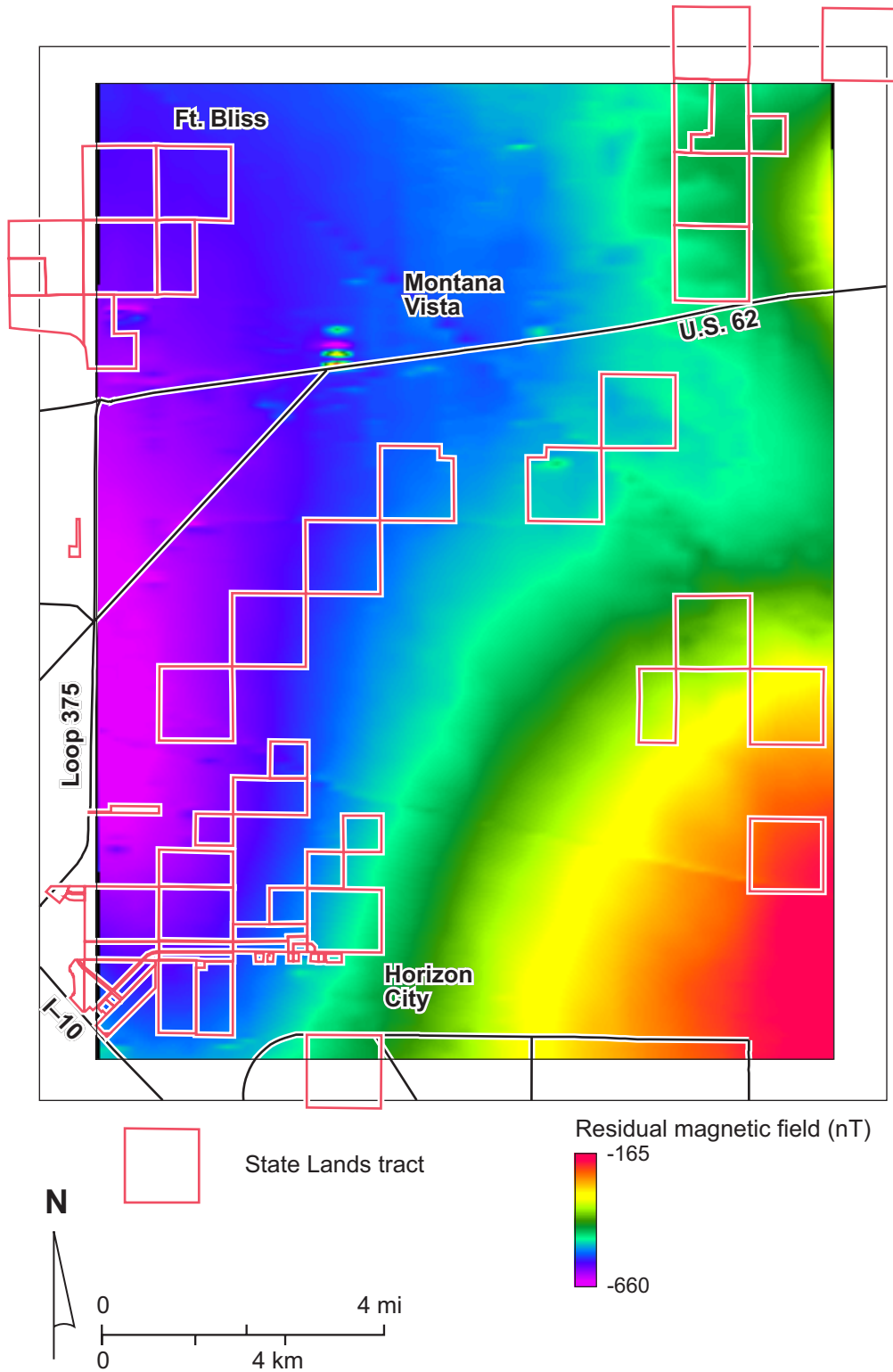


Figure 24. Residual magnetic field strength measured with an airborne magnetometer. Values are displayed relative to the IGRF field strength.

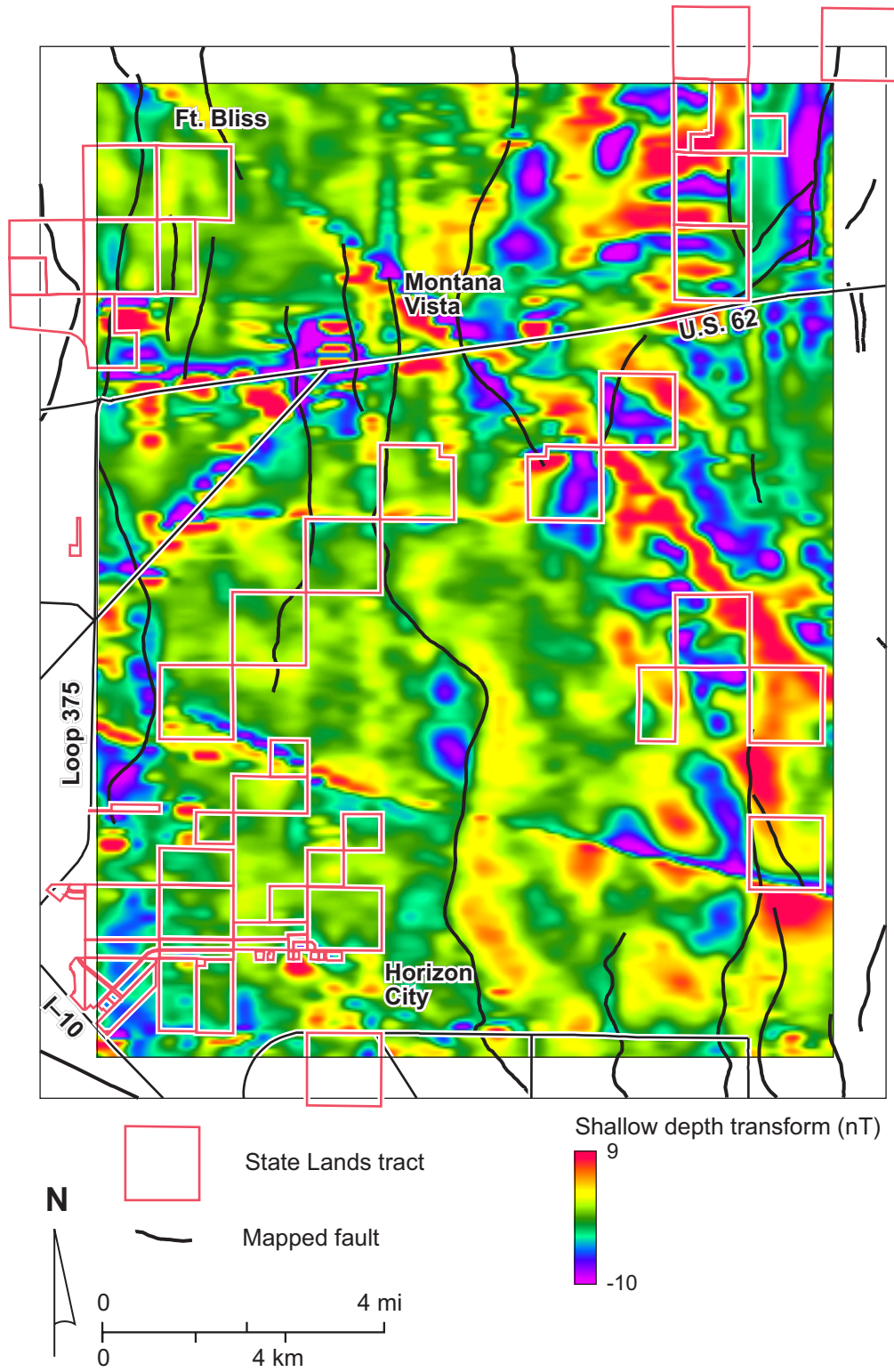


Figure 25. Shallow-depth transform of magnetic field data acquired using an airborne magnetometer. Also shown are faults mapped in the area by Collins and Raney (2000).

analysis of the processed data. Assuming the instrument is operating properly and the exploration objectives are reasonable, the level of background EM noise can strongly influence the actual exploration depth achieved and the usefulness of the recorded data. EM noise is generated by many sources, including electrical power lines, thunderstorms, solar activity, radio antennas, and other significant electrical devices. As is true for ground-based TDEM data, the transient signal is small even at its strongest and decays rapidly with time. Because penetration depth increases with the length of the recordable signal, EM noise affects late-time (deeper) measurements more severely than it does early-time measurements. More powerful transmitters such as that in the Megatem II system can overcome some EM noise, but noise levels in developed areas can limit the ability to acquire good data.

For these reasons and because noise from electrical power lines is the most common noise source, power-line noise is monitored during airborne geophysical surveys. During our survey, noise levels ranged from a low of 11 to a high of 351 mV (fig. 26). Relatively low values were recorded over most of the survey area. Noise levels high enough to severely impact data quality were detected in narrow corridors along a major power line, roads such as U.S. 62 and Interstate 10, and in relatively dense communities such as Horizon City and Montana Vista. We consider the airborne data to be unreliable in these areas and have excluded them from further analysis.

The apparent conductance map (fig. 27) depicts the relative ability of the ground to conduct electricity within the exploration depth range of the airborne instrument, with little regard for depth distribution. It is a single value calculated for each measurement location based on the strength and shape of the transient decay. It can be used to identify highly conductive areas of mineralization or salinization. Because the transients are strongest at early times, the apparent conductance value is strongly influenced by the electrical properties of the relatively shallow subsurface. Apparent conductances range from 185 to 5,524 mS. High apparent conductances are found in more heavily developed areas such as Horizon City, Montana Vista, and along U.S. 62 and Interstate 10, suggesting that EM noise associated with these developments has influenced the data in these areas. Elsewhere, apparent conductance patterns do follow the curvilinear trends

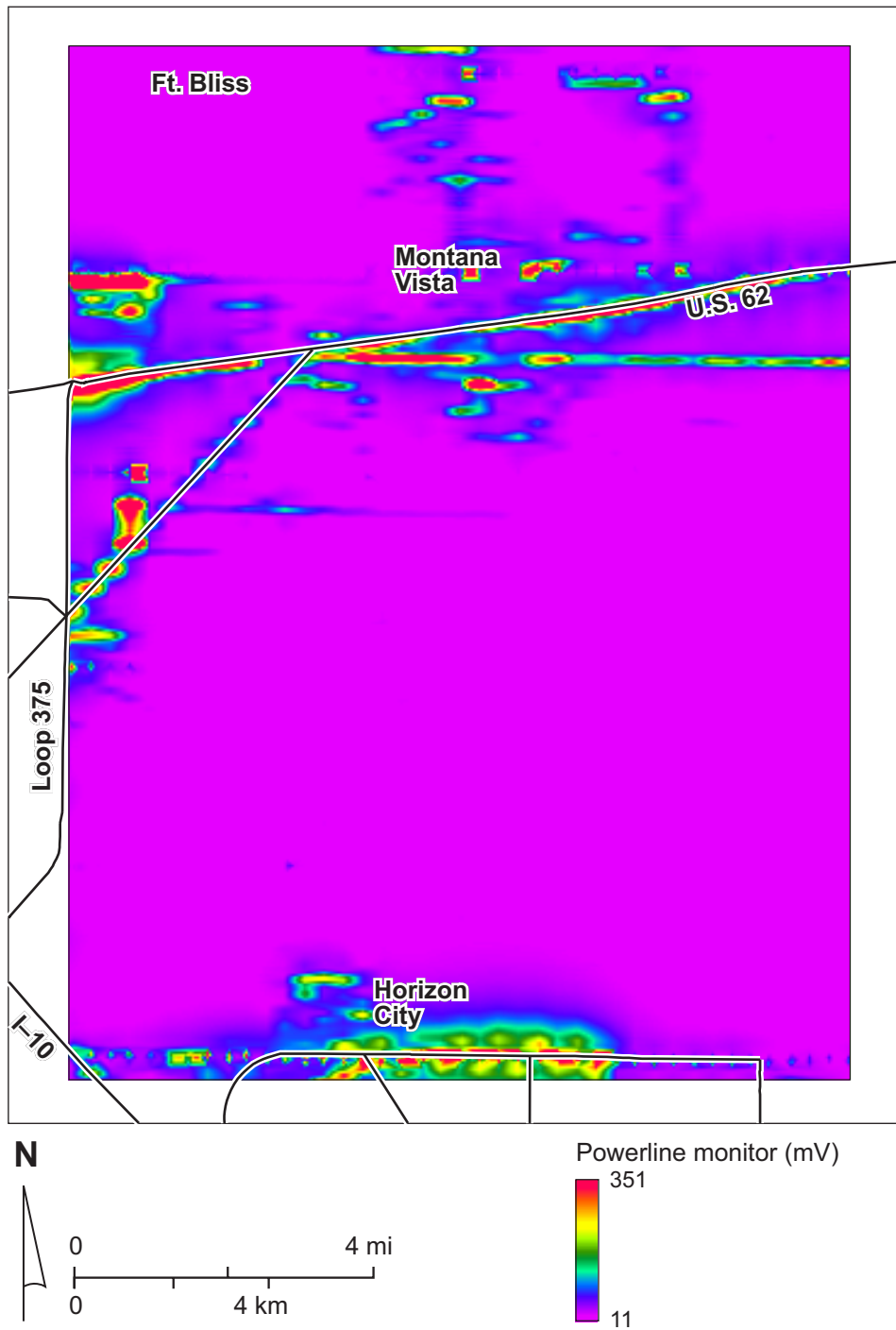


Figure 26. Powerline noise intensity measured during the airborne survey.

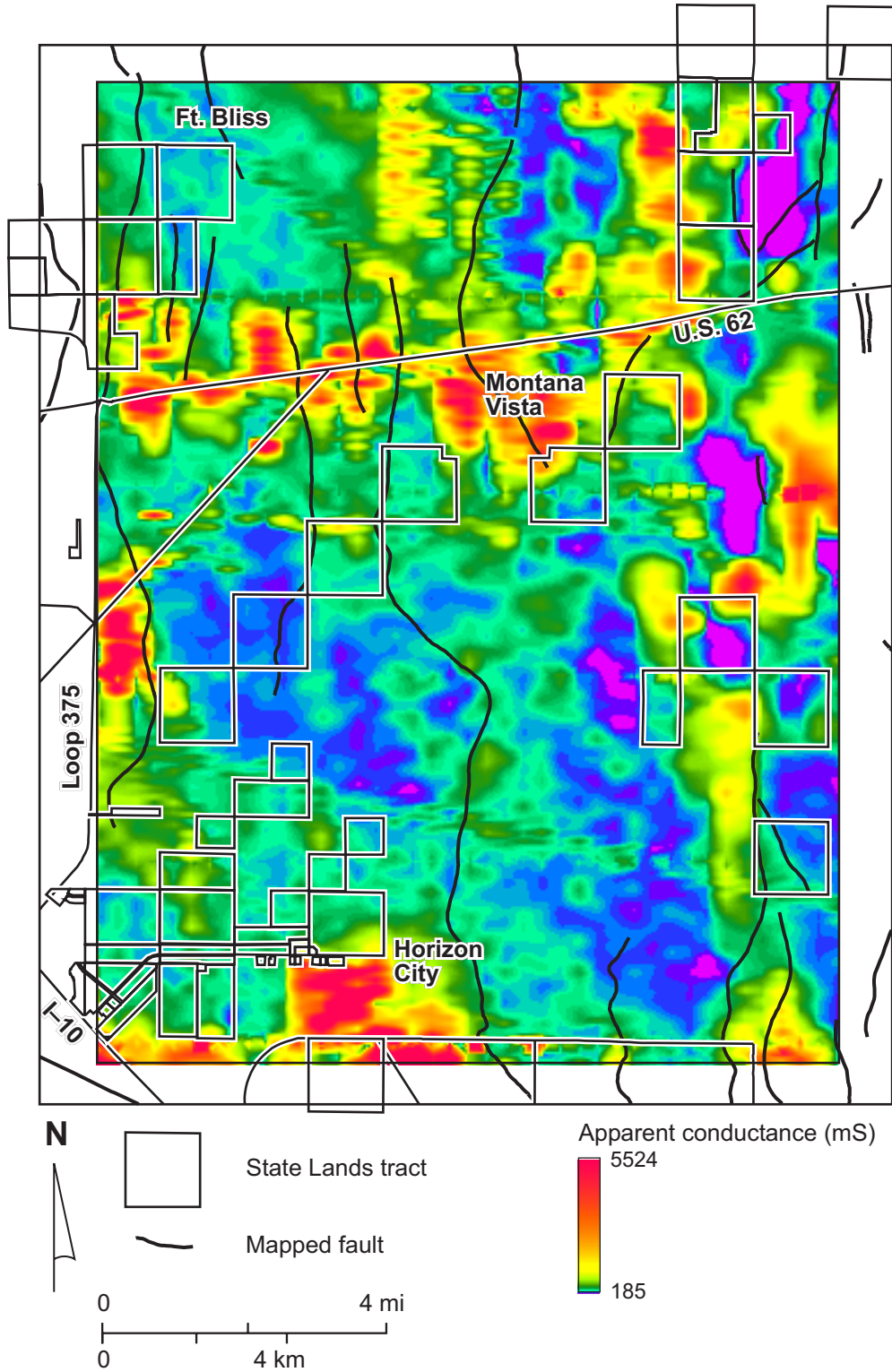


Figure 27. Apparent conductance calculated from TDEM data collected during the airborne survey.

of some of the mapped faults. A long, linear feature extending northwest–southeast from the northwest corner of the survey area passes about 1 km east of Horizon City. A more subtle but parallel linear feature is visible about 4 km east of this one, particularly north of U.S. 62. These features cross the principal flight lines obliquely; they are unlikely to be acquisition or processing artifacts. They may represent deeper structural elements such as fault-bounded sub-basins within the larger Hueco Bolson, but their orientation differs from that of the faults mapped at the surface.

High conductances might also be caused by the presence of relatively saline water within the exploration depth range, particularly if the water table is shallow. Relatively fresh groundwater would be expected in areas of relatively low conductance. In this area, where groundwater depths are generally 100 m or more, inversions of the EM data are more useful than apparent conductance values because the inversions produce estimates of apparent conductivity that vary with depth.

Average Conductivity Profile and Achieved Exploration Depth

By transforming each of the 64,773 recorded transient decay curves into a conductivity versus depth profile, we can examine conductivity changes with depth that can be related to changes in lithology, water saturation, and water quality. To get a generalized conductivity profile for the entire survey area, we extracted conductivity values at 10-m depth intervals, averaged all values for a given interval, and plotted the averages with depth (fig. 28). Average apparent conductivities increase with depth in the upper 100 m, increasing from relatively low values of 32 to 57 mS/m in the upper 50 m to the highest average values of 98 mS/m at depths of 110 and 120 m. Below these depths, average apparent conductivity decreases downward, declining to 43 mS/m at 200 m and 10 mS/m at 300 m.

Different transients achieved different exploration depths that largely depended upon the noise levels and the conductivity of the ground. The percentage of conductivity models consid-

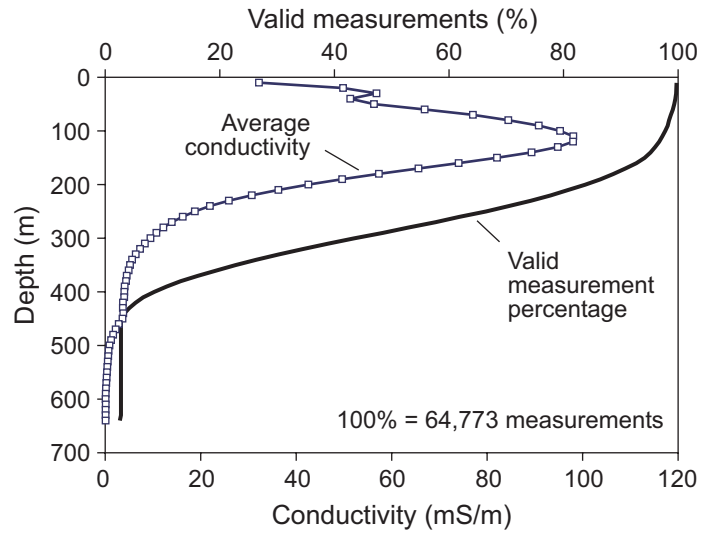


Figure 28. Average conductivity over the geophysical survey area calculated from airborne survey conductivity models at 10-m depth intervals. Also shown is the percentage of valid conductivity values at the same 10-m intervals.

ered to be valid at a given depth across the survey area is a rough measure of the exploration depth actually achieved (fig. 28). More than 90 percent of the conductivity values are valid to a depth of 170 m, well below the depth to water in the survey area (fig. 5). More than 50 percent of the models have valid apparent conductivities to a depth of 280 m, a depth that could be considered the actual exploration depth achieved over most of the area. This range compares well with estimates of 192 to 383 m based on measurement time and measured ground conductivity (fig. 19).

For comparable depth ranges, the average conductivity profile calculated from the airborne data is similar to those that fit the ground-based TDEM data (table 3). All of the profiles calculated for the ground-based data show increasing conductivity with depth in the upper 100 m; three of the nine ground profiles indicate a subsequent decrease in apparent conductivity similar to that shown in the average profile from airborne data at depths greater than 136 m (location TDEM-9, fig. 13), 173 m (TDEM-4), and 218 m (TDEM-3). All of these profiles are located on the eastern part of the survey area, where depth to resistive bedrock is interpreted to be shallow. Farther to the west, where bedrock is interpreted to be deeper, ground TDEM profiles show increasing conductivity with depth and do not explore deeply enough to detect resistive bedrock. The average airborne profile does show a decrease in conductivity below about 120 m, suggesting that either bedrock is shallower than expected over much of the survey area, or that the airborne system did not accurately measure the conductivity below the conductive zone at and below the water table. In the depth slices produced at 10-m intervals from the airborne EM data, we expect the absolute conductivity values to be reasonably accurate for the upper 150 m. Below this depth, we expect the conductivity values to be only accurate relative to values at the same depth but perhaps somewhat lower than actual conductivity at those depths.

Conductivity–Depth Slices

One of the biggest advantages of airborne EM is its ability to examine lateral changes in apparent conductivity at critical depths across a survey area. High-resolution coverage of an area allows the context of individual soundings to be considered and helps identify geological and hydrological features that would be difficult or impossible to recognize from sparse borehole data or ground-based geophysical studies. By combining data from wells, ground-based surveys, and airborne surveys, we can better interpret the airborne data and reduce the uncertainty associated with many types of geophysical data.

Appendix A includes 20 images (figs. A1 through A20) that depict apparent conductivity across the survey area at 10-m depth intervals from 10 m below the surface (fig. A1) to 200 m below the surface (fig. A20). Each of these images has been displayed such that warmer colors represent conductive areas relative to other conductivities at that depth, and cooler colors represent low conductivities relative to others at that depth.

Depth slices between 10 and 90 m are above the water table across most of the area. At these depths, conductivities are relatively low and should be more heavily influenced by variations in moisture and clay content than by the dissolved constituents in pore water. Prominent features evident on the 10- to 90-m depth slices include a broad zone of relatively low conductivity that is about 4 to 6 km wide and extends from the northwest corner of the survey area to its southern boundary just east of Horizon City (figs. A1 through A9). Higher apparent conductivities are found east of an abrupt curvilinear boundary passing a short distance west of Montana Vista. Apparent conductivity is low where bedrock is exposed at higher surface elevations (figs. 3 and 4) on the east side of the survey area. This area forms the eastern boundary of the Hueco Bolson.

A significant area of relatively high conductivity is located near and north of Horizon City. This north–south trending feature becomes more strongly developed between 40 and 90 m below the surface; it forms the western boundary of the broad zone of low conductivity that crosses the

entire survey area. Local areas of elevated apparent conductivity are located in developed areas, along roads, and at power lines. These are likely to be artifacts of EM noise.

Conductivity patterns at these relatively shallow depths correspond strongly to geologic features. Superimposed on the 70-m depth slice are the known and inferred faults (fig. 29) that have been mapped in the area (Collins and Raney, 2000). In general, areas of similar but low apparent conductivity are separated from other areas of similar but high apparent conductivity by abrupt boundaries that coincide with mapped faults. In most instances, low conductivities are found on the downthrown side of the fault, whereas higher conductivities are found on the upthrown side. Low conductivities in this depth range are also associated with mapped bedrock outcrops. Higher conductivities in the basin fill sediments are likely to be found where clay-rich sediments have been deposited; poorly conductive areas within the basin fill are likely to have higher sand, gravel, or caliche contents.

At depths that are within the water-saturated zone, water quality can become the dominant control on measured conductivity. Few water wells produce from depths less than about 100m, but at and below this level there are many wells with reported water-quality analyses that can be used to help infer the distribution of relatively fresh water in the subsurface.

At 110 m (fig. A11), low-conductivity areas form three north–northwest to south–southeast trending zones (east, central, and west) that are separated by similar-trending zones with higher apparent conductivities. As depth increases, the conductive zones expand until depth of 160 m or more are reached, at which point only the eastern low-conductivity zone covers a significant total area.

Between 100 and 150 m (figs. A10 to A15), the central zone of low conductivity that was prominent at shallower depths narrows considerably and is barely discernable on the 150-m depth slice. Other significant areas of relatively low conductivity in this depth range are found in the northwest corner, an area northwest of Horizon City measuring about 4 km north–south and east–west, and a large north–south trending area in the northern and eastern quadrant where bedrock is exposed. The low in the northeastern quadrant remains prominent (and enlarges) to

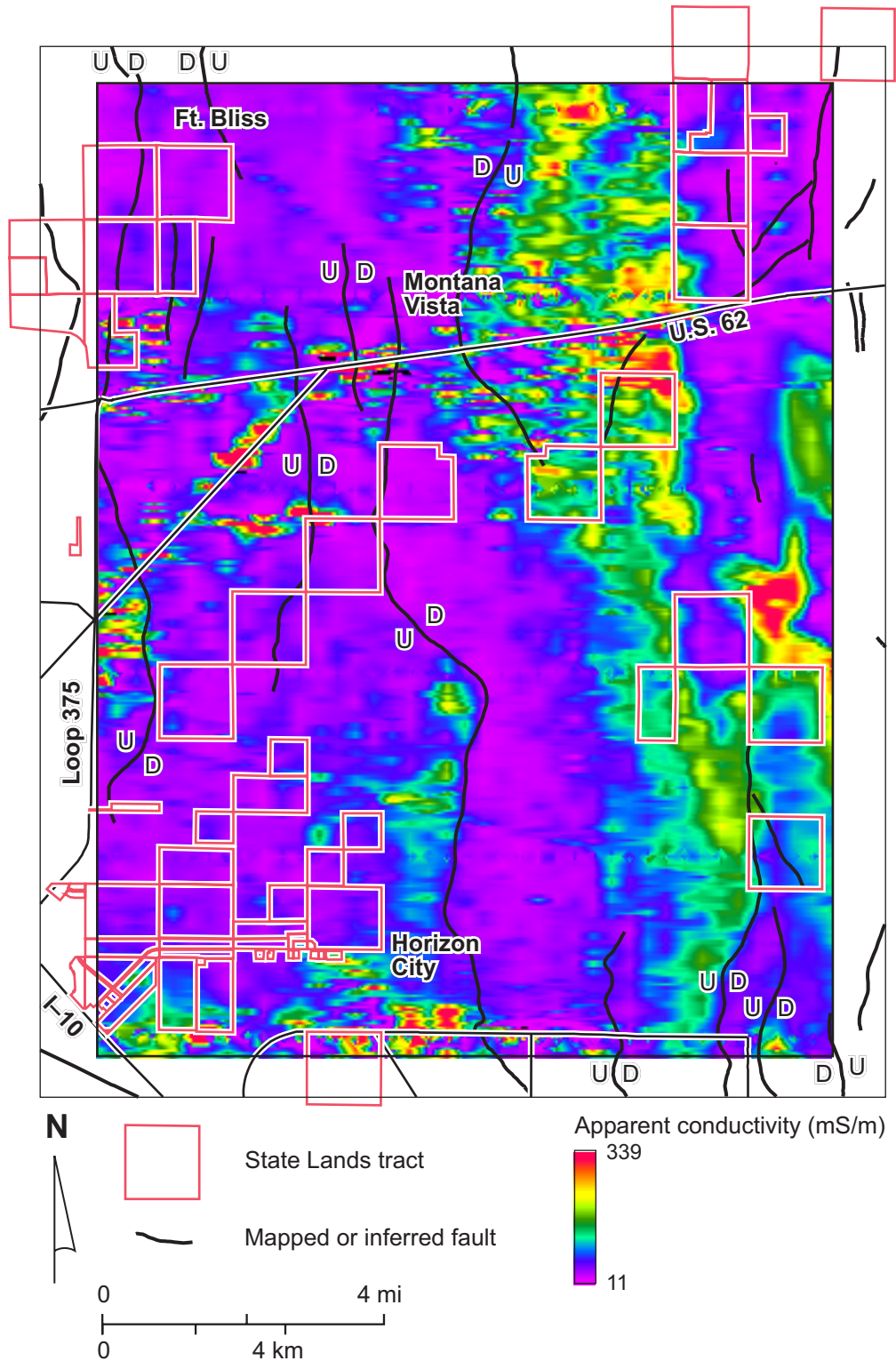


Figure 29. Apparent conductivity at a depth of 70 m. Also shown are faults mapped in the area by Collins and Raney (2000). Labels “U” and “D” denote interpreted upthrown and downthrown sides of fault.

the deepest level considered (200 m, fig. A20), but the area northwest of Horizon City diminishes greatly with depth and is nearly indiscernible at 150 m (fig. A15). The eastern boundary of the low-conductivity zone near Fort Bliss migrates westward with depth; by 150 m it has diminished to an area measuring about 2 km east–west by 4 km north–south. Low conductivities persist in this corner of the survey area to depths of at least 200 m (fig. A20).

RELATIONSHIP BETWEEN WATER QUALITY AND CONDUCTIVITY

At depths that are within the water-saturated zone, water quality can become the dominant control on measured conductivity. Few water wells produce from depths less than about 100 m, but at and below this level there are many wells with reported water-quality analyses that can be used to help infer the distribution of relatively fresh water in the subsurface. To illustrate the apparent correlation between conductivity measured by an airborne instrument and the TDS concentration in groundwater, we selected two wells (49-15-404 and 49-15-509, fig. 30) that were located near flight lines, had similar depths, and had substantially different TDS concentrations. Well 49-15-509, located near Montana Vista, has a reported water depth of 125 m, a slotted casing from 119 to 140 m, and a fresh TDS value of 410 mg/L. Well 49-15-404, located about 6 km west of well 49-15-509, has a water depth of 105 m, two slotted casing sections from 107 to 125 m and from 180 to 192 m, and a slightly saline TDS value of 1,935 mg/L. A conductivity profile located about 30 m from the fresh-water well 49-15-509 shows consistently low apparent conductivity values throughout the depth range potentially sampled by the adjacent well (fig. 31). A conductivity profile located about 70 m from the more saline-water well 49-15-404 shows apparent conductivity values that are considerably higher than those near well 49-15-509 throughout the depth range that could have produced the more saline water.

We can also qualitatively evaluate the influence of water quality on the EM data by superimposing TDS values from wells that produce water from a given depth range onto images of apparent conductivity at that depth. Depths that are most critical for water resource assessment in

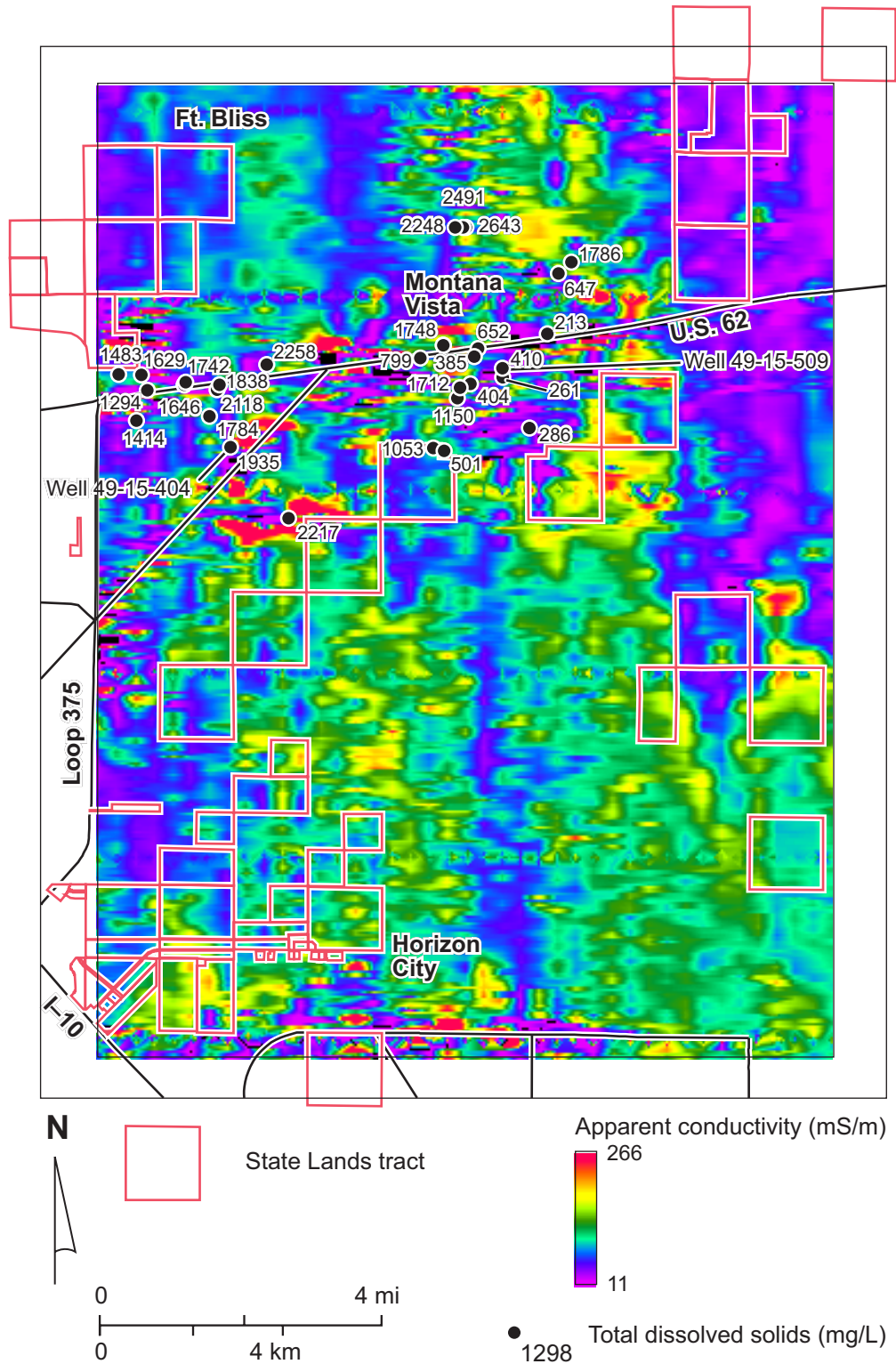


Figure 30. Apparent conductivity at a depth of 120 m. Also shown are TDS values for water samples from wells that have water levels above this level and are screened at this level.

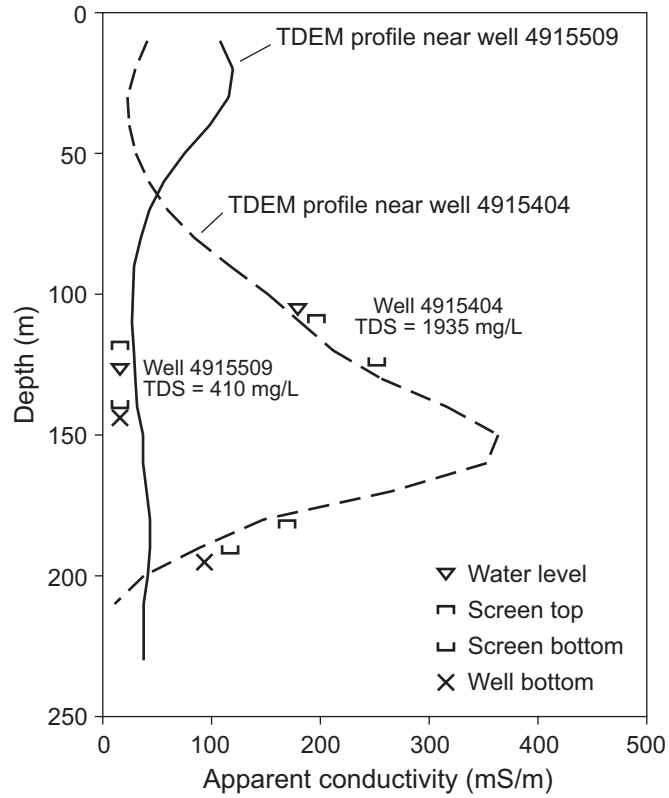


Figure 31. Comparison of TDS values from one low-TDS water well and one high-TDS water well with conductivity profiles calculated for transients acquired during the airborne survey nearest the well locations.

an unconfined aquifer are those at and below the water table. Considering water depths, depths to the top and bottom of slotted casings, well depths, and the fact that water salinity is reported to increase with depth in this area, the most critical depth slices are those between about 100 and 150 m.

For water depths shallower than 100 m, there is only one well with a reported TDS value within the airborne survey area. This well, located east of Horizon City, reports slightly saline water that is being produced from some depth between the water level at 32 m and the bottom of the slotted casing at about 75 m. On depth slices between 40 and 70 m (figs. A4 to A7), this TDS value falls within an area of low apparent conductivity.

At deeper depths, more wells are available for a more meaningful analysis of the relationship between TDS and apparent conductivity measured using an airborne instrument. At 120 m, for example, there are 31 wells with water levels shallower than this depth, slotted casing at or deeper than this depth, and reported TDS values (fig. 30). Qualitatively, the highest TDS values (greater than 2,000 mg/L) are generally located in the most conductive areas and the fresher values (TDS less than 1,000 mg/L) tend to be found in areas where apparent conductivities are lower. A similar relationship can be seen on depth slices at greater depths (figs. A12 through A20), although the number of wells with reported TDS values decreases with depth from a peak of 32 at 130 m to 12 at 170 m to 1 at 200 m. The relationship is also limited by the fact that most wells are located near developed areas where EM noise is the highest and data quality most suspect.

A more quantitative assessment of the relationship between water quality and apparent conductivity can be carried out by plotting the TDS value reported for a well against the apparent conductivity indicated by the conductivity profile located closest to the well (fig. 32). In most cases, there is more than one conductivity value for each TDS value because apparent conductivity slices at more than one depth fall between depths reported for the water level and the top and bottom of slotted casing.

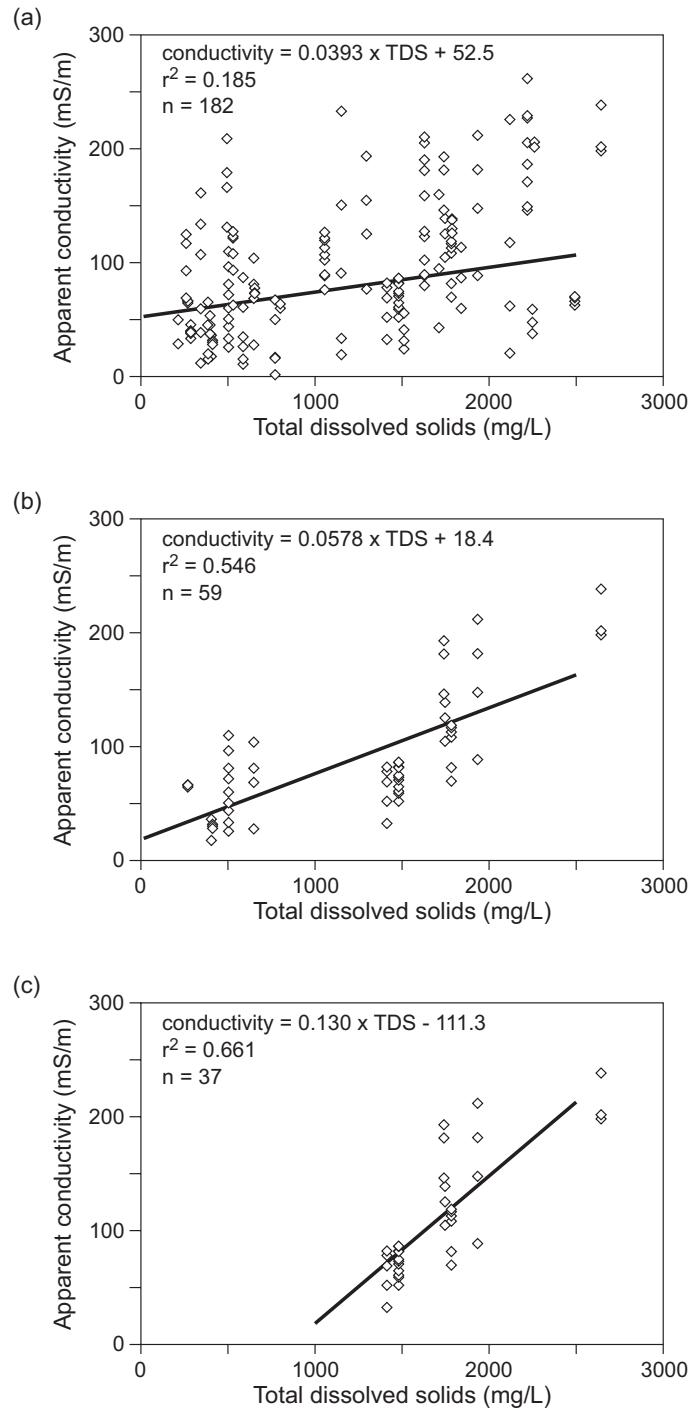


Figure 32. Relationship between TDS concentration in groundwater samples from the airborne survey area and apparent conductivities calculated from airborne data for depths below the water level and within the screened intervals of each well. (a) Data pairs and best-fit relationship using all available wells in the study area; (b) data pairs and best-fit relationship using only those wells that have been accurately located using GPS and are within 100 m of an airborne measurement; and (c) data pairs and best-fit relationship using wells that meet the criteria listed in (b) and have TDS concentrations greater than 1,000 mg/L.

If all possible wells are used regardless of TDS value, the accuracy of the well location, and the distance between the closest conductivity profile and the well location, there is only a vague relationship between water quality and apparent conductivity (fig. 32a). For these 182 data pairs, there is a hint of the expected increase in apparent conductivity that should accompany increasing TDS values, but the correlation coefficient for a best-fit line through the data is low at 0.185.

A considerably better fit is obtained when we restrict the data pairs used in the analysis to wells with the most accurately known locations (located by TWDB using GPS instruments) and only those wells located within 100 m of a flight line (fig. 32b). The straight-line fit through the 59 remaining data pairs from 11 wells has a reasonably good correlation coefficient of 0.546.

Most of the increase in apparent conductivity occurs at relatively high TDS values (fig. 32b), suggesting that, for groundwater that is fresh or toward the fresh end of the slightly saline classification, the apparent conductivity is within a range that is as strongly influenced by sediment or rock properties as it is by dissolved ionic concentrations. Taking data only from wells that meet the strict location and distance criteria of fig. 32b and further removing data pairs with TDS values less than 1,000 mg/L, the linear fit to the 37 remaining data pairs improves to a correlation coefficient of 0.661 (fig. 32c).

Where GPS instruments have been used to locate wells, the locational accuracy will be similar to the 10-m accuracy estimated for the airborne data (Hefford, 2001). Nevertheless, there remain sources of potential error in the quantification of the relationship between water quality and apparent conductivity, most notably the uncertainty in the actual depth range contributing to the reported TDS value, water from different stratigraphic levels mixing in the well bore before sampling, and the date of the analysis. We used the most recent analyses in this comparison, but the analysis dates ranged from 1952 to 2001. In particular, TDS values for the older analyses could differ substantially from values at the time the survey was flown.

FAVORABLE GROUNDWATER EXPLORATION AREAS

The most favorable groundwater exploration areas can be selected based on the foregoing analysis of the airborne and ground-based geophysical data, the distribution of fresh to moderately saline water reported in existing wells, the depths to water and slotted well casing, and the presence of geological features that may control deposition within the Hueco Bolson. This analysis indicates that there is more confidence associated with identifying likely low-salinity groundwater than there is in identifying locations for highly productive zones. In a simplified sense, we are seeking to identify laterally and vertically extensive areas at or below the current groundwater levels that have low apparent conductivities. Because saline water is more conductive than fresh water, sediments saturated with fresh water will have lower conductivities than similar sediments saturated with saline water. Secondly, we know that clayey basin-fill sediments are more electrically conductive than sandy or gravelly sediments; significant deposits of these strata also should be manifested as areas of relatively low conductivity.

At the most relevant depths of 110 to 130 m, there are two relatively extensive areas with low apparent conductivity. The largest is area A (figs. 33 and 34), which covers about 23 km² on the depth slice at 120 m. It is the broad zone of low conductivity trending north–northwest to south–southeast across the survey area and passing west of Montana Vista. It appears to be bounded on the west, and perhaps on the east, by faults that have dropped this area downward relative to adjacent blocks. Fresh water has been produced from a well along the eastern margin of this area near Montana Vista (fig. 30); the apparent conductivities at the well producing fresh water are higher than those within much of area A. Little data on lithology is available in this area, but a driller's log from a well near the margin of this area indicates relatively coarse sediments are present in this depth range. One possible geological interpretation of this feature is that it represents a former drainageway that focused deposition of relatively coarse sediment moving southward toward the ancestral Rio Grande. If coarser sediments are present within this down-

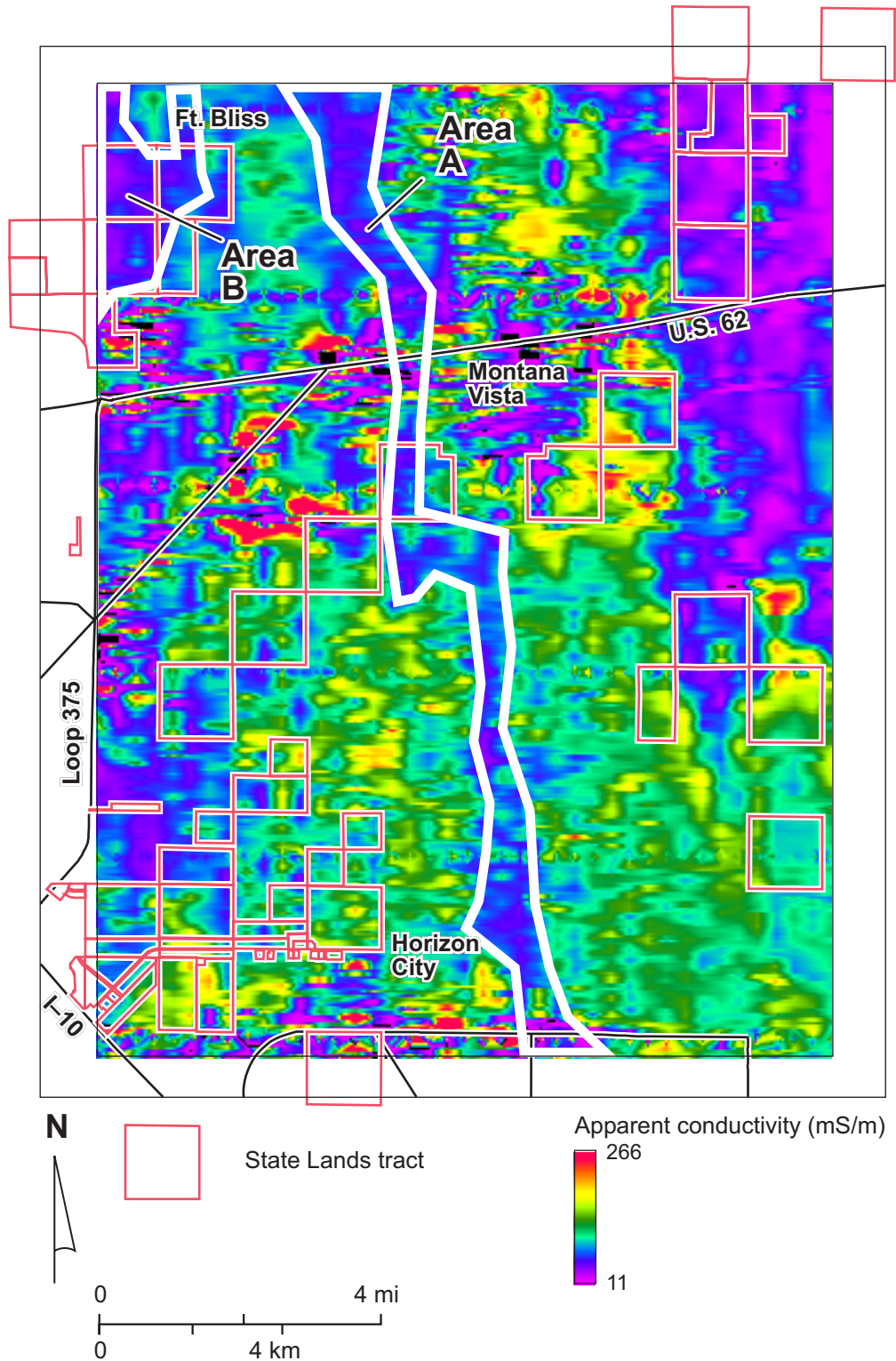


Figure 33. Favorable exploration areas for relatively low-TDS groundwater at a depth of 120 m within the survey area.

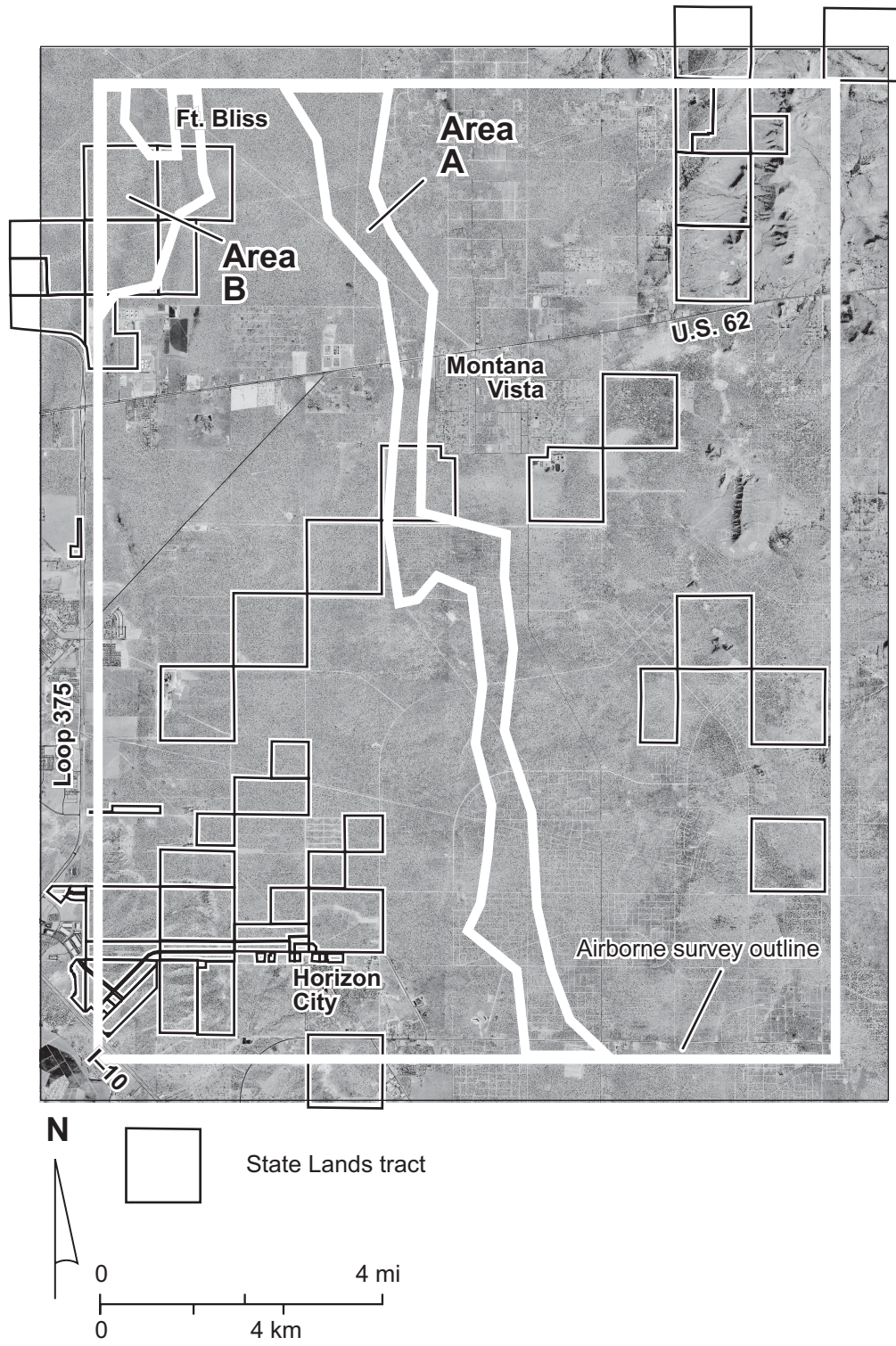


Figure 34. Favorable exploration areas for relatively low-TDS groundwater superimposed on an aerial photograph.

dropped block, wells could be expected to yield higher specific capacities than the low values reported for nearby wells outside the low-conductivity zone (fig. 11).

Two State-owned tracts, section 18 of block 78T2 and section 48 of block 79T2 in the T&P Railroad survey, occupy part of area A (figs. 2, 33, and 34). Section 18 appears to be the most favorably located above the thickest low-conductivity zone, particularly in the western part of the block. Good airborne coverage exists in this area; four principal flight lines and one tie line cross section 18. Any exploratory well in this area should be sited east of the fault mapped along the western boundary of section 18. It should also be located along the tie line at an intersection with one of the principal flight lines to provide the best correspondence with the airborne geophysical data.

Area B, located in the northwestern part of the study area (figs. 33 and 34), may represent the eastern extension of an extensive area of fresh water interpreted to exist on the eastern flank of the Franklin Mountains (Gates and others, 1980). Here the low-conductivity zone covers an area of about 8 km² within the survey area, migrates westward with depth, and extends from the depth to water at about 100 m to at least 160 m in some areas. There are three State tracts within area B: sections 15, 16, and 21 of block 79T2 in the T&P Railroad survey (figs. 2, 33, and 34). Based on airborne geophysical data, the most favorable areas should be in sections 16 and 21 along a north–south line passing near the center of sections 16 and 21.

Airborne and ground-based geophysical data and available water-well data indicate that fresh-water resources exist in the study area. These resources are underlain by saline water and do not appear to be laterally or vertically extensive enough to support local high-volume production without accompanying water-level decline and salinity increase.

CONCLUSIONS

Airborne and ground-based geophysical studies have been combined with an analysis of available water-well data to identify potential groundwater resources in eastern El Paso County.

Results of this investigation are summarized as follows:

- Fresh to slightly saline groundwater is present at depths of 90 to 130 m over most of the study area;
- Ground-based geophysical measurements demonstrate that EM data are influenced by water content and water quality, that the saturated zone is within the exploration depth range of EM instruments, and that groundwater salinity increases with depth;
- Magnetic field and TDEM data acquired during the airborne survey both provided information that helped delineate basinal faults that may influence groundwater flow and resource quality;
- Conductivity-depth slices produced from airborne TDEM data revealed prominent geological features at depths shallower than the water table;
- At depths below the water table, apparent conductivity values in conductivity-depth slices correlate reasonably well to water quality for accurately located wells near flight lines;
- Two low-conductivity zones evident on conductivity-depth slices at depths within the upper part of the water-saturated section (110 to 150 m) are interpreted to be the most favorable areas for groundwater exploration within the survey area. The larger area includes one State-owned tract southwest of Montana Vista. The smaller area includes parts of three State-owned tracts in the northwest corner of the survey area; and
- Fresh groundwater resources are present, but geophysical and available well data suggest that they are not extensive enough to support local high-volume production without significant water-level decline and salinity increase.

ACKNOWLEDGMENTS

This project was funded by the General Land Office under Interagency Cooperation Contracts No. 01-546R and 02-306R. Project direction was provided by Jeff Frank of the General Land Office. Texas Water Development Board staff William Mullican, Robert Mace, and Brent Christian assisted the project design and provided water well data. Airborne geophysical data were acquired and processed by Fugro Airborne Surveys staff Andrew Marshall and Leo Denner and Voyageur Airways staff Bruce Waines, Steven Christeas, Nick Craig, and Brendon Fisher. Andy Graham assisted in the acquisition of ground-based geophysical data.

REFERENCES AND RELATED PUBLICATIONS

- Albritton, C. C., Jr., and Smith, J. F., Jr., 1965, Geology of the Sierra Blanca area, Hudspeth County, Texas: U.S. Geological Survey Professional Paper 479, 131 p.
- Alvarez, H. J., and Buckner, 1980, Ground-water development in the El Paso region, Texas, with emphasis on the resources of the lower El Paso Valley: Texas Department of Water Resources, Report 246, 346 p.
- Ashworth, J. B., 1990, Evaluation of ground-water resources in El Paso County, Texas: Texas Water Development Board, Report 324, 25 p.
- Ashworth, J. B., and Hopkins, J., 1995, Aquifers of Texas: Texas Water Development Board, Report 345, 69 p.
- Brock, R. D., Buszka, P. M., and Godsy, E. M., 1994, Hydrogeologic and water-quality data from wells near the Hueco Bolson Recharge Project Area, El Paso, Texas, 1990 and 1991: U. S. Geological Survey, Open-File Report 94-329, 85 p.

- Buszka, P. M., Brock, R. D., and Hooper, R. P., 1994, Hydrogeology and selected water-quality aspects of the Hueco Bolson aquifer at the Hueco Bolson Recharge Project Area, El Paso, Texas: U. S. Geological Survey, Water-Resources Investigations Report 94-4092, 41 p.
- Cliett, Tom, 1969, Groundwater occurrence of the El Paso area and its related geology, *in* Cordoba, D. A., Wengerd, S. A., and Shomaker, John, eds., Guidebook of the border region, Chihuahua and the United States: New Mexico Geological Society Twentieth Field Conference, p. 209–214.
- Collins, E. W., and Raney, J. A., 1991, Tertiary and Quaternary structure and paleotectonics of the Hueco Basin, Trans-Pecos Texas and Chihuahua, Mexico: The University of Texas at Austin, Bureau of Economic Geology, Geological Circular 91-2, 44 p.
- Collins, E. W., and Raney, J. A., 2000, Geologic map of west Hueco Bolson, El Paso region, Texas: The University of Texas at Austin, Bureau of Economic Geology, Miscellaneous Map No. 40, scale 1:100,000, 25-p. text.
- Davis, M. E., and Leggat, E. R., 1965, Reconnaissance investigation of the ground-water resources of the Rio Grande Basin, Texas: Texas Water Commission, Bulletin 6502, variously paginated.
- Davis, M. E., and Leggat, E. R., 1967, Preliminary results of the investigation of the saline-water resources in the Hueco Bolson near El Paso, Texas: U. S. Geological Survey Open-File Report, 27 p.
- Freeze, R. A., and Cherry, J. A., 1979, Groundwater: Englewood Cliffs, New Jersey, Prentice-Hall, Inc., 604 p.
- Frischknecht, F. C., Labson, V. F., Spies, B. R., and Anderson, W. L., 1991, Profiling using small sources, in Nabighian, M. N., ed., Electromagnetic methods in applied geophysics _ applications, part A and part B: Tulsa, Society of Exploration Geophysicists, p. 105-270.

- Gates, J. S., White, D. E., Stanley, W. D., and Anderson, H. D., 1980, Availability of fresh and slightly saline ground water in basins of westernmost Texas: Texas Department of Water Resources, 108 p.
- Geonics Limited, 1992, Protem 47 operating manual: Mississauga, Ontario, variously paginated.
- Geraghty & Miller, Inc., 1995, A review and evaluation of the available hydrologic data on the groundwater resources under the El Paso County Water Authority and Fabens WCID leases: Geraghty & Miller, Inc., contract report prepared for the El Paso County Water Authority, 41 p.
- Groschen, George E., 1994, Simulation of ground-water flow and the movement of saline water in the Hueco Bolson aquifer, El Paso, Texas, and adjacent areas: U. S. Geological Survey, Open-File Report 92-171, 87 p.
- Gustavson, T. C., 1991, Arid basin depositional systems and paleosols: Fort Hancock and Camp Rice Formations (Pliocene–Pleistocene), Hueco Bolson, West Texas and adjacent Mexico: The University of Texas at Austin, Bureau of Economic Geology Report of Investigations No. 198, 49 p.
- Hawley, J. W., Kottlowski, F. E., Seager, W. R., King, W. E., Strain, W. S., and LeMone, D. V., 1969, The Santa Fe Group in south-central New Mexico border region, *in* New Mexico Bureau of Mines & Mineral Resources Circular 104, p. 52–76.
- Hefford, S., 2001, Airborne magnetic and Megatem II electromagnetic multicoil survey, El Paso County: Fugro Airborne Surveys, Ottawa, Canada, Logistics and Processing Report, Job 744, 21 p.
- Henry, C. D., and Price, J. F., 1985, Summary of the tectonic development of Trans-Pecos Texas: The University of Texas at Austin, Bureau of Economic Geology, Miscellaneous Map No. 36, scale 1:500,000, 8-p. text.

- Kaufman, A. A., and Keller, G. V., 1983, Frequency and transient soundings: Elsevier, Amsterdam, Methods in Geochemistry and Geophysics, No. 16, 685 p.
- Knowles, T., and Kennedy, Ground-water resources, Hueco Bolson, Texas: U. S. Department of the Interior, Geological Survey, Water-Supply Paper 1426.
- Lee Wilson and Associates, 1981, Water supply alternatives for El Paso: contract report prepared for El Paso Water Utilities Public Service Board, El Paso, Texas, variously paginated.
- Mack, G. H., and Seager, W. R., 1990, Tectonic control on facies distribution of the Camp Rice and Palomas Formations (Pliocene–Pleistocene) in the southern Rio Grande rift: Geological Society of America Bulletin, v. 102, no. 1, p. 45–53.
- Mattick, R. E., 1967, A seismic and gravity profile across the Hueco Bolson: Texas Geological Survey Research 1967, Professional Paper 575-D, p. D85-D91.
- Mayer, W. D., and Gordon, J. D., 1972, Development of ground water in the El Paso District, Texas, 1963-1970: Texas Water Development Board, Report 153, 51 p.
- Muehlberger, W. R., and Dickerson, P. W., 1989, A tectonic history of Trans-Pecos Texas, *in* Muehlberger, W. R., and Dickerson, P. W., eds., Structure and stratigraphy of Trans-Pecos Texas: 28th International Geological Congress, Field Trip Guidebook T317, p. 35–54.
- Mullican, William F., III, Dutton, Alan R., Mace, Robert E., and Blum, Martina, 1997, Reevaluation of ground-water resources on state lands in eastern El Paso county: topical report prepared for the Texas General Land Office by the Bureau of Economic Geology, The University of Texas at Austin, 17 p.
- Mullican, W. F., III, and Senger, R. K., 1992, Hydrologic investigations of deep ground-water flow in the Chihuahuan Desert, Texas: The University of Texas at Austin, Bureau of Economic Geology, Report of Investigations No. 205, 60 p.

- Myers, B. N., 1969, Compilation of results of aquifer tests in Texas: Texas Water Development Board, Report 98, 532 p.
- Parasnis, D. S., 1973, Mining geophysics: Amsterdam, Elsevier, 395 p.
- Parasnis, D. S., 1986, Principles of applied geophysics: Chapman and Hall, 402 p.
- Ramberg, I. B., Cook, F. A., and Smithson, S. B., 1978, Structure of the Rio Grande rift in southern New Mexico and West Texas based on gravity interpretation: Geological Society of America Bulletin, v. 89, no. 1., p. 107–123.
- Rees, R. W., 1987, Records on wells, water levels, pumpage, and chemical analyses from selected wells in parts of the Trans-Pecos region, Texas, 1968-1980: Texas Water Development Board.
- Robinove, C. J., Langford, R. H., and Brookhart, J. W., 1958, Saline-water resources of North Dakota: U.S. Geological Survey, Water-Supply Paper 1428, 72 p.
- Rust Lichliter/Jameson, 1994, Preliminary engineering report for the creation of El Paso County Municipal Utility District No. 2: Contract report for the Texas Natural Resource Conservation Commission, variously paginated.
- Sayre, A. N. and Livingston, Penn, 1945, Ground-water resources of the El Paso area, Texas: U. S. Geological Survey Water-Supply Paper 919, 190 p.
- Seager, W. R., 1980, Quaternary fault system in the Tularosa and Hueco Basins, southern New Mexico and West Texas, *in* Dickerson, P. W., Hoffer, J. M., and Callender, J. F., eds., Trans-Pecos region, southeastern New Mexico and West Texas: New Mexico Geological Society Guidebook No. 31, p. 131–135.
- Slichter, C. J., 1905, Observations on the ground waters of the Rio Grande Valley: U. S. Geological Survey Water-Supply Paper 141, 83 p.

- Spies, B. R., and Frischknecht, F. C., 1991, Electromagnetic sounding: in Nabighian, M. N., ed., Electromagnetic methods in applied geophysics_ applications, part A and part B: Tulsa, Society of Exploration Geophysicists, p. 285-386.
- Strain, W. S., 1966, Blancan mammalian fauna and Pleistocene formations, Hudspeth County, Texas: Texas Memorial Museum Bulletin No. 10, 55 p.
- Strain, W. S., 1971, Late Cenozoic bolson integration in the Chihuahua tectonic belt, *in* Hoffer, J. M., ed., Geologic framework of the Chihuahua tectonic belt: West Texas Geological Society Publication 71-59, p. 167–173.
- Stuart, C. J., and Willingham, D. L., 1980, Late Tertiary and Quaternary fluvial deposits in the Mesilla and Hueco Bolsons, El Paso area, Texas: Sedimentary Geology, v. 38, no. 1/4, p. 1–20.
- Vanderhill, J. B., 1986, Lithostratigraphy, vertebrate paleontology, and magnetostratigraphy of Plio-Pleistocene sediments in the Mesilla Basin, New Mexico: The University of Texas at Austin, Ph.D. dissertation, 305 p.
- West, G. F., and Macnae, J. C., 1991, Physics of the electromagnetic induction exploration method, in Nabighian, M. N., ed., Electromagnetic methods in applied geophysics _ applications, part A and part B: Tulsa, Society of Exploration Geophysicists, p. 5-45.
- Williams, Dewayne, Thompson, C. M., and Jacobs, J. L., 1977, Soil survey of Cameron County, White, D. E., 1987, Summary hydrologic information in the El Paso, Texas, area, with emphasis on ground-water studies, 1903-1980: Texas Water Development Board, Report 300, 75 p.

Page intentionally blank

APPENDIX A: CONDUCTIVITY-DEPTH SLICES

Page intentionally blank

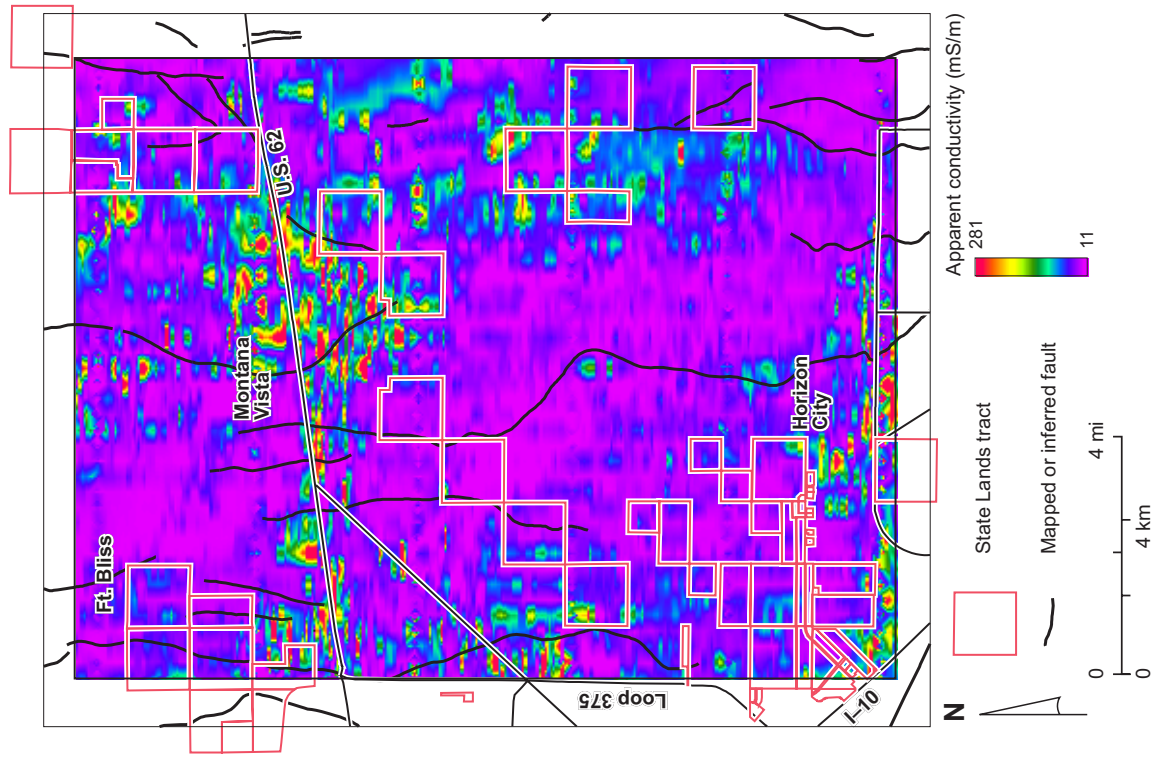


Figure A2. Apparent conductivity at a depth of 20 m.

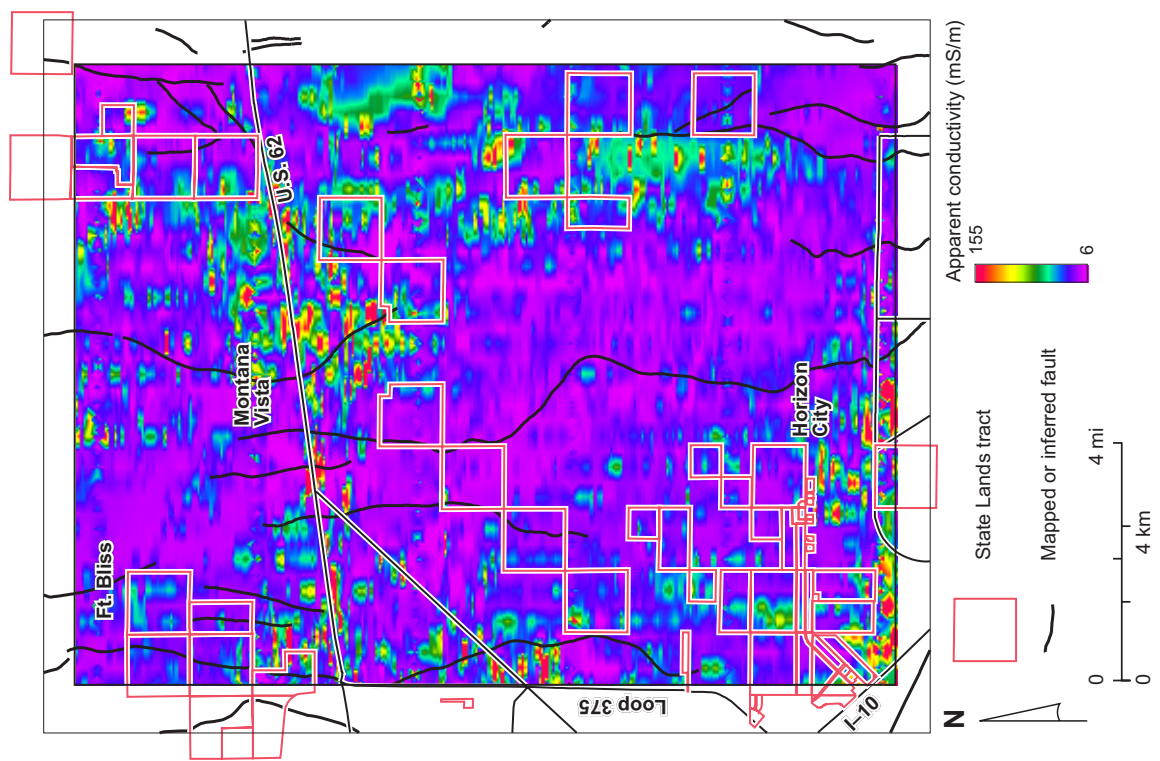


Figure A1. Apparent conductivity at a depth of 10 m.

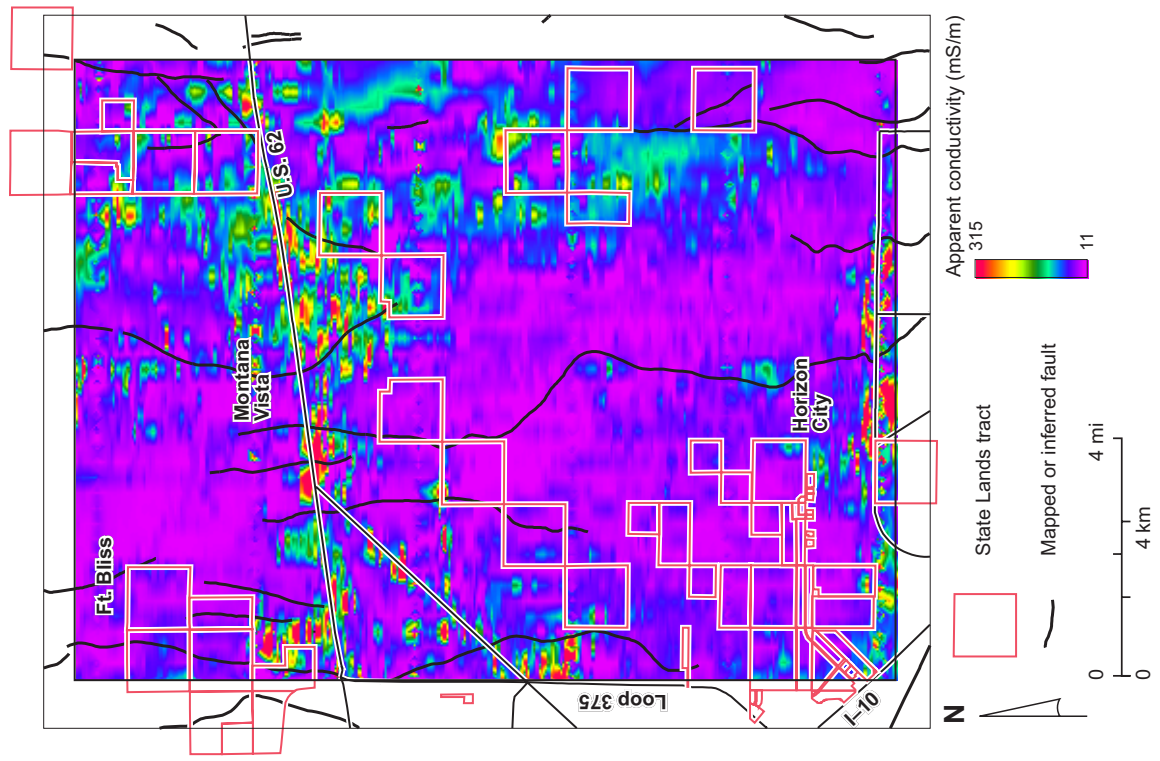


Figure A3. Apparent conductivity at a depth of 30 m.

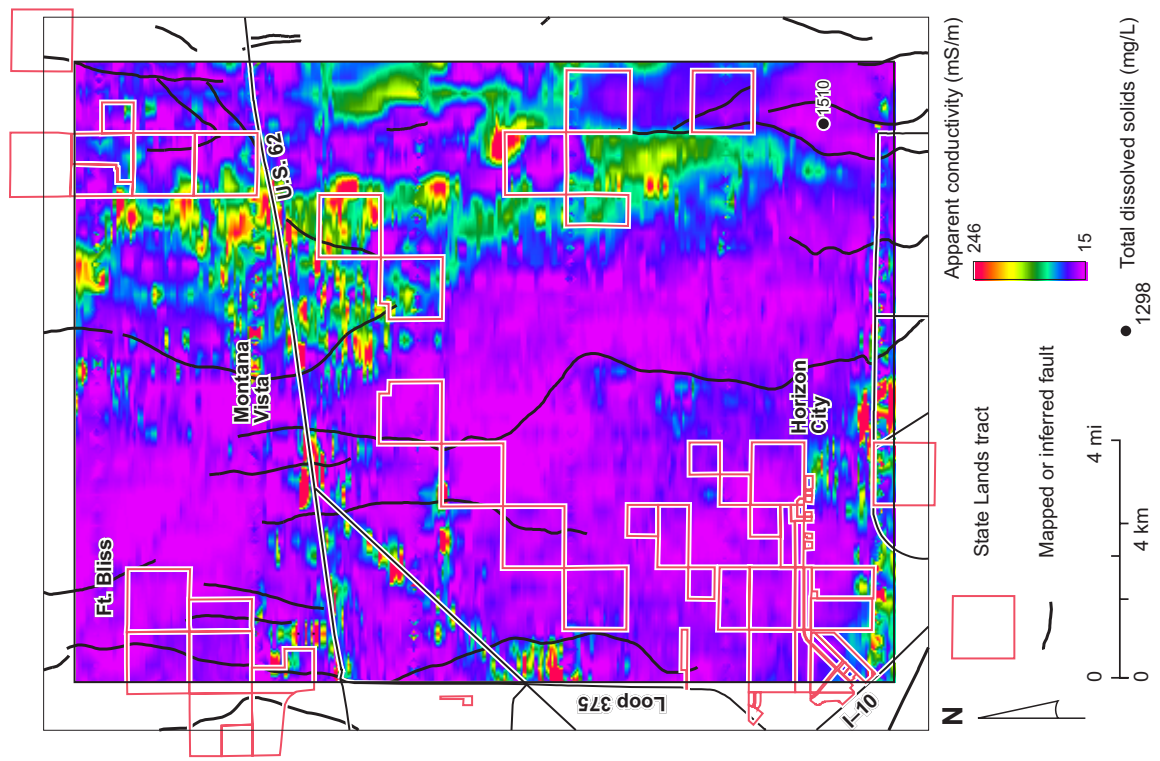


Figure A4. Apparent conductivity at a depth of 40 m. Also shown are TDS values for water samples from wells that have water levels above this level and are screened at this level.

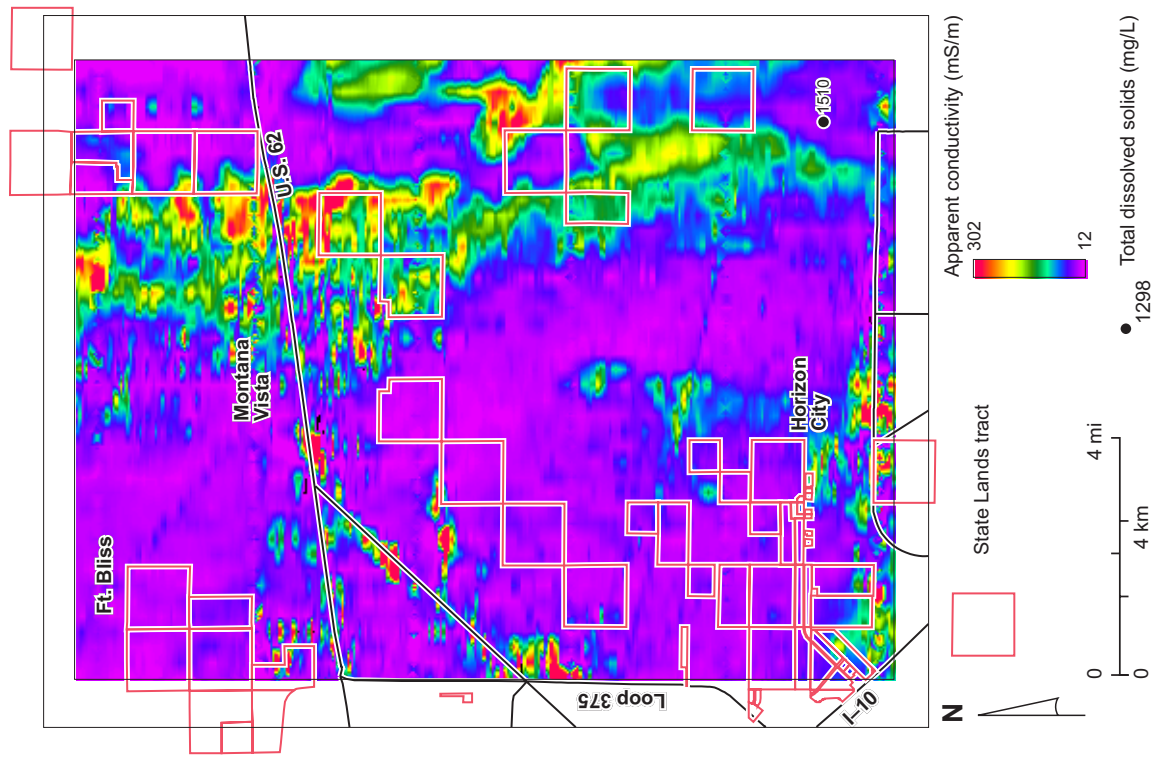


Figure A6. Apparent conductivity at a depth of 60 m. Also shown are TDS values for water samples from wells that have water levels above this level and are screened at this level.

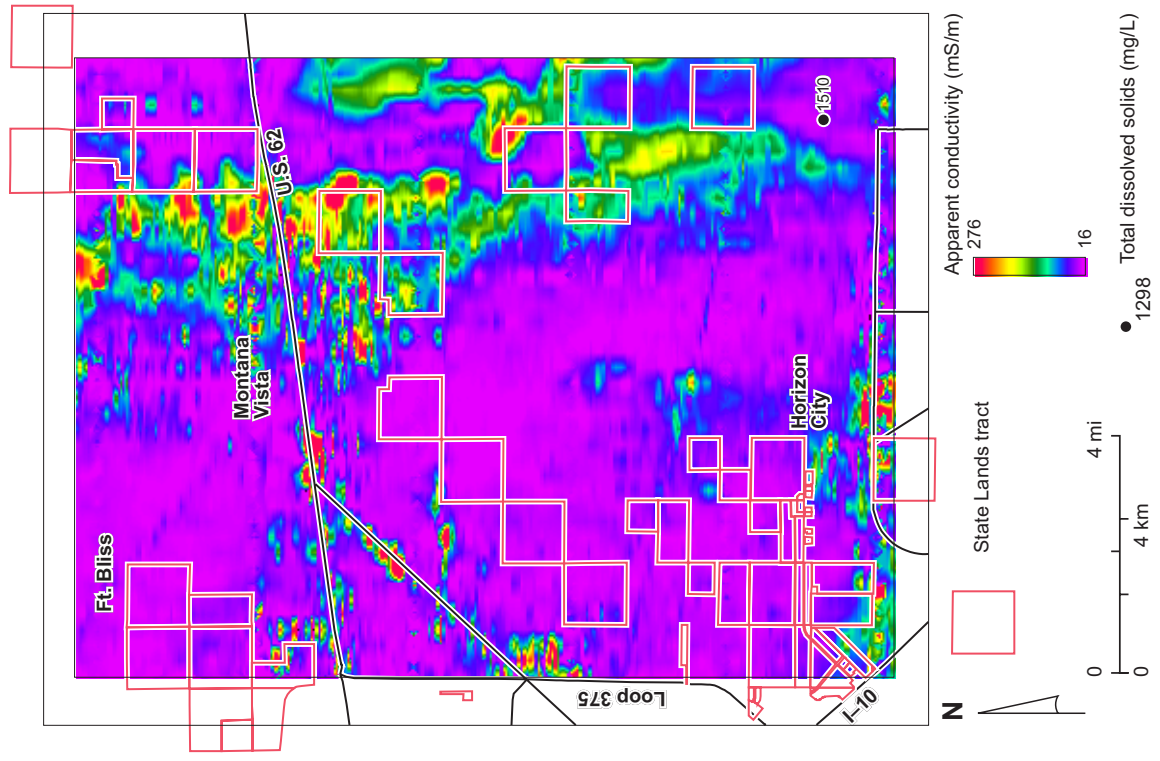


Figure A5. Apparent conductivity at a depth of 50 m. Also shown are TDS values for water samples from wells that have water levels above this level and are screened at this level.

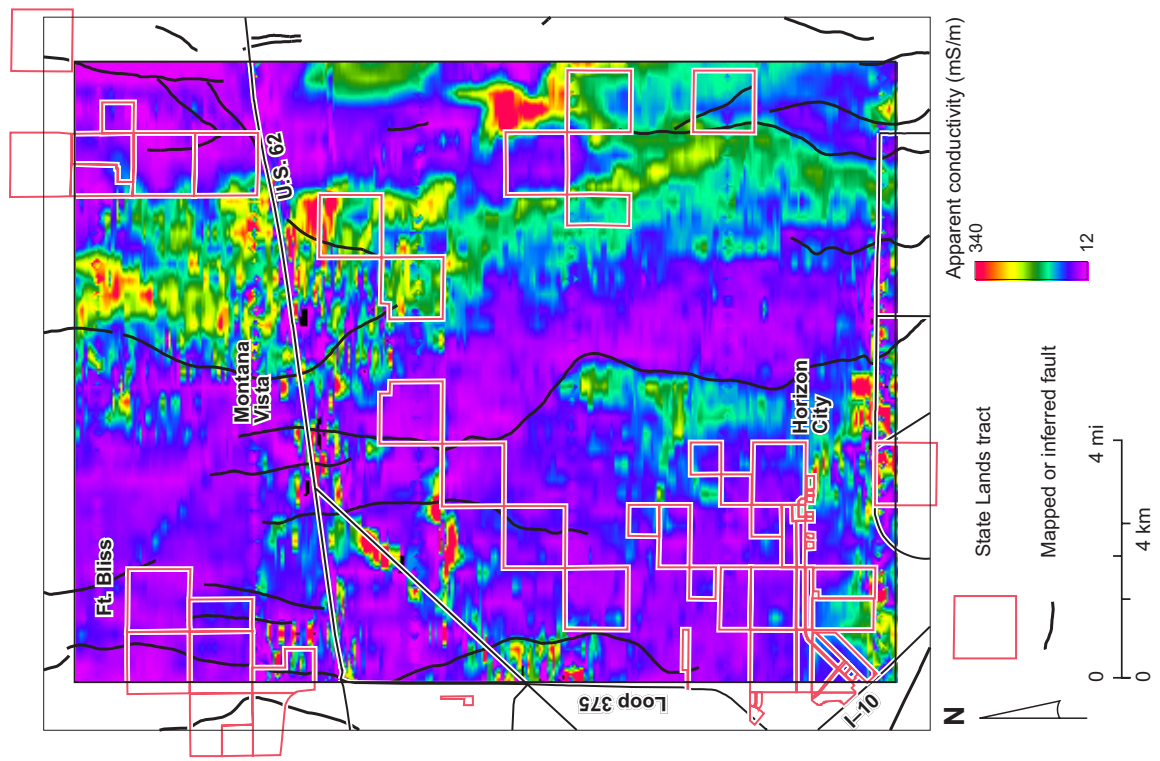


Figure A8. Apparent conductivity at a depth of 80 m

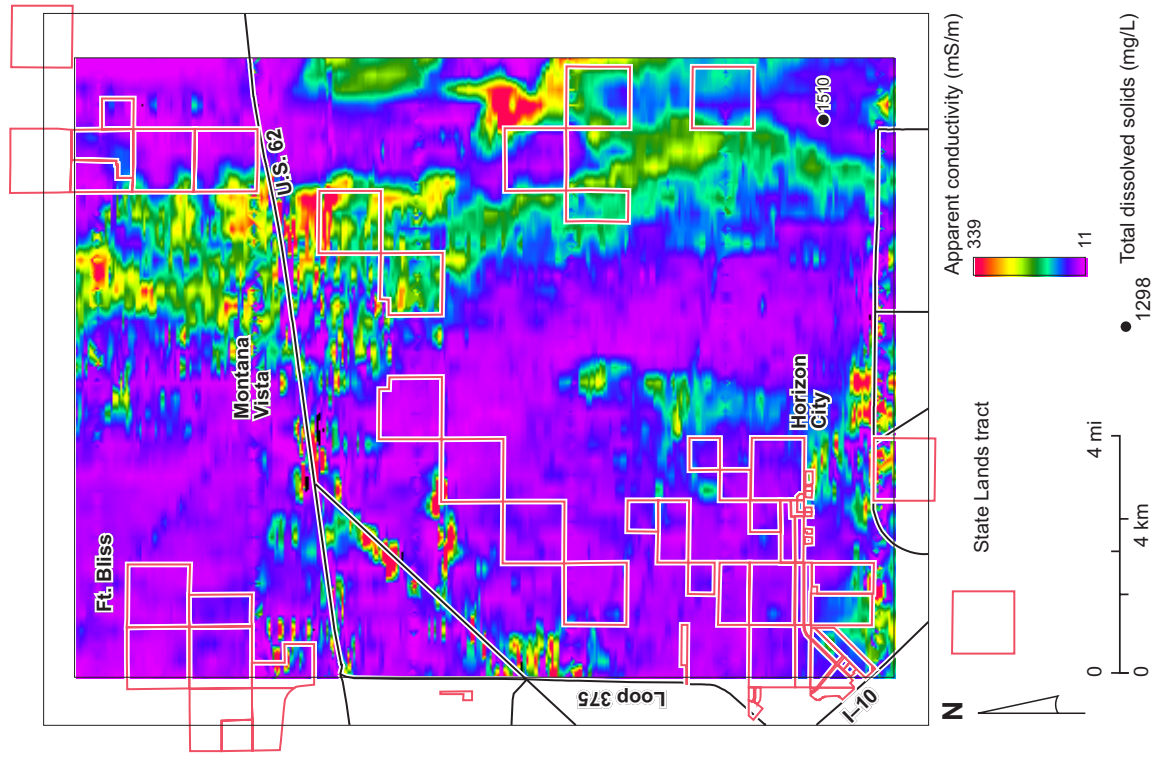


Figure A7. Apparent conductivity at a depth of 70 m. Also shown are TDS values for water samples from wells that have water levels above this level and are screened at this level.

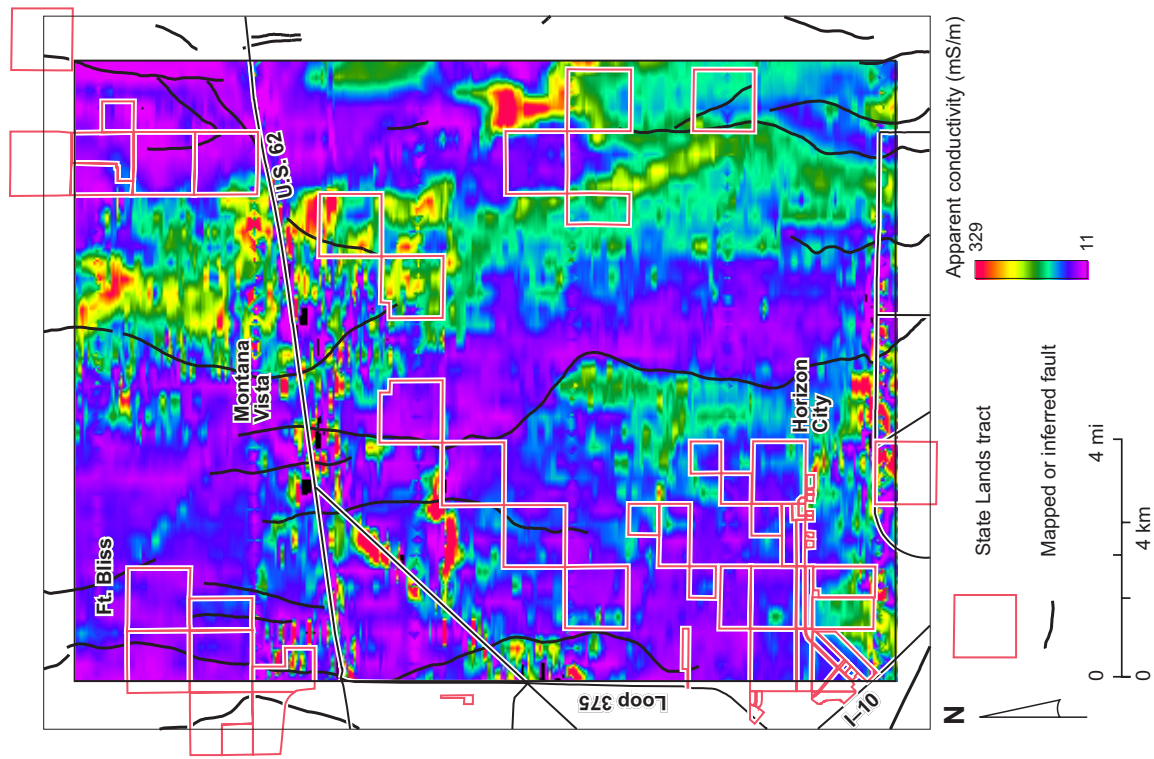


Figure A9. Apparent conductivity at a depth of 90 m.

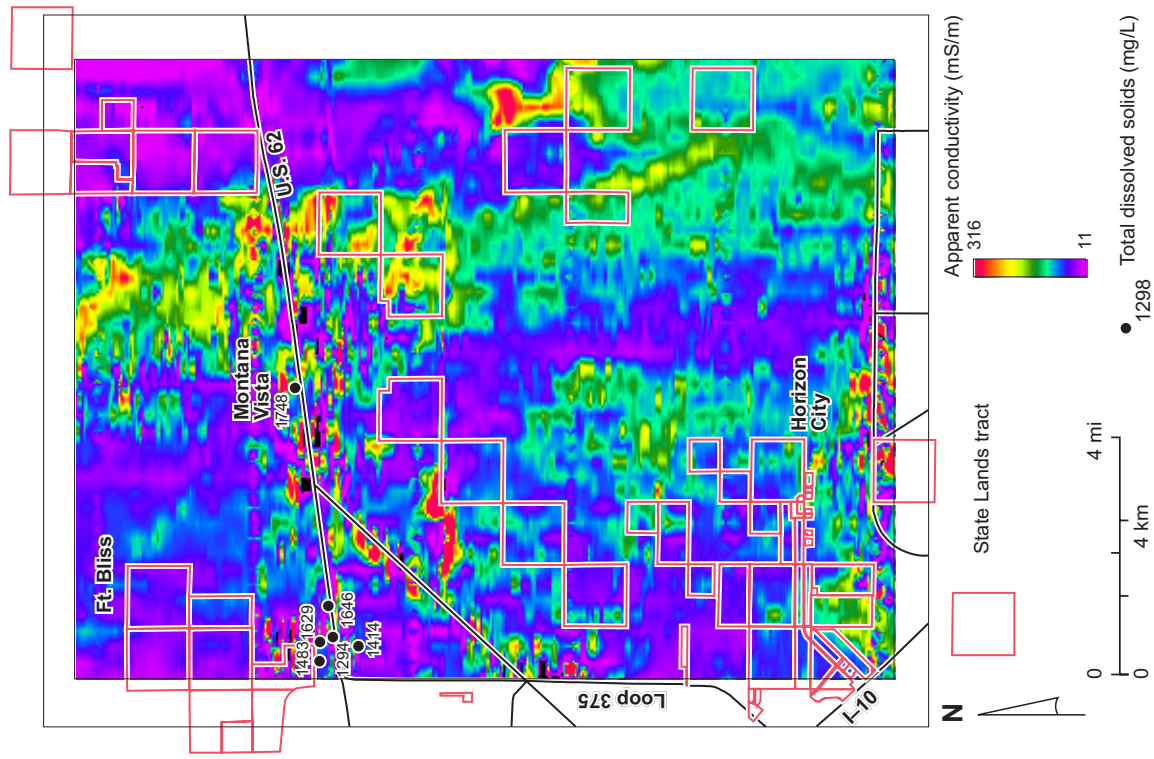


Figure A10. Apparent conductivity at a depth of 100 m. Also shown are TDS values for water samples from wells that have water levels above this level and are screened at this level.

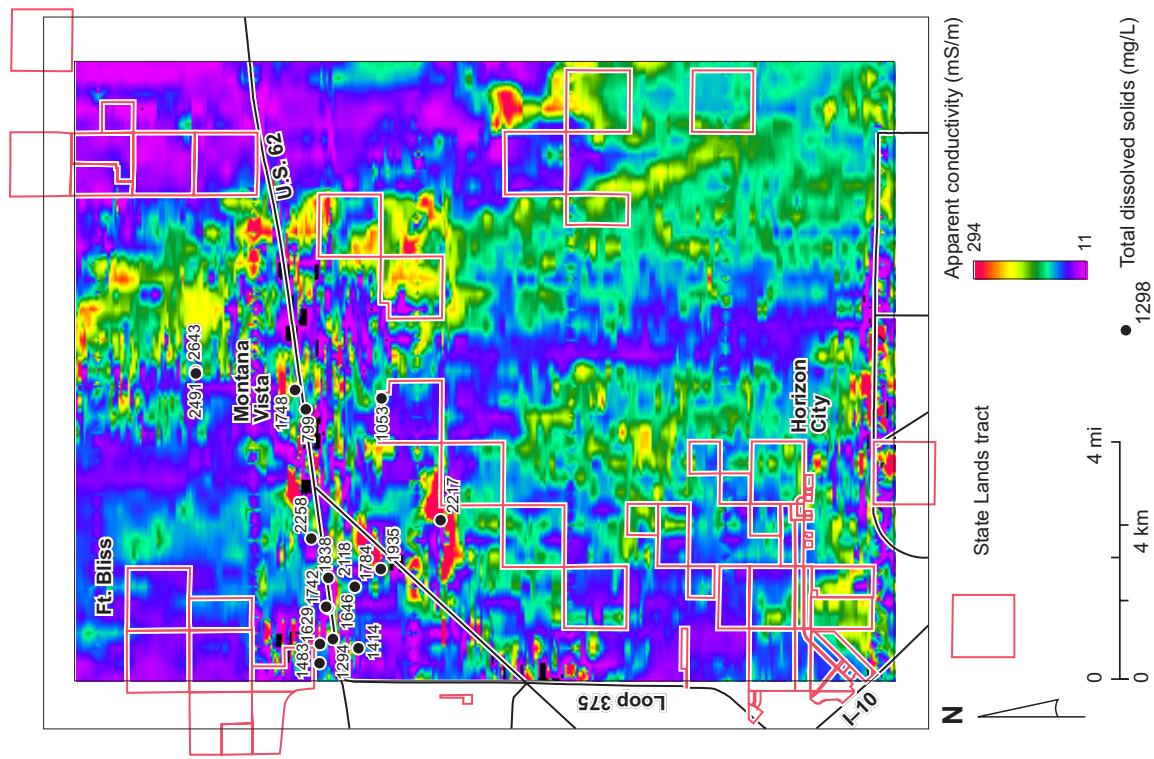


Figure A11. Apparent conductivity at a depth of 110 m. Also shown are TDS values for water samples from wells that have water levels above this level and are screened at this level.

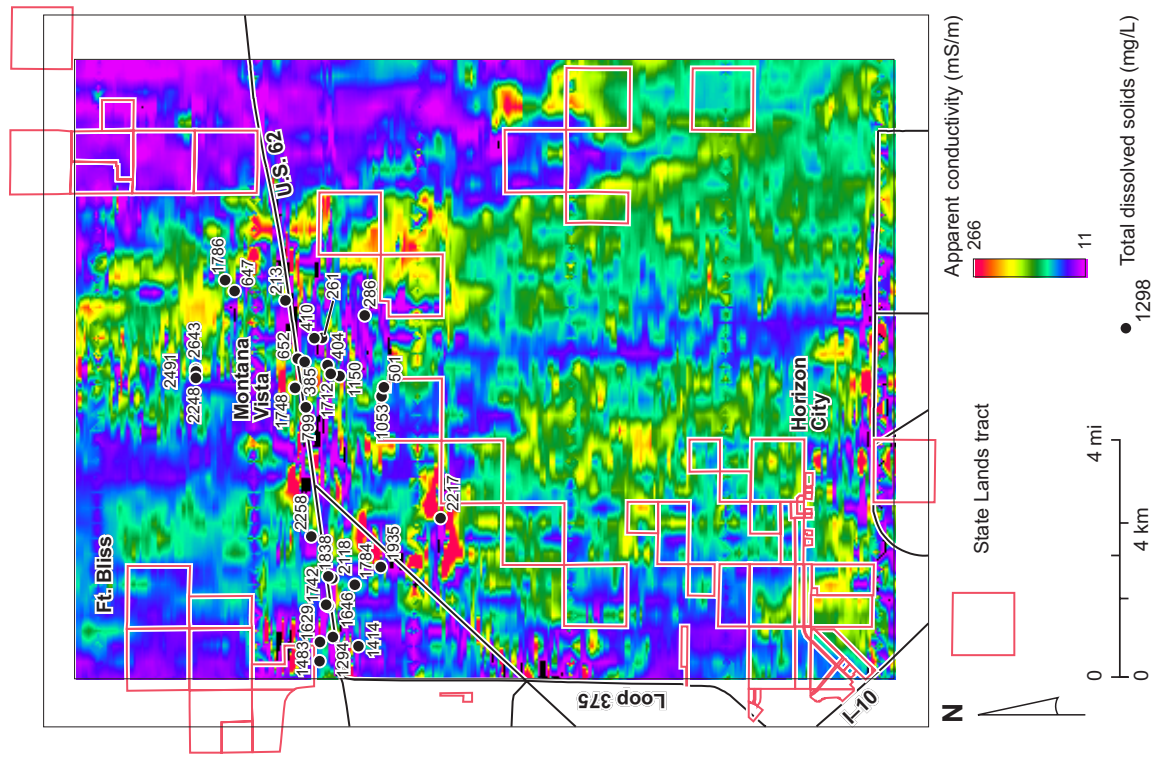


Figure A12. Apparent conductivity at a depth of 120 m. Also shown are TDS values for water samples from wells that have water levels above this level and are screened at this level.

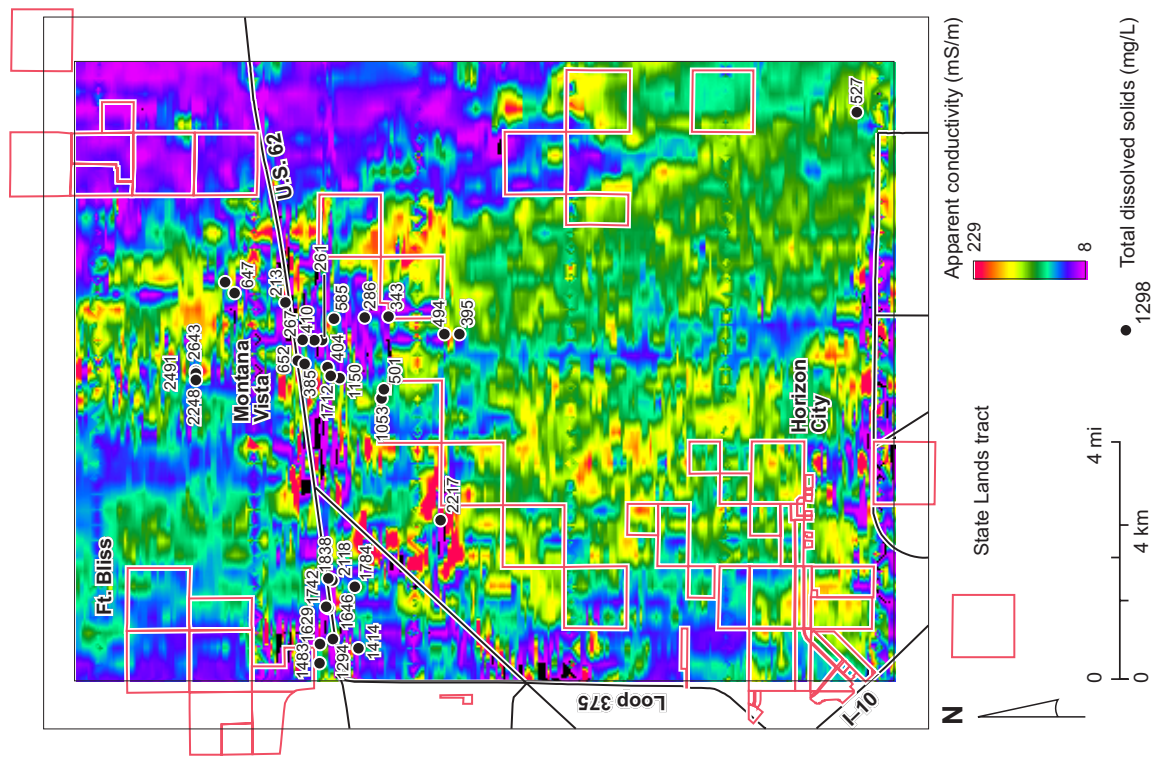


Figure A13. Apparent conductivity at a depth of 130 m. Also shown are TDS values for water samples from wells that have water levels above this level and are screened at this level.

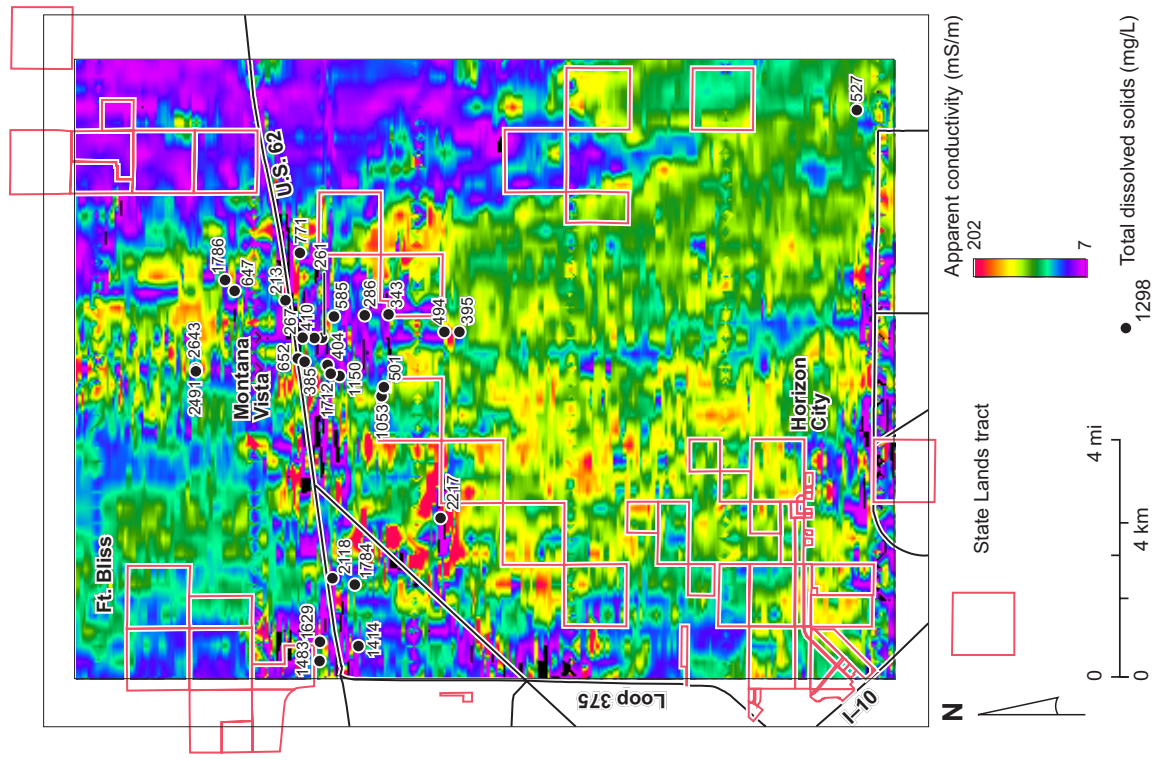


Figure A14. Apparent conductivity at a depth of 140 m. Also shown are TDS values for water samples from wells that have water levels above this level and are screened at this level.

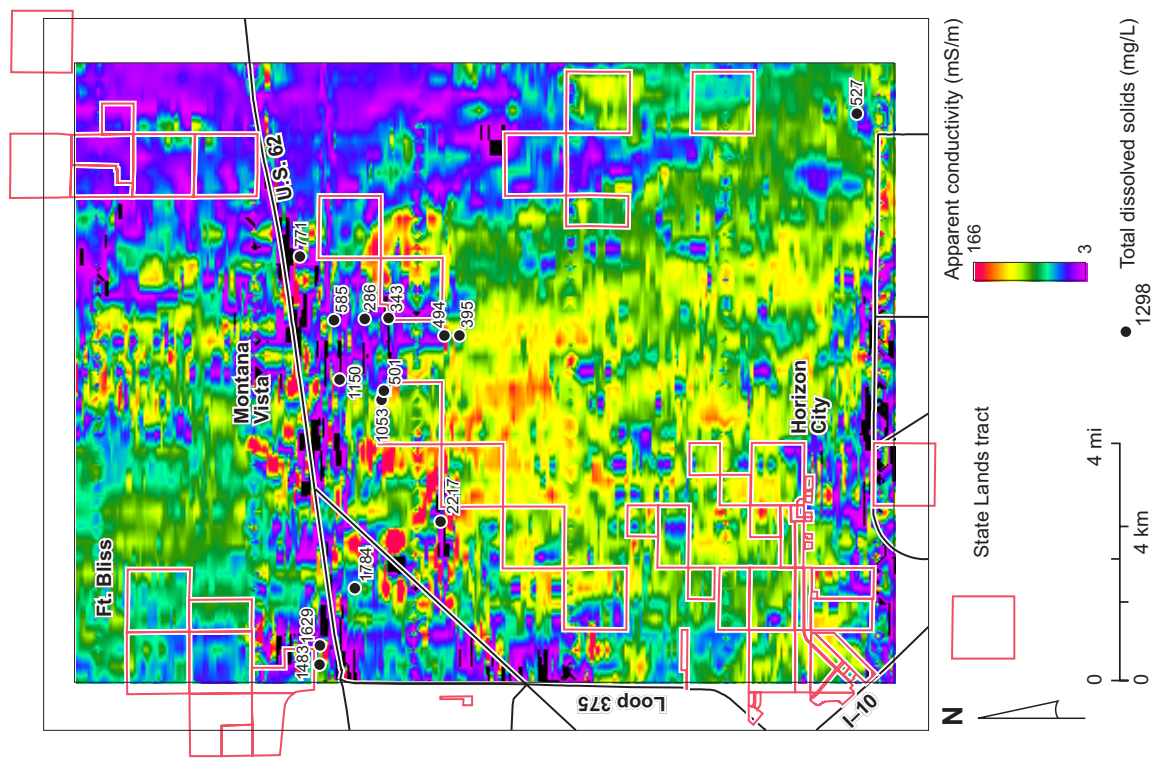


Figure A16. Apparent conductivity at a depth of 160 m. Also shown are TDS values for water samples from wells that have water levels above this level and are screened at this level.

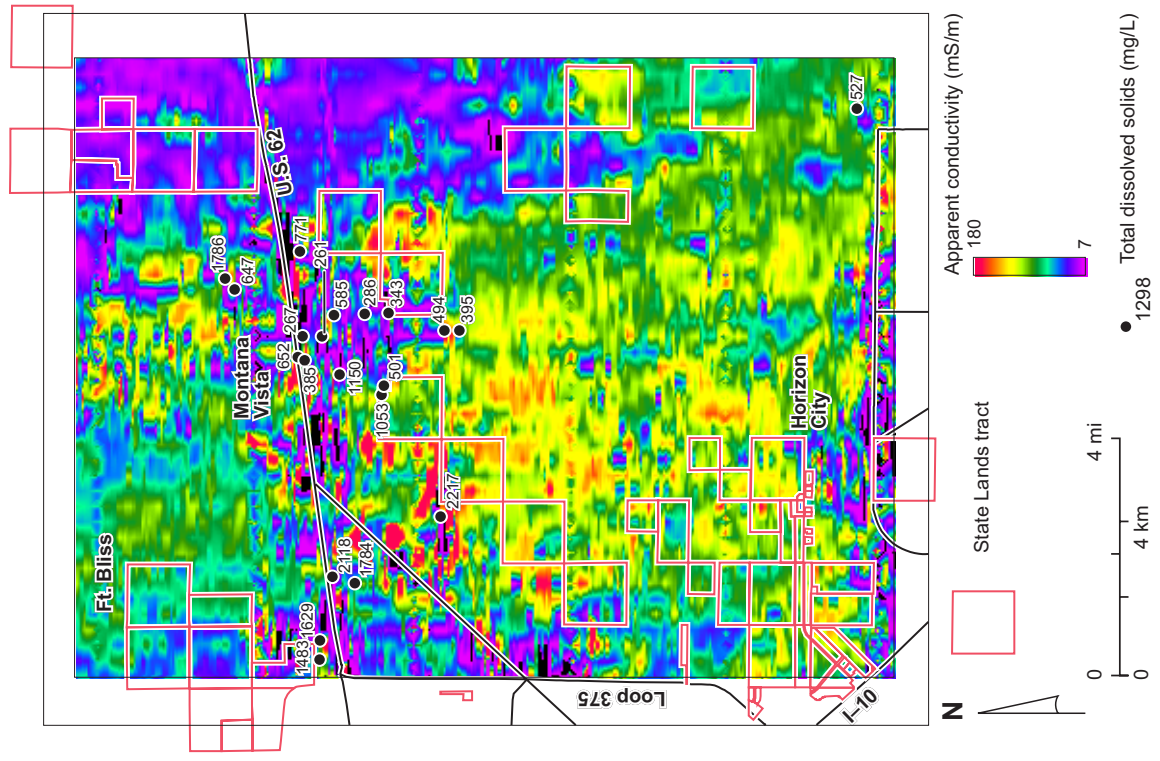


Figure A15. Apparent conductivity at a depth of 150 m. Also shown are TDS values for water samples from wells that have water levels above this level and are screened at this level.

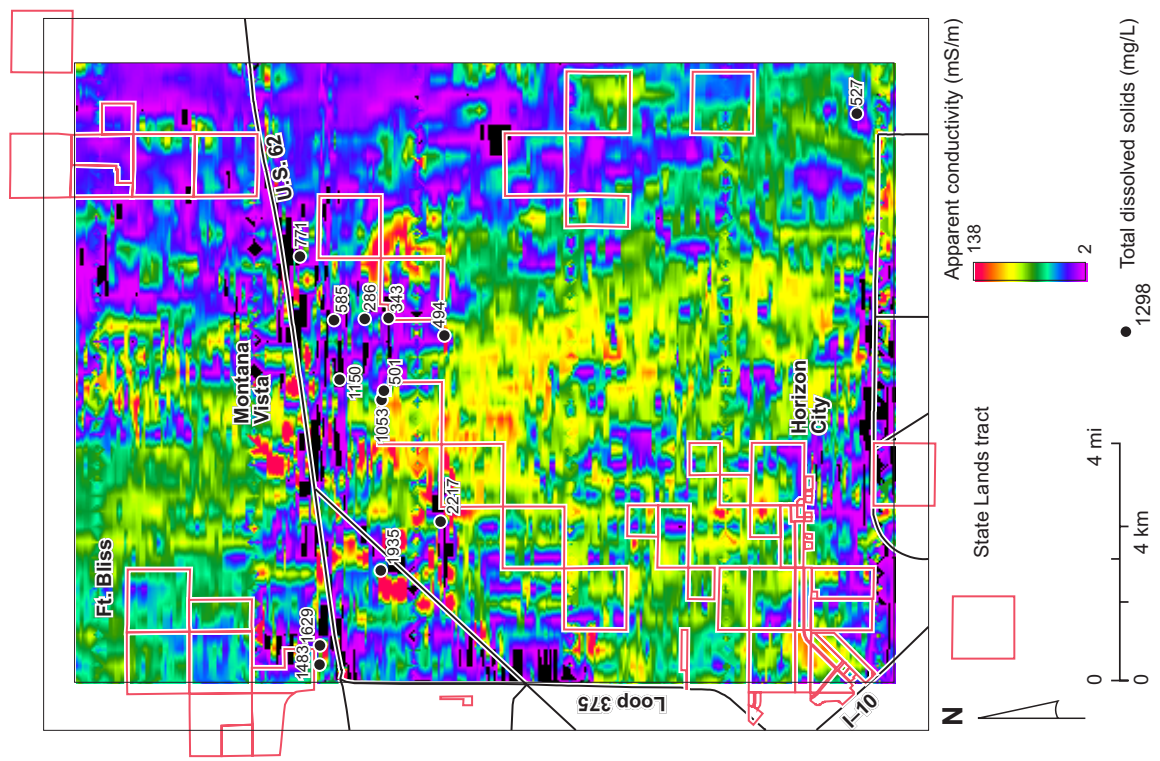


Figure A18. Apparent conductivity at a depth of 180 m. Also shown are TDS values for water samples from wells that have water levels above this level and are screened at this level.

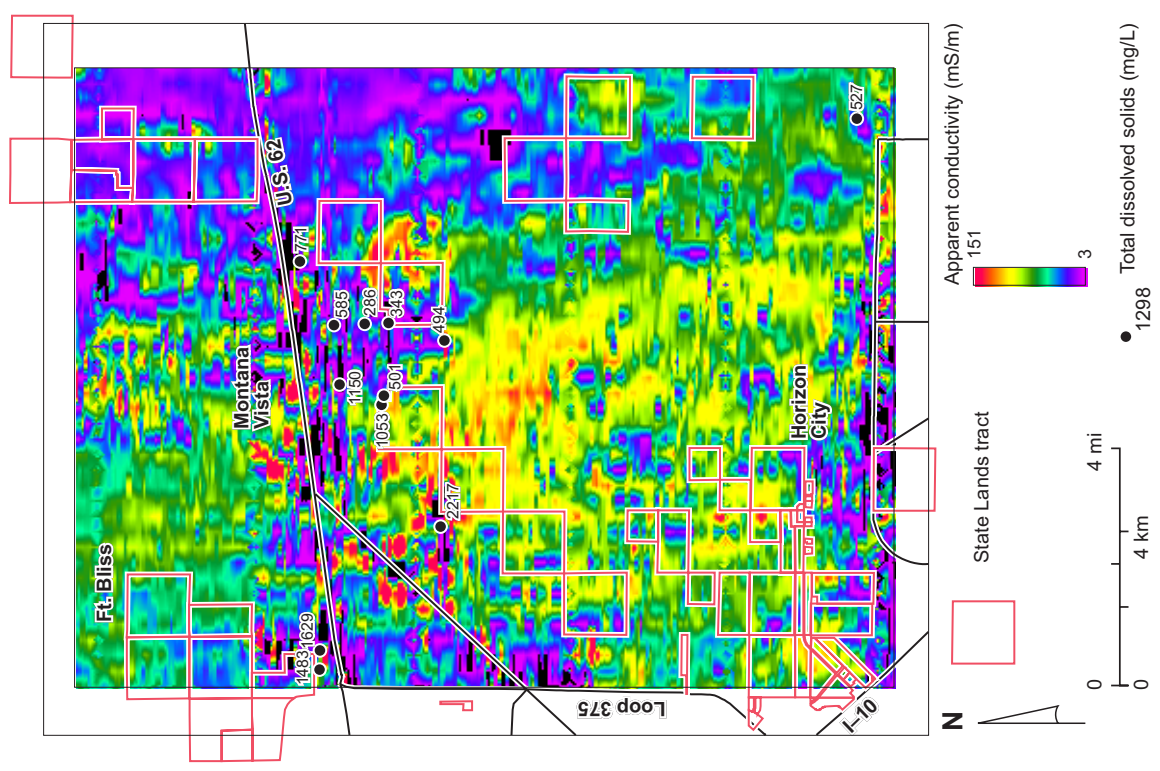


Figure A17. Apparent conductivity at a depth of 170 m. Also shown are TDS values for water samples from wells that have water levels above this level and are screened at this level.

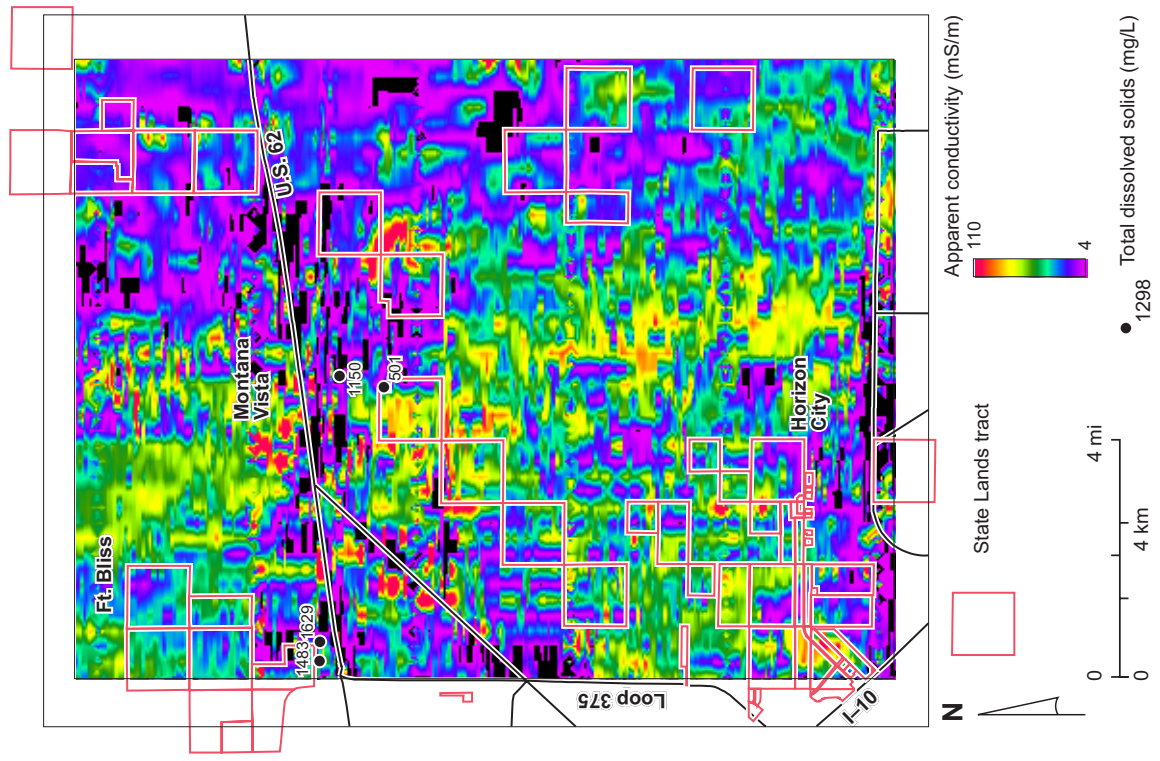


Figure A20. Apparent conductivity at a depth of 200 m. Also shown are TDS values for water samples from wells that have water levels above this level and are screened at this level.

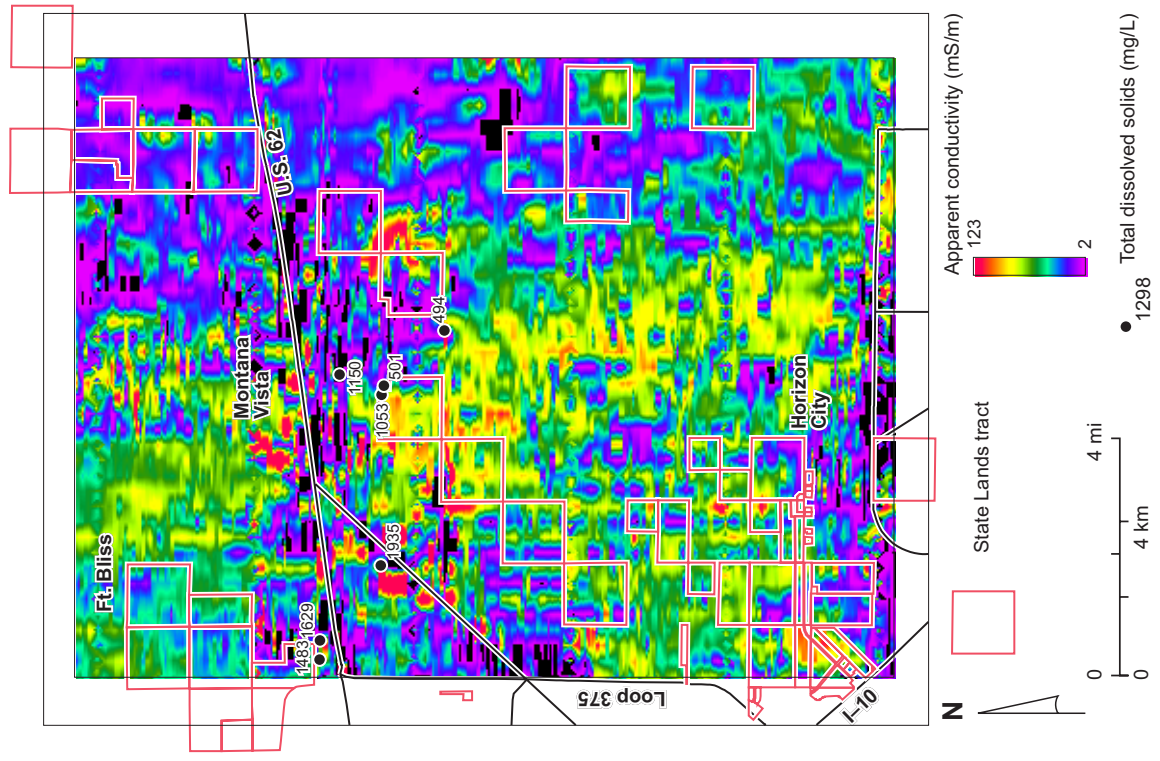


Figure A19. Apparent conductivity at a depth of 190 m. Also shown are TDS values for water samples from wells that have water levels above this level and are screened at this level.

APPENDIX B: CD-ROM CONTENTS

Electronic Report

Electronic versions of this report are included in the "report" directory of the CD-ROM accompanying the report. There are two versions in Adobe pdf format: one optimized for printing (glo_elpaso_print.pdf) and one optimized for screen display (glo_elpaso_screen.pdf). They can be viewed and printed using Acrobat Reader, a free pdf viewer available from Adobe. There is also a version in Adobe Pagemaker format (version 6.5 for Microsoft Windows) in the "pagemaker" subdirectory. Report graphics for the Pagemaker document are in the "eps" and "tiff" subdirectories.

GIS Data Set

The GIS data set, located in the "gis" directory, consists of spatial data that were used in the analysis of the El Paso County airborne geophysical data acquired in August 2002. Included are aerial photographic mosaics, water well data, geology, roads, airborne geophysical data, water well data, and State Lands tracts. To use these files, create an ArcView project and add the shape files and raster images as needed to an unprojected view with map units in meters. All files are compatible with ArcView version 3 GIS software. Files are either ArcView shapefiles or georeferenced tiff images.

Datum and Projection

All project shape files and geotiff images have been projected in meters using the Universal Transverse Mercator (UTM) projection, zone 13 north, 1983 North American Datum.

Airborne Subdirectory

The airborne geophysical data are included as raster (tif) images with intensity values that are color-coded for each image. Data ranges are not included in the images. Scale ranges and measurement units are listed in table B1.

Table B1. File name, measurement units, low and high data values for color scale range, and short file description.

Image	Units	Scale range		Description
		Low	High	
mag_igrf.tif	nT	49168	49295	Geomagnetic reference field (IGRF2001.67)
mag_res.tif	nT	-660.4	-164.5	Residual magnetic field intensity
mag_sdt.tif	nT	-10.3	8.5	Magnetic field shallow depth transform
mag_tmi.tif	nT	48531	49034	Total magnetic field intensity
terrain.tif	m	1185	1352	Elevation
powerline.tif	mV	10.7	350.9	Power line noise
cond_app.tif	mS	184.6	5523.6	Apparent conductance
con_010.tif	mS/m	5.9	155.2	Apparent conductivity at 10 m
con_020.tif	mS/m	10.7	280.6	Apparent conductivity at 20 m
con_030.tif	mS/m	11.4	315.3	Apparent conductivity at 30 m
con_040.tif	mS/m	15.1	245.8	Apparent conductivity at 40 m
con_050.tif	mS/m	15.5	275.6	Apparent conductivity at 50 m
con_060.tif	mS/m	11.5	301.8	Apparent conductivity at 60 m
con_070.tif	mS/m	11.2	338.8	Apparent conductivity at 70 m
con_080.tif	mS/m	11.6	339.9	Apparent conductivity at 80 m
con_090.tif	mS/m	11.3	329.0	Apparent conductivity at 90 m
con_100.tif	mS/m	11.4	316.3	Apparent conductivity at 100 m
con_110.tif	mS/m	11.0	293.8	Apparent conductivity at 110 m
con_120.tif	mS/m	11.1	265.8	Apparent conductivity at 120 m
con_130.tif	mS/m	7.8	229.0	Apparent conductivity at 130 m
con_140.tif	mS/m	7.3	201.6	Apparent conductivity at 140 m
con_150.tif	mS/m	6.9	179.8	Apparent conductivity at 150 m
con_160.tif	mS/m	3.2	165.5	Apparent conductivity at 160 m
con_170.tif	mS/m	2.7	151.1	Apparent conductivity at 170 m
con_180.tif	mS/m	1.7	137.5	Apparent conductivity at 180 m
con_190.tif	mS/m	2.4	123.3	Apparent conductivity at 190 m
con_200.tif	mS/m	3.7	109.6	Apparent conductivity at 200 m
con_210.tif	mS/m	2.3	96.3	Apparent conductivity at 210 m
con_220.tif	mS/m	2.6	83.7	Apparent conductivity at 220 m
con_230.tif	mS/m	2.6	69.2	Apparent conductivity at 230 m
con_240.tif	mS/m	1.5	62.0	Apparent conductivity at 240 m

con_250.tif	mS/m	1.6	55.2	Apparent conductivity at 250 m
con_260.tif	mS/m	2.3	47.2	Apparent conductivity at 260 m
con_270.tif	mS/m	2.6	42.3	Apparent conductivity at 270 m
con_280.tif	mS/m	1.0	38.8	Apparent conductivity at 280 m
con_290.tif	mS/m	1.1	32.7	Apparent conductivity at 290 m
con_300.tif	mS/m	1.0	28.9	Apparent conductivity at 300 m

boundary: subdirectory containing shapefile of the airborne survey boundary.

cond_app.tif: geotiff image depicting apparent conductance. Conductance range is shown in table B1.

con_depth: subdirectory containing shapefile of conductivity-depth profiles at 10-m intervals from 10 to 400 m below the land surface. Conductivity values expressed in mS/m.

depth_slices: subdirectory containing geotiff images of the El Paso County survey area depicting apparent electrical conductivity of the subsurface on depth slices at 10-m intervals between 10- and 300-m depth (con_010 through con_300) using the land surface as datum. Conductivity ranges for each slice are shown in table B1.

flight_lines: subdirectory containing the shapefile of airborne geophysical measurement locations.

magnetics: subdirectory containing the files mag_igrf.tif (the International Geomagnetic Reference Field, IGRF 2001.67); mag_res.tif, the residual magnetic field strength obtained by subtracting the measured magnetic field strength from the IGRF; mag_sdt.tif, the shallow depth transform of the magnetic field data; and mag_tmi, the total magnetic field intensity measured by the airborne instrument.

powerline.tif: geotiff image depicting power-line noise. Noise intensity range is shown in table B1.

terrain.tif: geotiff image depicting land-surface elevation as measured using airborne GPS and a radar altimeter. Elevation range is shown in table B1.

Airphoto Subdirectory

el_paso_mosaic_2m_gs.tif: 2-m resolution aerial photographic mosaic (grayscale) of the El Paso County survey area produced from 1-m resolution Digital Orthophoto Quarter Quadrangle (DOQQ) images from the Texas Natural Resource Information System.

el_paso_mosaic_8m_gs.tif: 8-m resolution aerial photographic mosaic (grayscale) of the El Paso County survey area produced from 1-m resolution Digital Orthophoto Quarter Quadrangle (DOQQ) images from the Texas Natural Resource Information System.

Faults Subdirectory

Subdirectory containing shapefile of mapped and inferred faults within the survey area. Data from Collins and Raney (2000).

Favorable_areas Subdirectory

Subdirectory containing shapefile of favorable areas for groundwater exploration within the 110 to 130-m depth range based on airborne geophysical data.

Geology Subdirectory

Subdirectory containing shapefile of mapped geologic units intersecting the survey area. Map data from Collins and Raney (2000).

Roads Subdirectory

Subdirectory containing shapefile of survey area roads from the ESRI data base.

State_lands Subdirectory

state_fee: Subdirectory containing shapefile of State Lands classified as State fee (code 04).

surface_mins: Subdirectory containing shapefile of State Lands classified as surface minerals (code 19).

surface_only: Subdirectory containing shapefile of State Lands classified as surface only (code 17).

TDEM_ground Subdirectory

Subdirectory containing shapefile of ground-based TDEM measurements acquired in March 2001.

TWDB Subdirectory

`casing`: Subdirectory containing shapefile of well casing information for water wells in the survey area. Data from the Texas Water Development Board, April 2002.

`spec_cap`: Subdirectory containing shapefile of specific capacities for water wells in the survey area. Data from the Texas Water Development Board, April 2002.

`water_level`: Subdirectory containing shapefile of water levels in the survey area. Data from the Texas Water Development Board, April 2002.

`water_quality`: Subdirectory containing shapefile of water-quality analyses in the survey area. Data from the Texas Water Development Board, April 2002.

`well_data`: Subdirectory containing shapefile of water-well data in the survey area. Data from the Texas Water Development Board, April 2002.

El Paso Depth-Slice Animation

The "animation" directory on the CD-ROM contains a movie (`elpaso_movie.avi`) of progressively deeper slices through the conductivity volume of the El Paso County survey area. These animations contain 30 lateral slices at 10-m intervals between the surface and 300-m depth, using the land surface as the vertical datum. Each frame depicts conductivity variations across the area, ranging from high conductivities portrayed as "hot" colors (reds, oranges, and yellows) and low conductivities portrayed as "cool" colors (purple, blue, and green). The animation is stored in Windows movie format (`.avi` suffix). Animations can be played using the Windows movie player on Windows platforms, using the Quicktime Movie Player on Windows, MacOS, and other platforms, or using most other video viewers.